ABSTRACT

An abstract of the thesis of Michael Leslie Hekkers for the Master of Science in Geography presented October 21, 2009.

Title: Climatic and Spatial Variations of Mount Rainier's Glaciers for the Last 12,000 Years

Regional paleoclimatic proxies and current local climate variables and were analyzed to reconstruct paleoglaciers in an effort to assess glacier change on Mount Rainier. Despite the dry and generally warm conditions (sea surface temperatures (SST) -0.15°C to +1.8°C relative to current temperatures), the previously documented McNeeley II advance (10,900-9,950 cal yr B.P.) was likely produced by air temperature fluctuations. The average SST record and the terrestrial climate proxies show cooling temperatures with continued dryness between McNeeley II and the Burroughs Mountain advance (3,442-2,153 cal yr B.P.). The paleoclimate during the Burroughs Mountain advance was both cool and warm (SST temperatures -0.55°C to +0.5°C) and was the wettest of the Holocene.

A combination of statistical and deterministic equilibrium line altitude (ELA) models was used to produce Holocene ELAs between 1,735 -2,980 m. Glacial advances were predicted 10,990, 10,170, 9,260, 8,200, 6,490, 3,450 and 550-160 cal yr. B.P. Two glacier flow models were produced simultaneously to constrain glacial extent through the Holocene. Model 1 is based on current mass balance parameters and produced lengths for the Nisqually and Emmons glaciers 3.7-14.2 km and 4.2-17.1 km

respectively. Glaciated area ranged from 26 to 327 km^2. Model 2 is tuned to the Garda advance and produced lengths 2.6-10.6 km and 2.3-13.9 km. Glaciated area ranged from 11 to 303 km^2. The first two advances were similar in elevation and GIS-modeled extent to McNeely II moraines. The following three advances were not detected in the geologic record. The 3,450 cal yr. B.P. advance was the largest of the late-Holocene (ELA 1,800-1,817 m) and was ~200 m lower than the geologic record. The ELAs of the Garda advance were modeled (1,944-1,983 m) and are similar to previous reconstructions. North-south spatial variations in glacial extent increase during periods of recession as the southern glaciers receive more ablation than northern glaciers.

Early humans could have accessed the alpine environments as high as 1,730-2,980 m. The early Holocene glacial extent allowed the highest (2,980 m) 11,150 cal yr. B.P. and lowest (1,730 m) 10,990 cal yr. B.P. alpine access. Glacial retreat (2,727 m 10,400 cal yr. B.P.) was followed by an advance (1,929 m 10,170 cal yr. B.P.) and another retreat (2,951 m 10,050 cal yr. B.P.). Ice gradually descended and limited access to 1,820 m 6,490 cal yr. B.P. Glacial extents remained largely unchanged until the historic era when paleohumans would have had access to alpine environments at 2,000 m.

Climatic and Spatial Variations of Mount Rainier's Glaciers for the Last 12,000 Years

by

Michael Leslie Hekkers

A thesis submitted in partial fulfillment of the
requirements for the degree of

Master of Science
in
Geography

Thesis Committee:
Andrew G. Fountain, Chair
Martin D. Lafrenz
Jiunn-Der Geoffrey Duh
Gregory Burtchard, National Park Service

Portland State University

ACKNOWLEDGMENTS

I would like to thank my advisor, Andrew G. Fountain, for his honesty and forthright comments throughout this mountainous process. This endeavor could not have happened without the immense support from my wife, Di and understanding from our son, Aubrey and even our dog, Dawa. This project was funded by Mount Rainier National Park under the supervision of Greg Burtchard, Darin Swinney, and Paul Kennard. Thanks for your comments, patience, and the opportunity to contribute to the scientific understanding of park history. It was a great project that met my climatological and glaciological interests. Greg and Paul thanks for hiking with me out to glacial and paleo-human sites. Thanks to Greg, Geoffrey, and Martin for the comments that made this more accessible to the general public.

TABLE OF CONTENTS

LIST OF TABLES

LIST OF FIGURES

1. INTRODUCTION

The glaciers of the Cascade Range in the western U.S. have left geologic evidence of prior stable advanced positions that have been linked with cooler and/or wetter climates (Heine, 1998; Marcott and others, 2009; Thomas, 2000). But to understand the full range of regional paleoclimate variations that may or may not have also affected glaciers, other regional climate proxies must be addressed. Paleoclimate proxies, such as ocean sediment cores and lake sediment cores e.g. (Barron and others, 2003; Gavin and others, 2001; Tweiten, 2007), offer a more complete climate record than the geologic evidence left by glaciers. Understanding the range of paleoclimate variation during the Holocene epoch, approximately the last 12,000 years, is important for understanding the range of glacier extent. Past glacier extents affect how and where early human habitants used periglacial environments at Mount Rainier in the past (Burtchard, 1998). Over the last couple centuries as glaciers have receded, treeline advanced (Baker and Moseley, 2007; Butler and DeChano, 2001), and early human habitants would have followed treeline for their resource harvesting (Burtchard, 1998). Understanding the paleoclimate-paleoglacier relationship is also important for modeling future glacier extent in light of global warming and general worldwide glacial recession (IPCC 2007).

In this thesis I examine the entire Holocene climate and glacial record to illustrate how glaciers changed over this period. First, I reconstruct Mount Rainier's climate over the last 12,000 years using geomorphic data including moraines whose time of formation has been determined, and regional paleoclimate proxies for temperature and precipitation.

This continuous high-elevation climate and reconstructed glacial record will aid our understanding of Holocene climate-glacier dynamics at Mount Rainier and the greater Pacific Northwest. Second, the local glacier-climate relationship (temperature and precipitation) is estimated and its change over the Holocene. The third and final goal is to reconstruct glacial extent and its changes over the Holocene. These findings will be used by National Park Service archeologists to assess early Holocene human habitats.

1.1 Study Site

The climate at Mount Rainier is largely determined by its height and its proximity to the Pacific Ocean (Whiteman, 2000). Mount Rainier, located in central southwestern Washington (46.85°N, 121.75°W), is the tallest mountain (4,392 m) in the Cascade Range (Figure 1) and is only 180 km east of the Pacific Ocean. It receives 17 m of snow annually (1.9 m weq snowpack) at the Paradise Visitor Center, elevation 1,645 m) from marine systems advecting from the Pacific Ocean (Miller, 2002) (Figure 2). Winter and summer temperatures at Paradise range from -6°C to +2°C and 6°C to 18°C, respectively (Whiteman, 2000). Above 2,500 m elevation, heavy snowfall and cool summer temperatures create the most extensively glaciated mountain in the continental U.S. (Driedger and Kennard, 1984; Nylen, 2001).

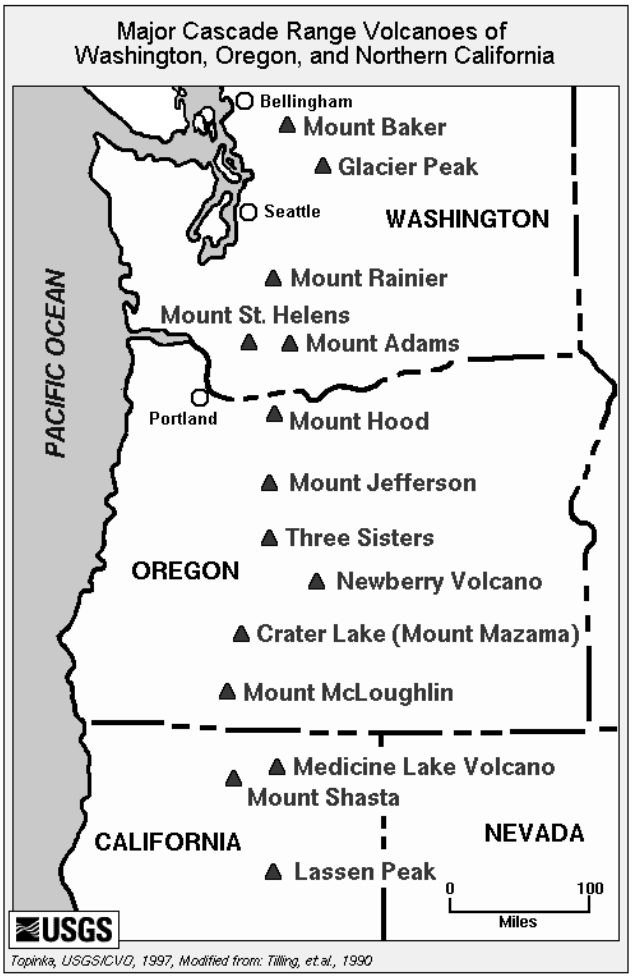

Figure 1. Volcanoes of the Cascade Range (Topinka, 1997).

Twenty-six glaciers and numerous unnamed snow fields occupy the slopes of Mount Rainier with a total area of 87.4 km^2 and ice volume of 4.21 km^3 as of 1994 (Nylen, 2001) (Figure 2). Carbon Glacier is the largest glacier by volume of ice, 0.74 km^3, and the Emmons has the greatest area, 11.21 km^2. The Nisqually Glacier, because of its access by roads and proximity to Paradise on the south slopes is the most studied glacier (Nylen, 2001).

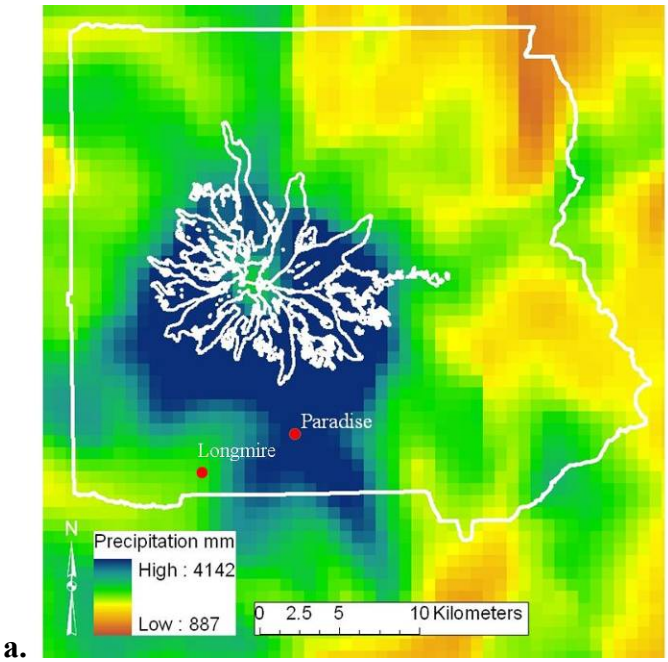

a.

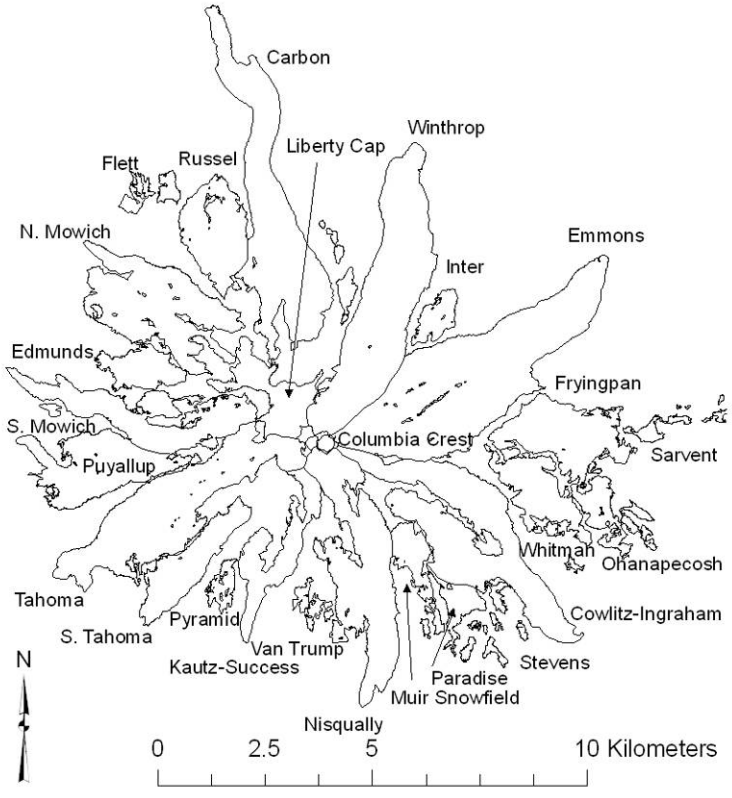

b.

Figure 2. a) Precipitation normals for the Mount Rainier National Park (boundary shown) area 1971-2000 30-arcseconds, 800 (Daly and others, 1994). Glacier outlines are shown for reference. b) Glaciers of Mount Rainier, USGS 1998.

Numerous Holocene volcanic eruptions and debris flows melted or covered the glaciers on Mount Rainier. Twenty-two tephra (ash and pyroclastic debris) layers have been deposited during the Holocene, eleven from Mount Rainier and eight falling between ~7,425 and 4,440 cal years B.P. (Mullineaux, 1974). Dates have been converted from radiocarbon years B.P. (Stuiver and Reimer, 1993). The most widespread and voluminous tephra deposited on the mountain is the layer C tephra, 2-30 cm thick, dated to ~2,150 cal years B.P. (Scott and others, 1995). At least three large debris flows ($>2x10^8$ m^3), which extended to Puget Sound, occurred in the last 5,000 years (Scott and others, 1995). The most notable debris flows of these are the Osceola and Paradise dating to 5,725 and 5,070 cal years B.P., which could have been caused by a summit collapse during eruption that removed the upper 500 m, decreased its volume by 3 km^3, and thus potentially changed the climate and mass balance of the glaciers (Scott and Vallance, 1995), (Kennard, Scott, Valance pers. comm.).

1.2 Glacial History

The glacial history in the Pacific Northwest produced a somewhat unclear picture as glaciers advanced at different times in different locations. The Younger Dryas cooling event is widely documented (Alley and Clark, 1999; Peteet, 1993), (Alley and others, 1997; Alley and Clark, 1999; Peteet, 1993) throughout the Northern Hemisphere (12,900-11,600 cal yr. B.P.) and is quantified by Greenland ice core records (-9.0°C) (Alley and others, 1997; Alley, 2000) (Figure 3). However, the Younger Dryas cold event did not

produce glacial advances on all the glaciated areas in western coastal North America because the timing of the advance occurs before, during or after the event (Davis and others, 2009; Menounos and others, 2009). Younger Dryas climate coincides with glacial advances in the Canadian Rockies (Reasoner and others, 1994), southern British Columbia (Friele and Clague, 2002), and perhaps the Enchantment Lakes area of the North Cascades (Bilderback, 2004), and the Three Sisters peaks in central Oregon (Marcott and others, 2009). Post-Younger Dryas advances are found on Mount Rainier and the Wallowa Mountains (Heine, 1998; Licciardi and others, 2004) and because of dating uncertainty, perhaps at the Three Sisters.

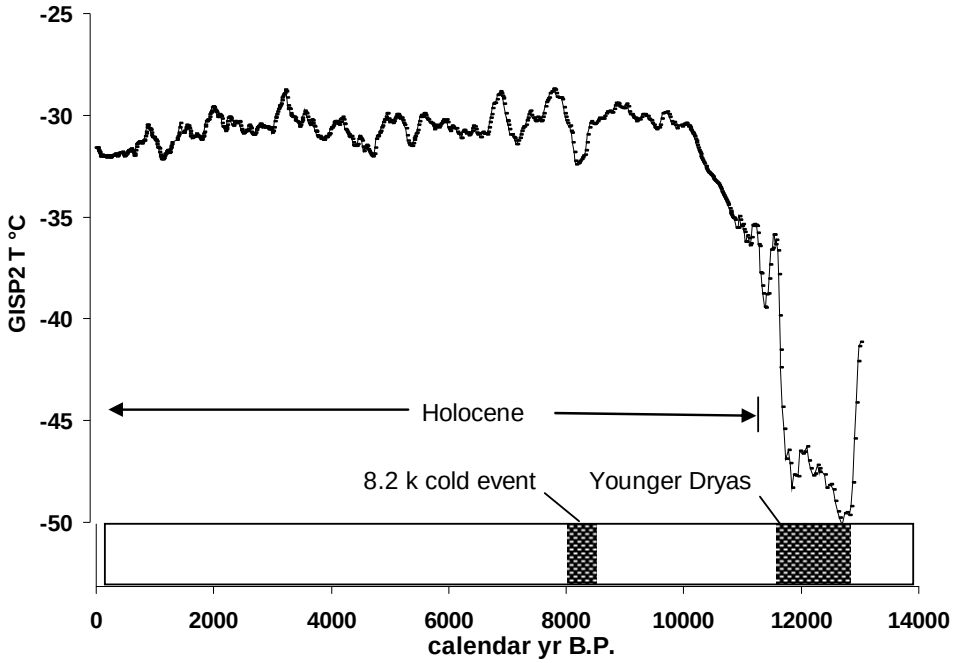

Figure 3. Central Greenland air temperatures with northern hemisphere climate reversals (shaded areas): Younger Dryas 12,900-11,600 cal yr. B.P., 8,200 cold event 8,400-8,000 cal yr. B.P. (Alley and others, 1997; Alley, 2000).

Four other time periods had some synchronous Holocene glacial advances. Glacial evidence for the 8,200 cal yr. B.P. cold event is present at two sites in southern British Columbia (Menounos and others, 2004; Osborn and others, 2007). Another advance at 4,200 cal yr. B.P. was found in the Canadian Rockies and the southern Coast Mountains of British Columbia (Osborn and others, 2007; Reasoner and others, 1994). Evidence for a 3,400 cal yr. B.P. advance is present at Mount Rainier (Crandell and Miller, 1974) and the Canadian Rockies (Osborn and others, 2007) Based on stratigraphy, the approximate end of that advance on Mount Rainier was also synchronous Three Sisters (Marcott and others, 2009) at about 2,200 cal yr B.P. During the Little Ice Age (LIA), a worldwide glacial advance broadly defined as 12th to late 19th centuries (Menounos and others, 2009) but more specifically ~1550-1850 A.D., (Green and Dolman, 1988), moraines were ubiquitous on glaciated peaks in the region (Figure 4; Table 1).

In summary, the evidence indicates that Mount Rainier, despite that it is the highest glaciated peak in the region, had glacial advances generally more synchronous with its southern neighbors than the northern ones. Mount Rainier has no evidence of a Younger Dryas glacial advance but a post-Younger Dryas advance is synchronous with advances in the Wallowa Mountains and possibly Three Sisters, Oregon (Licciardi and others, 2004; Marcott and others, 2009). Also notably absent on Mount Rainier is evidence for the 8,200 cal yr. B.P. cold event seen on mountains to the north e.g. (Menounos and others, 2004; Osborn and others, 2007). The only synchronous advance with a northern mountain is in the Canadian Rockies 3,400 cal yr. B.P. (Osborn and

others, 2007). Otherwise the end of that glacial advance on Mount Rainier is again synchronous with Three Sisters, Oregon (Marcott and others, 2009). Like most mountains in the region, Mount Rainier had extensive advances during the LIA.

Figure 4. Map showing glacier advance sites that have been dated to the last 12,000 years.

Holocene glacial extents have been extensively mapped at Mount Rainier but few of the moraines have been dated (Crandell, 1969; Crandell and Miller, 1974). The three mapped Holocene moraines are McNeeley Drift, Burroughs Mountain Stade, and the Garda Stade (Table 2) (Figure 5). The Garda Stade is the local geologic name for the

Table 1. Summary of glacial advances for western Pacific North America (k= thousands of calendar years B.P.) Hemispheric cold periods are shown in gray: * Little Ice Age 50-450 years B.P., **8.2k cold event 8,000-8,200 years B.P, ***Younger Dryas 11,600-12,900 B.P.

Location	0k*	1k	2k	3k	4k	5k	6k	7k	8k**	9k	10k	11k***	12k***	Reference
Canadian Rockies												11.5		Reasoner and others, 1994
	0.25±0.2													Luckman, 2000
					4.0 ± 0.2									Menounos and others, 2008
S. Coast Mountains, B.C.				3.2 ± 0.3	4.2 ± 0.2[1]		6.8 ± 0.1		8.3 ± 0.3					Osborn and others, 2007
									8.3 ± 0.3					Menounos and others, 2004
	0.25-0.9													Koch and others, 2007
													12.7 ± 0.2	Friele and Clague, 2002
Mount Baker, WA	undated								8.9 ± 0.5					Thomas and others, 2000
Enchantment Lakes, WA	0.8-0.47+											> 11.3		Bilderback, 2004
Mount Rainier, WA	**0.4 ± 0.3**		**2.8 ± 0.6**								**10.4 ± 0.5**			Heine, 1998;
														Crandell and Miller, 1974
Wallowa Mountains, OR											10.2 ± 0.6			Licciardi and others, 2004
	0.21 ± 0.13													Kiver, 1974
Three Sisters, OR	0.2 ± 0.1		2.1 ± 0.4			5.5 ± 1.0						11 ± 1[2]		Marcott, 2009
Mount Thielsen, OR	0.2 ± 0.1													Lafrenz, 2001
Sierra Nevada, CA	0.2 ± 0.1													Clark and Gillespie, 1997

[1] Authors noted as a probable glacier advance because of limited datable material

[2] Fountonnour advance late Pleistocene or early Holocene

Little Ice Age glacial advance. Techniques used included tephrochronology, lichenometry and bracketing tephra for relative dating.

Table 2. Geologic-climate units in western Washington and correlative deposits in the southeastern part of the Puget Sound lowland and the Cascade Range (Crandell and Miller, 1974).

	Inferred years before the present	Major geologic-climate unit	Subdivisions of major units	Deposits	
				Southeast Puget Sound lowland	Cascade Range
Holocene	3,000	Winthrop Creek Glaciation "Hypsithermal interval"	Garda Stade Burroughs Mountain Stade		Garda Drift
	10,000		Sumas Stade		McNeeley Drift
Late Pleistocene	11,500 12,500		Everson Interstade		
		Fraser Glaciation	Vashon Stade	Vashon Drift	Vashon Drift
			Evans Creek Stade	Evans Creek Drift	Evans Creek Drift
	20,000?	Olympia Interglaciation			
	35,000?				

The McNeeley moraines are characterized by elevations 1,720-1,805 m with an average ELA elevation of 1,815 m and are typically located in small, mid-elevation cirques, but some have been noted down valley from the large glaciers, including Carbon, Cowlitz, Ohanapecosh, and Paradise (Crandell and Miller, 1974; Heine, 1998). Flooding events may have washed away moraines of large valley glaciers (Heine, 1998), and subsequent glacial advances may have overridden McNeeley moraines elsewhere on the mountain. McNeeley moraines were mapped and dated in the northeast corner of Mount Rainier National Park. A tephra Layer R ~ 8,750 ^{14}C yr B.P. overlays the moraines, and

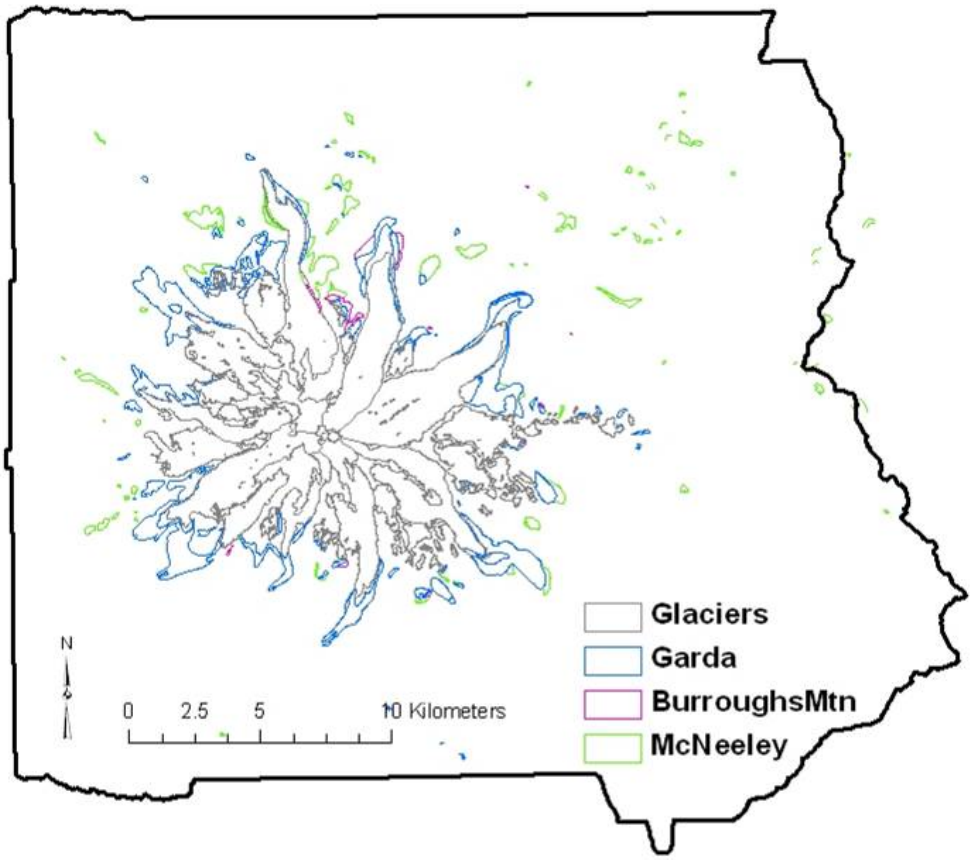

Figure 5. Mount Rainier National Park boundary with 1998 glaciers and the three mapped sets of Holocene moraines: Garda, Burroughs Mountain, and McNeeley.

therefore the moraines must have formed before this time (Crandell and Miller, 1974). Heine (1996) redated the Layer R tephra to 8,850 ^{14}C yr B.P. (9,880 cal yr B.P.) and improved dating accuracy of the McNeeley moraines using radiocarbon dating of embedded organic material in the moraine, and sediments in a nearby proglacial lake and noted two McNeeley advances. McNeeley I was dated late-glacial (13,320-12,880 cal yr. B.P.), prior to the Younger Dryas cold reversal and beginning of the Holocene (Heine, 1998) and is thereby disregarded in this thesis. McNeeley II was dated to the Holocene 10,900-9,950 cal yr B.P. (Figure 6) and was similar in glacial extent (Heine, 1998).

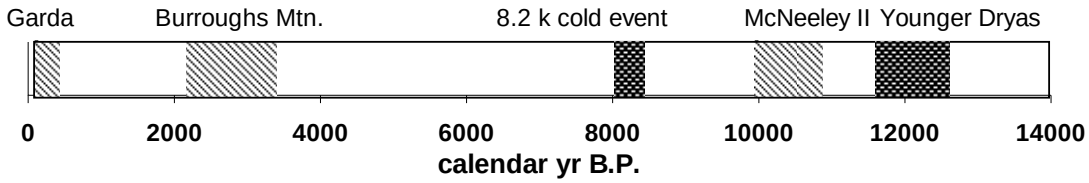

Figure 6. Northern Hemisphere climate reversals (dark shaded areas) and glacial advances (diagonal shaded areas) on Mount Rainer: McNeeley II 10,900-9,950 cal yr B.P., Burroughs Mountain 3,442-2,153 cal yr B.P., Garda 500-90 cal yr B.P.

A later Holocene advance marked by the Burroughs Mountain moraines, average elevation 1,943 m, are bracketed by tephra 3,442-2,153 cal yr B.P. (Crandell and Miller, 1974). These moraines are not common and typically lie only short distances beyond the most recent advance, the Garda Stade, which occurred 750-100 cal yr B.P. The Garda moraines may have overridden the Burroughs Mountain moraines in some valleys (Crandell and Miller, 1974). Based on the range of dates for the Burroughs Mountain and Garda stades (advances), Crandell and Miller (1974) believe the interval between the two advances to be as short as 1,200 years.

The Garda advance reached their maximum extents in the 15th, 17th, and 18th centuries (Crandell and Miller, 1974) with terminus elevations of 977- 1,404 m (1,206 m average) and an average ELA of 1,943 m (Burbank, 1981). However, half of the glaciers on Mount Rainier reached their maximum between 1830 and 1860 A.D. (Crandell and Miller, 1974). Historic photographs, surveys, and tree-ring records also support the geologic evidence of these advances (Harrison, 1956). Since 1750 A.D., Garda glaciers responded in synchrony as shown by lichenometry (Burbank, 1981).

Since the Garda, the historic variation showed that smaller glaciers on the south and west-facing aspects retreated more than the larger north or east-facing glaciers over the last century largely due to incoming solar radiation, size, and elevation range (Nylen

and others, 2000; Nylen, 2001). Over the last several decades, debris cover has shaded ice on several glaciers e.g. Winthrop, Carbon, and Emmons, thus preserving greater ice extents and volumes (Driedger and Kennard, 1984; Nylen, 2001).

2. PALEOCLIMATE

Paleoclimate at Mount Rainier is inferred from continental-hemispheric proxies, insolation, a combination of coastal sea surface temperatures (SST), and regional terrestrial proxies. The continental-hemispheric scale proxies and insolation trends are used to provide a context for the regional scale SST and local terrestrial climate proxies. SST reconstructions off the western coast of North America offer evidence of atmosphere-ocean interactions affecting Mount Rainer's climate. Qualitative terrestrial proxies, examined because of their proximity to Mount Rainier, are considered after evaluating the broader trends in continental-scale multi-proxy climate reconstructions and insolation.

Multi-proxy climate reconstructions for the Northern Hemisphere offer high resolution but are generally limited to the late Holocene. The reconstructions are based on fossil pollen, tree rings, terrestrial borehole temperatures, lake sediments, ice cores, fossil sea shells, and more recently, instrumented temperature records (Huang, 2004; Mann and others, 1999; Mann and Jones, 2003; Rutherford and others, 2005) (Figure 7). Insolation is also included in one multi-proxy study (Mann and others, 1999). Subsurface terrestrial borehole temperature records, such as Mann and others (2003), are thought to be good indicators of long-term surface temperature trends while multi-proxy analyses tuned with historical temperature records are thought to offer better temporal resolution (Huang, 2004).

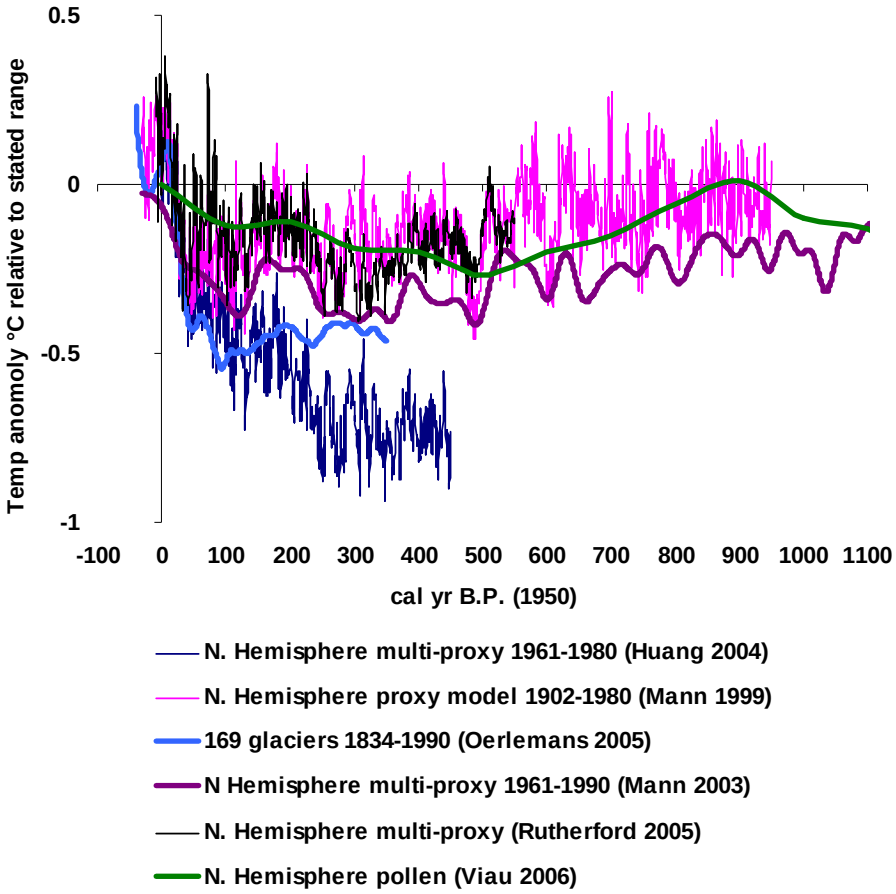

Figure 7. North American temperature reconstructions reflecting multi-proxy studies, pollen and tree rings. Where noted in the legend, stated date ranges reflect the mean against which other records are compared.

The majority of the reconstructions chart a cooling which began 1,000 cal yr. B.P. reaching a low point between 500 and 40 cal yr. B.P. From the historical 400 year global glacier length record, temperatures were inferred, and the coldest point was 85 cal yr B.P. (Oerlemans, 2005) (Figure 7). The North American pollen record captures these general trends and is unique because it extends through the Holocene (Figure 8).

Holocene trends in paleoclimate at Mount Rainier are likely influenced by variations in insolation. Astronomical forcing, reduced insolation, is thought to have decreased long-term temperatures since the mid-Holocene by -0.01 to -0.04°C per

century (Berger, 1988). Northern hemisphere summer insolation peaked in the early Holocene and is currently approaching insolation minima (Figure 9) (Huybers, 2006).

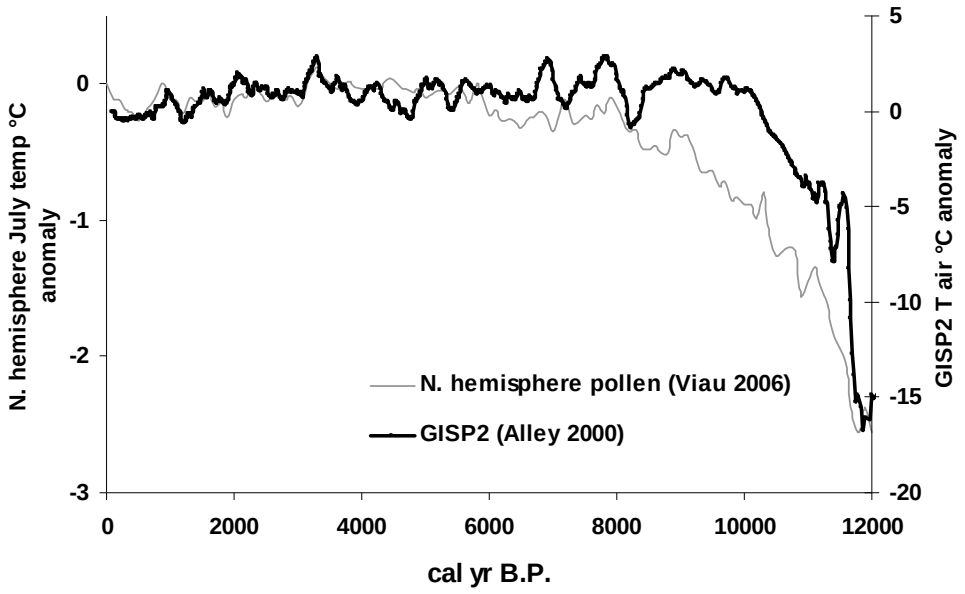

Figure 8. A broad-scale pollen-based temperature reconstruction for North America compared with the central Greenland air temperatures (Alley, 2000; Viau and others, 2006). Temperatures anomalies are from most recent temperatures.

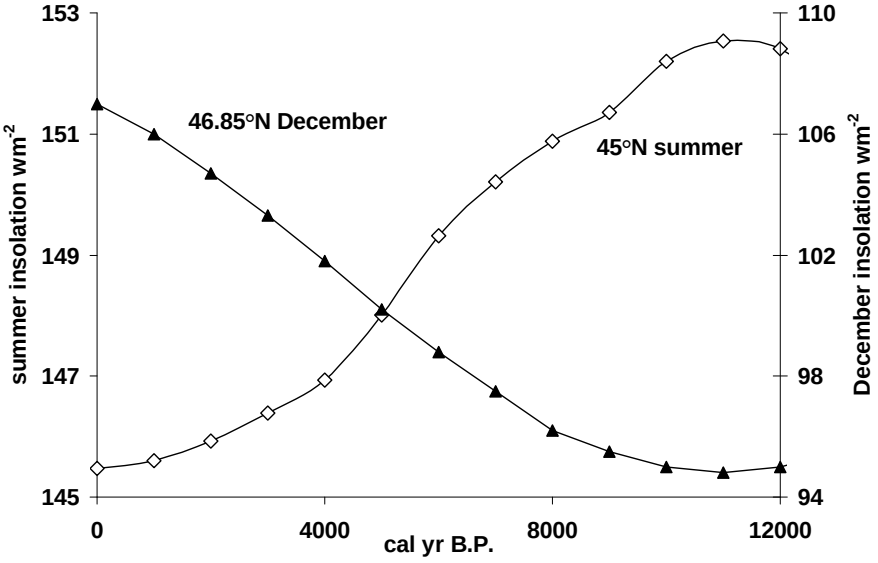

Figure 9. Northern hemisphere summer insolation at 45°N (Huybers, 2006). December insolation at 46.85°N (Corripio, 2007).

2.1 Paleo-Sea Surface Temperature

Sea surface temperatures off the west coast should be a good proxy for terrestrial air temperature variations given the dominant westerly wind flow at this latitude. The closest SST reconstructions to Mount Rainier are from off the coast of Vancouver Island, 440 km away, (Kienast and McKay, 2001) and ocean drilling program site 1019 off northern California, 620 km away (Barron and others, 2003) (Figure 10). The coastal northern California SST reconstruction is based on planktonic species, pollen, fraction of $CaCO_{3,}$ and total organic carbon while the Vancouver Island reconstruction is based on the temperature derived alkenones and carbon dating of different planktonic foraminifera. All of the proxy indicators eventually sink from the surface onto the sea floor where they are preserved in the ocean sediment (Williams and others, 1998).

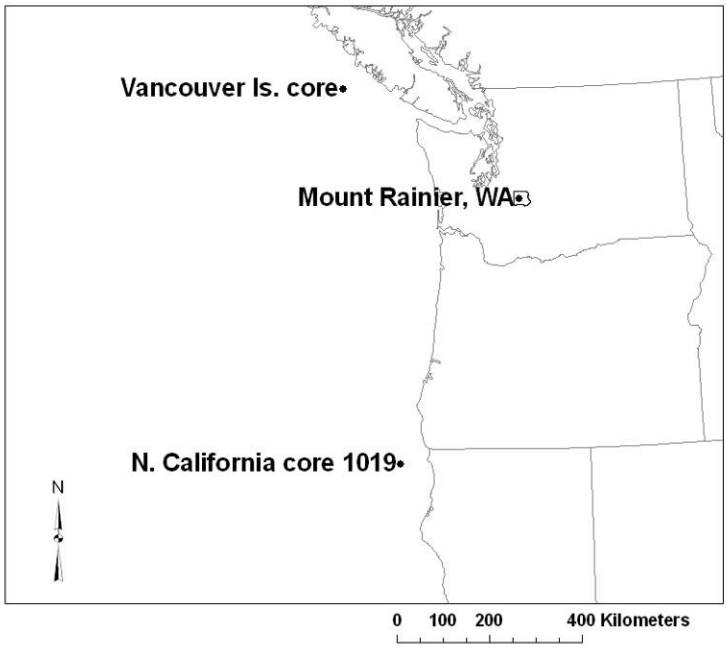

Figure 10. Locations of the Ocean Drilling Program (ODP) Site 1019 off northern California (41.682N, 124.93W, 620 km SSW from Mount Rainier, 980 m water depth) and core from southwest of Vancouver Is., British Columbia, Canada (48.911N, 126.89W, 440 km northwest of Mount Rainier, 920 m water depth).

The two SST records each have advantages and disadvantages. The northern California record is based on more proxies and it offers a higher temporal resolution than the Vancouver Island reconstruction. Most winter weather patterns approach Mount Rainier from the southwest making the northern California record perhaps more useful (Hayes and others, 2002; Miller, 2002; Mote, 2003). The coastal Vancouver Island record has a comparatively lower temporal resolution, but it is significantly closer to Mount Rainier. It also reflects climate of weather patterns approaching from the northwest.

To better compare temperature trends, I made the records coeval by correlating dates from the lower temporal resolution Vancouver Island record (within error bars) with similar trending temperatures where possible from the northern California record (average difference ±38 years, standard deviation 34 years). Dating preference was given to the northern California record because its error estimates are smaller and its SSTs are more coeval with the early Holocene GISP2 record (Figure 11). The SSTs are well correlated through the Holocene (*r=0.84, significance p<0.01*). Following the Younger Dryas, both records show dramatic warming followed by a slow cooling through the middle Holocene. The latter half of the Holocene, 4,700 cal yr. B.P. to present, is characterized by greater temperature differences and differing temperature trends between SST records.

Because it is unclear which record is more representative of Mount Rainier temperatures and despite the SST difference in the late Holocene, I simply averaged the two SST estimates to infer temperature changes at Mount Rainier. Data from the higher temporal resolution northern California record that did not have a corresponding

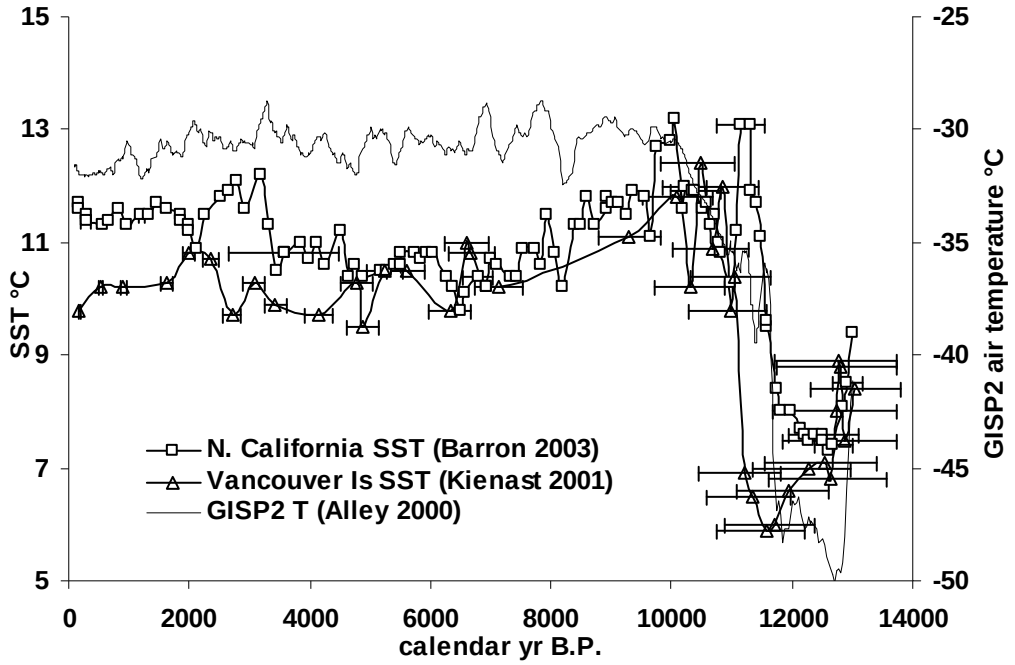

Figure 11. Sea surface temperatures (SST) and errors from Ocean Drilling Program (ODP) in the northeast Pacific Ocean 1019 core from off the coast of the Oregon-California border, and southwestern side of Vancouver Is. (*r=0.84, p=.01)*. The GISP2 ice core temperature records from central Greenland Ice Sheet. The uncertainties in the termination of the Younger Dryas in the GISP2 record (1% temporal error, 0.12% temperature error) were not plotted (Alley, 2000; Cuffey and others, 1995).

.

Vancouver Island date were eliminated from the average. Vancouver Island temperatures were visually interpolated from 8,600 to 7,940 cal yr B.P. from the GISP2 and northern California trends to capture the 8,200 cal yr. B.P. cold event that likely occurred near Vancouver Island and to add to the 1,900 year gap in the Vancouver record. The temperature anomalies of the two SST records, average SST, and GISP2 are plotted in Figure 12.

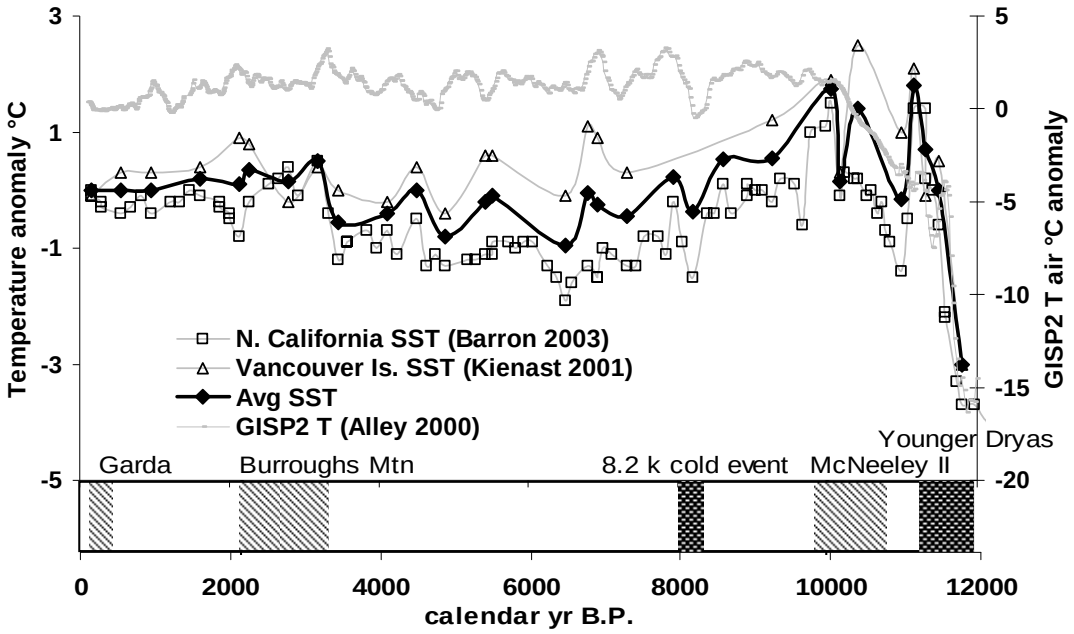

Figure 12. N. California SST, Vancouver Is. SST, and GISP2 air temperature. Corresponding SST fluctuations of the two records (within timing error estimates) were averaged (bold line). Northern Hemisphere climate reversals (dark shaded areas on lower timeline) and glacial advances (diagonal shaded areas) on Mount Rainer: McNeeley II 10,900-9,950 cal yr B.P., Burroughs Mountain 3,442-2,153 cal yr B.P., Garda 500-90 cal yr B.P. Temperatures anomalies are from most recent temperatures.

2.2 Qualitative Terrestrial Proxies for Temperature and Precipitation

Many local (<30 km radius from the summit of Mount Rainier) and regional (30-555 km radius from the summit of Mount Rainier) terrestrial qualitative proxies for temperature and precipitation are available around Mount Rainier and the greater Pacific Northwest e.g. (Burtchard, 1998; Dunwiddie, 1986; Tweiten, 2007; Whitlock and others, 2000) (Figure 13 and Table 3). Temporal resolution for the proxies ranges from 500-2,000 years. These proxies, including plant macrofossils, charcoal, pollen, and a speleothem, are only relative indicators and describe conditions as warmer, drier, colder, wetter, relative to previous times or today. For example, paleoclimatic proxies of pollen,

plant macrofossils, and charcoal, indicate colder temperatures during the McNeeley II period and thus support a glacial advance (Burtchard, 1998; Heusser, 1977). According to Burtchard's (Burtchard, 1998) proxy-based climate reconstruction for Mount Rainier, the mid-Holocene was the warmest period of the Holocene, called the Hypsithermal, a warm-dry period (~8,000 to 4,000 cal yr. B.P.) found elsewhere in the world. Fossil pollen and charcoal deposited in a lake and bog in the park support a colder and or wetter climate during the Burroughs Mountain advance (Dunwiddie, 1986; Tweiten, 2007). Burtchard's climate analysis (1998), the starting point for my re-examination, relies on pollen-based reconstructions by others (Dunwiddie, 1986; Heusser, 1977; Sea and Whitlock, 1995; Whitlock, 1992), and is the first to detail a continuous Holocene temperature record in the park (Figure 14).

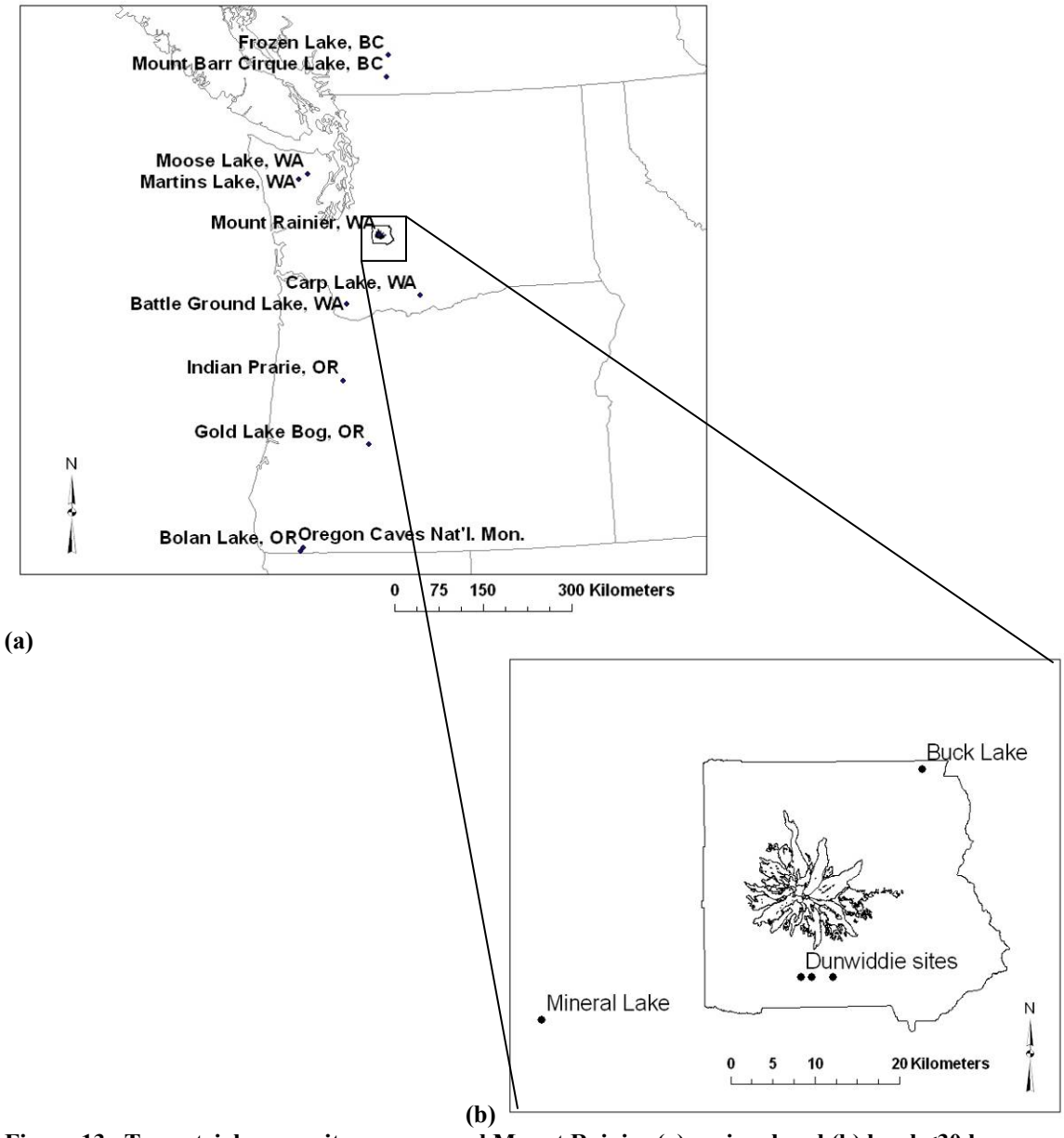

Figure 13. Terrestrial proxy site map around Mount Rainier (a) regional and (b) local <30 km radius from the summit of Mount Rainier.

Table 3. Local and regional terrestrial proxy sites. Distance is from Mount Rainier summit. Proxy key: p=pollen, m= plant macrofossils, c=charcoal, s=speleothem, multi=multi-proxy, 3= three vegetation types model.

Citation Location (# of sites)	Distance km	Elev. m	Date Range	Lat. °N	Long. °W	Proxy
Dunwiddie, 1986						
Jay Bath -Mt. Rainier	2	1,311	6,000	46°46'	121°46'	p, m, c
Log Wallow -Mt. Rainier	2	1,361	6,000	46°46'	121°45'	p, m, c
Reflection Pond 1 -Mt. Rainier	3	1,482	6,000	46°46'	121°43'	p, m, c
Tweiten, 2007						
Buck Lake, WA	13	1,700	8,000	46°59'10"	121°34'22"	p, c
Tsukada and others, 1981						
Mineral Lake, WA	30	433	Holocene	46°43'32"	122°10'18"	p, c
Heusser, 1977						
Western WA (6)	50-250		Quaternary			p
Whitlock and others, 2000						
Carp Lake, WA	125	714	125,000	45°55'	120°53'	p
Walsh and others, 2008						
Battle Ground Lake, WA	130	154	14,300	45°48'17"	122°29'37"	c
Gavin and others, 2001						
Martins Lake, WA	160	1,415	10,000	47°42'50"	123°32'25"	p, m, c
Moose Lake, WA	160	1,508	10,000	47°53'	123°21'	p, m, c
Brown and others, 2006						
Southern Vancouver, Is. (69)	260 (avg)		Holocene			p
Hallett and others 2003						
Mount Barr Cirque Lake, BC	265	1,376	11,000	49°16'	121°31'	c
Frozen Lake, BC	300	1,180	11,000	49°36'	121°28'	c
Sea and Whitlock, 1995						
Indian Prarie, OR	250	988	14,000	44°38'	122°34'30"	p
Gold Lake Bog, OR	355	1,465	14,000	43°39'	122°02'30"	p
Vacco and others, 2005						
Oregon Caves National Mon.	545	1,100	13,100	42°05'	123°25'	s
Briles and others, 2005						
Bolan Lake, OR	555	1,638	17,000	42°01'30"	123°27'30"	p, m, c
Thompson, 1993						
Pacific Northwest	n/a		18,000			multi
Bartlein, 1998						
Pacific Northwest	n/a		21,000			3

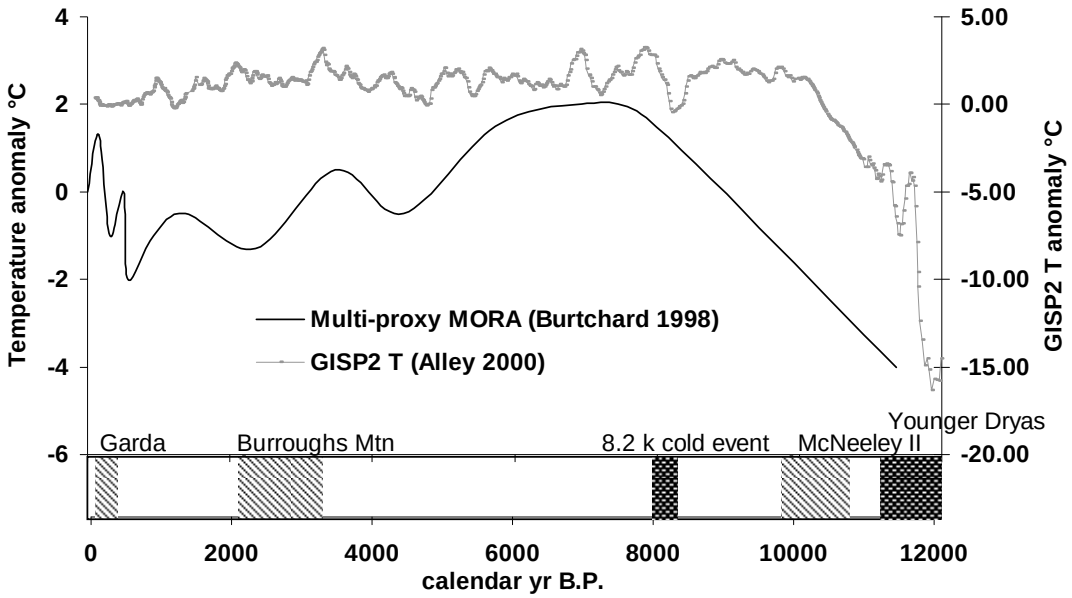

Figure 14. Multi-proxy-based temperature proxy record for Mount Rainier National Park compared to GISP2 air temperatures. Northern Hemisphere climate reversals (dark shaded areas on lower timeline) and glacial advances (diagonal shaded areas) on Mount Rainer: McNeeley II 10,900-9,950 cal yr B.P., Burroughs Mountain 3,442-2,153 cal yr B.P., Garda 500-90 cal yr B.P. Temperatures anomalies are from most recent temperatures.

To assess terrestrial qualitative proxies, I summarized their results (Table 4) and plotted quantitative values, temperature and precipitation relative to today, at 500-year rounded intervals throughout the Holocene despite generally lower temporal resolutions in the individual records. Increased precipitation is a positive value and colder temperatures are negative values (Figure 15). The magnitude of the values is +1 or -1 equating to the authors description of more (warmer) or less (colder) respectively. When the authors noted extremes such as coldest or driest, I assigned that proxy with an additional 0.5 (e.g. driest P= -1.5). All time scales converted to calendar years before present (1950 A.D.) based on Stuiver and Reimer (1993).

Table 4. Climate summaries for local and regional proxies (key: c=cool, w=warm, d=dry, m=moist, t=today's), (k= thousands of calendar years B.P.). Hemispheric cold periods are shown in gray: * Little Ice Age 50-450 years B.P., **8.2k cold event 8,000-8,200 years B.P, ***Younger Dryas 11,600-12,900 B.P. Mount Rainier glacial advances are shown: Garda, Burroughs Mountain, McNeeley II.

	Garda			Burroughs Mtn.																					McNeeley II	
Citation	*****	**1k**		**2k**		**3k**		**4k**		**5k**		**6k**		**7k**		**8k****	**9k**			**10k**		**11k**		**12k*****	
Dunwiddie, 1986	c, m	c, m	w	w	c, m	c, m	c, m	c, m	w, d	w, d	w, d	w, d	w, d	w, d												
Tweiten, 2007	d	t	t	d	w	c	c, m	c, m	w, d	w, d	w, d	c, m	c, d	c, d	c, d	w, d										
Tsukada and others, 1981										w, d	w,d	w,d	w,d	c, m	c, m	c, m	w, d	w, d	w, d	c, d	c, d	c, d	c, d	c, d	c, d	
Heusser, 1977													w	w	w	w	w			c	c	c				
Whitlock and others, 2000	m	m	m	m	m	m	m	w, d	w, d	w, d	w, d	w, d	w, d	w, d	w, d	w, d	w, d	w, d	w, d	c, m	c, m	c, m	c, m	c, m	c, m	
Walsh and others, 2008	m	d	d	m	m	m	m	m	m	d	d	d	d	d	d	d	d	d	d	d	d	d	d			
Gavin and others, 2001	m	m	m	m	m	m	m	m	m	m	w, m	c, m	c, m	c, m	c, m	c, m	c, m	w	w	w	w	w	c, d	c, d		
Brown and others, 2006	t	t	t	t	t	t	t	t	t	t	t	t	t	d	d	d	d	d	d	d	d	d	d			
Hallett and others 2003	w	w	t	d	d	w	t	d	d	t	w	w	w	w	t	t	t	t	d	d	d	d	w	w		
Sea and Whitlock, 1995	c, m	c, m	c, m	c, m	c, m	c, m	c, m	c, m	w, d	w, d	w, d	w, d	w, d	w, d	w, d	w, d	w, d	w, d	w, d	w	w	w	w	w		
Vacco and others, 2005				w	w	w	w	w										w	w	w	w	w	c	c		
Briles and others, 2005	t	t	t	t	c, m	c, m	c, m	c, m	c, m	c, m	c, m	c, m	w, d	w, d	w, d	w, d	w, d	w, d	w, d	w, d	w, d	w, d	w, m			
Thompson, 1993	c, d	c, d	c, d	c, d	c, d	c, d	c, d	c, d	c, d	c, d	c, d	d	t	t	t	t	m	d	t	t	t	t	t	c		
Bartlein, 1998												w, d										w, d				

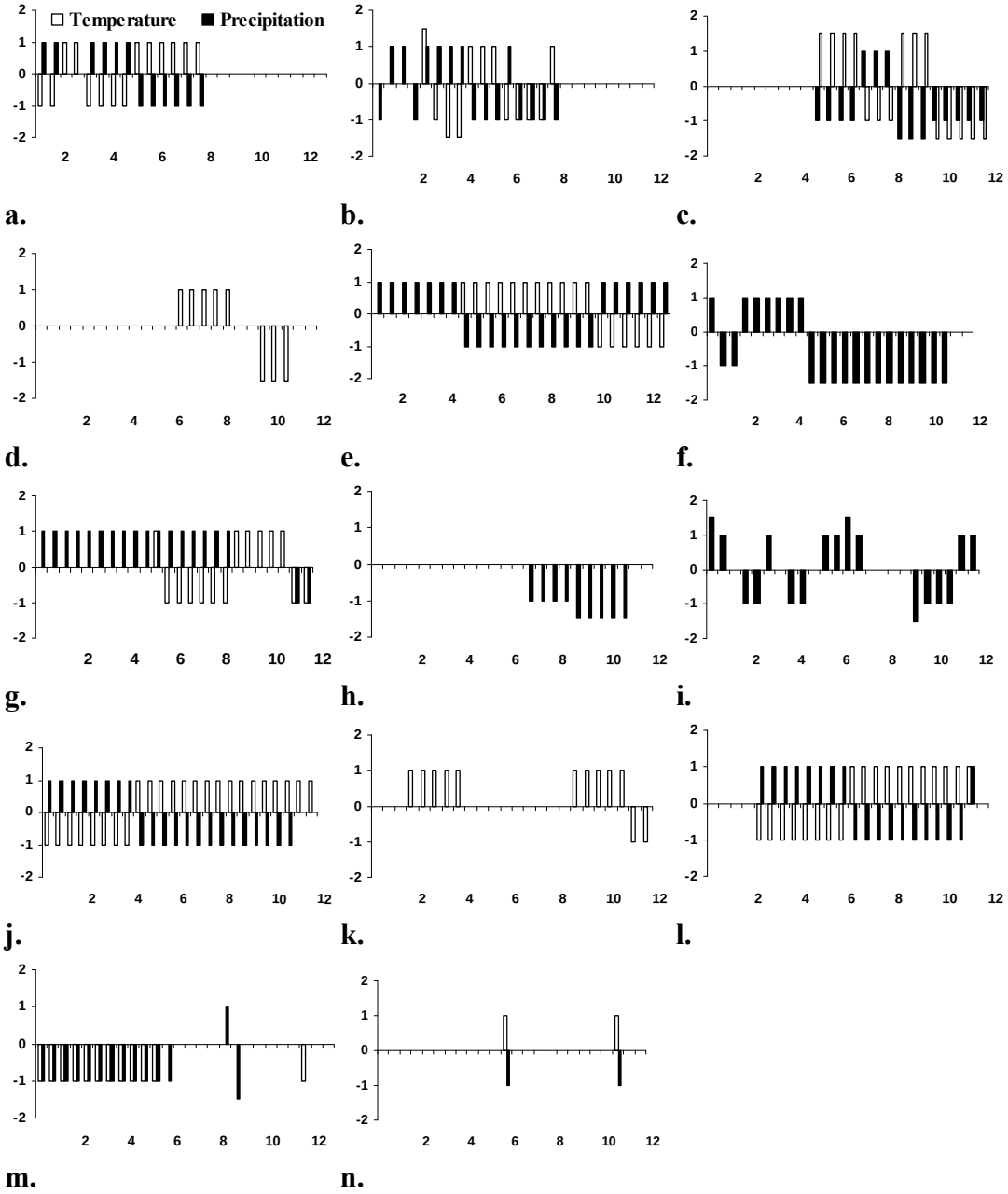

Figure 15. Temperature (hollow) and precipitation (solid) bars. Negative values depict colder and drier conditions while positive values are warmer and wetter. (a) Mount Rainier (Dunwiddie, 1986). (b) Buck Lake, Mount Rainier (Tweiten, 2007). (c) Mineral Lake, WA, (Tsukada and others, 1981). (d) Western WA (Heusser, 1977). (e) Carp Lake, WA (Whitlock and others, 2000). (f) Battleground Lake, WA (Walsh and others, 2008). (g) Olympic Peninsula, WA (Gavin and others, 2001). (h) Vancouver Is. (Brown and others, 2006). (i) Southwestern B.C. Canada (Hallett and others, 2003). (j) Central Cascade Range, OR (Sea and Whitlock, 1995). (k) Southern OR (Vacco and others, 2005). (l) Siskiyou Mountains, OR (Briles and others, 2005). (m) Western U.S. climate (Thompson and others, 1993). (n) Pacific northwest climate (Bartlein and others, 1998).

I gave each proxy equal weight and averaged all local and regional proxies to derive a broad climate signature at Mount Rainier and compared that to the average of local proxies (<30 km from Mount Rainier's summit) (Figure 16) (Table 5). The average of all proxies shows a slow warming from cold conditions 12,000 cal yr B.P. Very dry conditions start in the early Holocene 11,500 cal yr B.P. with the driest 9,000 cal yr B.P. Holocene warmth begins 9,500 cal yr B.P. peaking 9,000 cal yr B.P. Warmth continues with minimums 7,500 and 4,500 cal yr B.P. Dryness persists through the same period. Cooler and wetter conditions favoring glacier growth commence 3,500 ka and peak at 3,000 cal yr B.P. and minimize by 2,000 cal yr B.P. Renewed cool and moist conditions occur through the last millennia. The local climate proxies show similar general climate trends but with greater fluctuations than the regional proxies (Figure 16). The local proxies for precipitation and temperature compare well with regional trends (*correlation r=0.80, significance p<0.01)* (*correlation r=0.80, significance p<0.01)* respectively, indicating no significant statistical climatic anomalies near Mount Rainier. Local temperatures early in the Holocene remained cold until 10,000 cal yr. B.P. while regional temperatures were only slightly lower than current temperatures. Approximately 7,500 cal yr B.P. marked another brief cold spell near Mount Rainier that was not seen in the region on the whole. Local precipitation was drier earlier and remained drier than the region until 8,000 cal yr B.P. Local precipitation followed regional trends but tended to have greater severity through the rest of the Holocene.

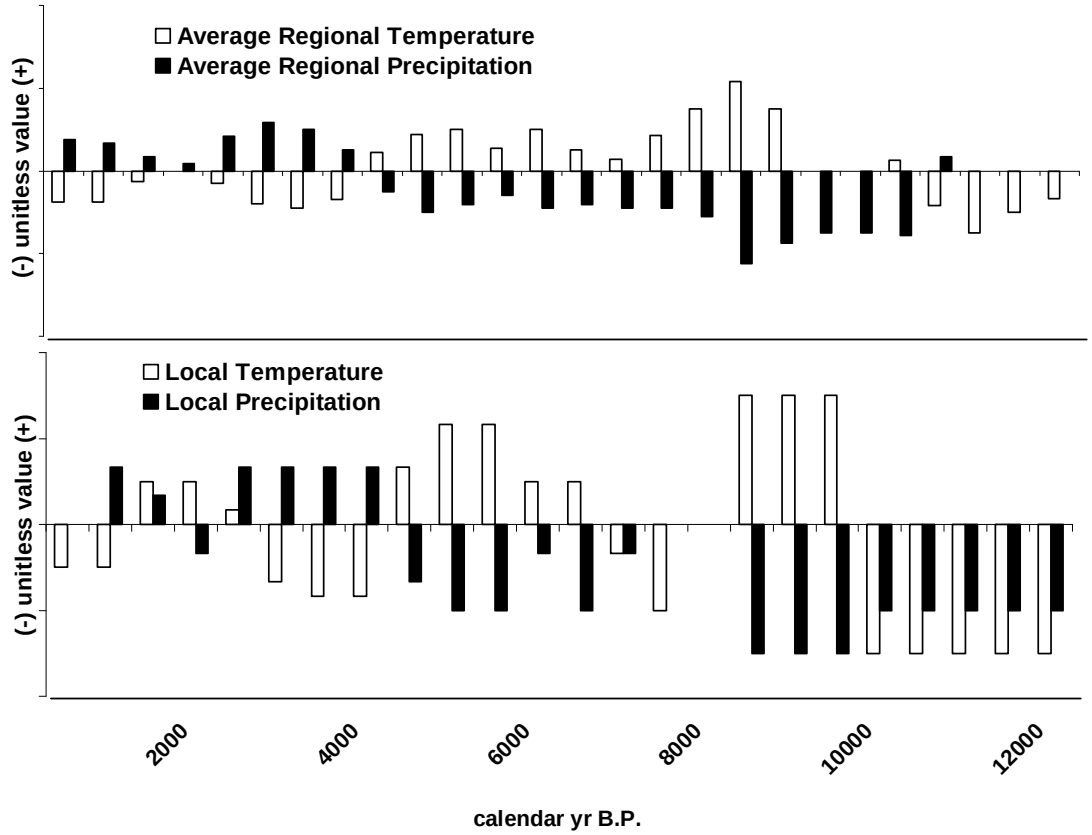

Figure 16. Averages of qualitative proxies relative to modern values. Top panel shows average of temperature and precipitation trends from all regional and local proxies, and bottom panel shows proxies local to Mount Rainier (<30 km from summit).

Table 5. Statistics for qualitative terrestrial temperature and precipitation proxies shown for all regional and local sites , and local sites (<30 km from Mount Rainier's summit, k= thousands of calendar years B.P.) . Hemispheric cold periods are shown in gray: * Little Ice Age 50-450 years B.P., **8.2k cold event 8,000-8,200 years B.P, ***Younger Dryas 11,600-12,900 B.P. Mount Rainier glacial advances are shown: Garda, Burroughs Mountain, McNeeley II. n/a= insufficient data.

	Garda		Burroughs Mtn.														McNeeley II							
	*	1k	2k		3k		4k		5k		6k		7k			8k**	9k		10k		11k		12k***	
Regional & Local																								
Average T	-0.4	-0.4	-0.1	0.0	-0.2	-0.4	-0.5	-0.4	0.2	0.4	0.5	0.3	0.5	0.3	0.1	0.4	0.8	1.1	0.8	0.0	0.0	0.1	-0.4	-0.8
Std Dev T	0.5	0.5	0.6	0.7	0.9	0.7	0.8	0.9	0.8	1.0	0.9	1.0	0.9	1.0	1.1	1.0	0.9	0.2	0.9	1.3	1.3	1.2	1.1	0.9
Average P	0.4	0.3	0.2	0.1	0.4	0.6	0.5	0.3	-0.3	-0.5	-0.4	-0.3	-0.5	-0.4	-0.5	-0.5	-0.6	-1.1	-0.9	-0.8	-0.8	-0.8	0.2	0.0
Std Dev P	0.8	0.8	0.7	0.8	0.8	0.7	0.7	0.9	0.9	0.9	1.0	1.0	1.0	1.0	0.9	0.9	1.0	0.5	0.9	0.8	0.8	0.8	1.0	1.2
Local																								
Average T	-0.5	-0.5	0.5	0.5	0.2	-0.7	-0.8	-0.8	0.7	1.2	1.2	0.5	0.5	-0.3	-1.0	0.0	1.5	1.5	1.5	-1.5	-1.5	-1.5	-1.5	-1.5
Std Dev T	0.7	0.7	0.7	0.7	1.3	0.6	0.8	0.8	0.6	0.3	0.3	1.3	1.3	1.2	0.0	1.4	n/a	n/a	n/a	n/a	n/a	n/a	n/a	n/a
Average P	0.0	0.7	0.3	-0.3	0.7	0.7	0.7	0.7	-0.7	-1.0	-1.0	-0.3	-1.0	-0.3	0.0	0.0	-1.5	-1.5	-1.5	-1.0	-1.0	-1.0	-1.0	-1.0
Std Dev P	1.0	0.6	0.6	0.6	0.6	0.6	0.6	0.6	0.6	0.0	0.0	1.2	0.0	1.2	1.4	1.4	n/a	n/a	n/a	n/a	n/a	n/a	n/a	n/a

Comparing the local terrestrial proxies to the two SSTs shows that climate was influenced by Vancouver Island SST and Northern California SST. The local terrestrial proxies show pervasive cold early in the Holocene while the SST's show considerable temperature variation (Figure 17). Comparing terrestrial and oceanic temperature trends, SSTs from N. California appear to have influenced Mount Rainier from 9,500-7,500 cal yr B.P. while the SSTs at Vancouver Island better correlated with the terrestrial during the rest of the Holocene.

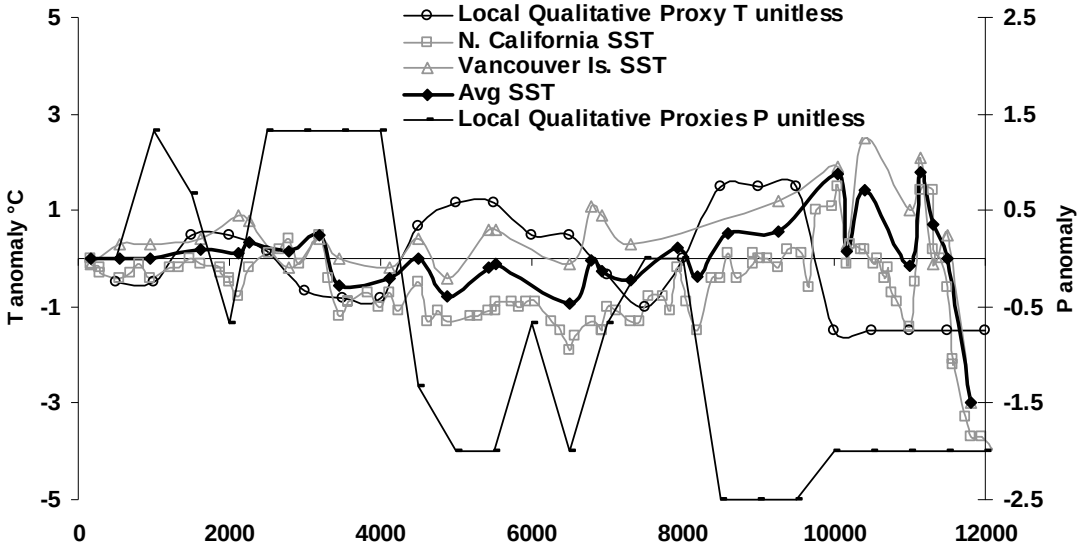

Figure 17. Local climate proxies and SST records.

2.3 Paleoclimate Summary

The final paleoclimatic data used to reconstruct glaciers through the Holocene are based on the combined regional and local qualitative precipitation proxies and average correlated SST (Figure 18). The regional proxies show a more complete and consistent climate record than the limited local proxies. I chose the SST record over the qualitative

terrestrial temperature proxies because SST trends generally represent terrestrial trends and they offer quantitative measures. I lowered the temporal resolution of the average SST to simplify paleoglacier reconstruction (Figure 18).

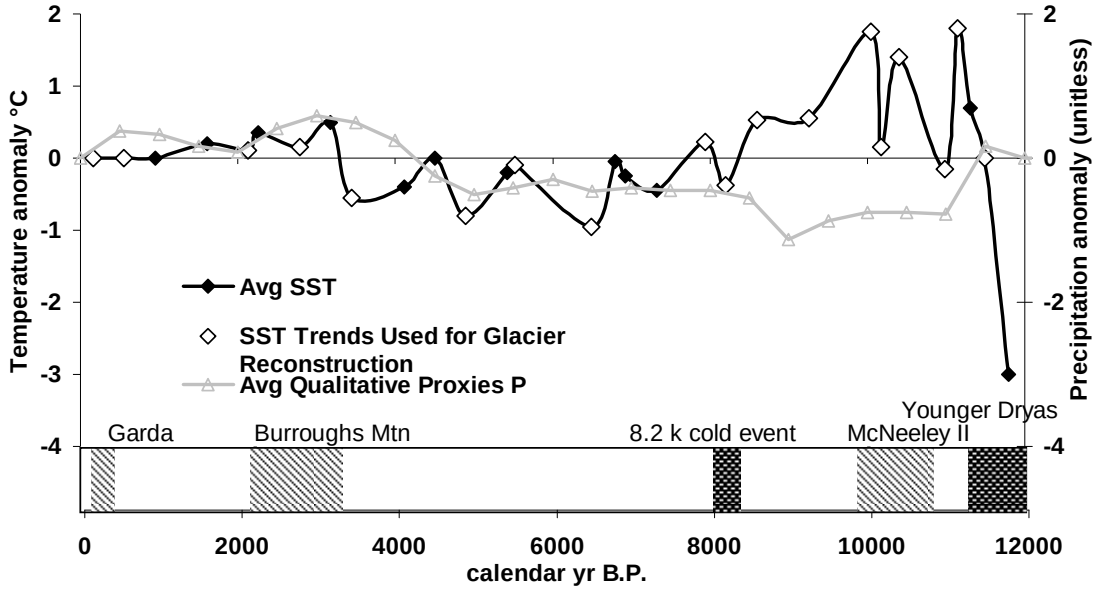

Figure 18. Holocene temperature and precipitation trends used for paleoglacier reconstruction. Northern Hemisphere climate reversals (dark shaded areas on lower timeline) and glacial advances (diagonal shaded areas) on Mount Rainer: McNeeley II 10,900-9,950 cal yr B.P., Burroughs Mountain 3,442-2,153 cal yr B.P., Garda 500-90 cal yr B.P. Temperatures anomalies are from most recent temperatures.

Based on my reconstruction, the Holocene started warm and dry, followed by cooling and increasing moisture to the mid-Holocene. Temperatures reached a minimum 6,500-3,500 cal yr. B.P. The mid-Holocene Hypsithermal (maximum warmth and dryness) is not recorded in either terrestrial temperature or SST proxies. Moist and cool conditions occurred from 4,500-3,500 cal yr. B.P. with peak Holocene precipitation occurring 3,000 cal yr. B.P. Warm temperatures began 3,000 cal yr. B.P., and late Holocene climate was moist with temperatures similar to current temperatures or slightly warmer.

3. MODERN CLIMATE AT MOUNT RAINIER

The first of two goals of this section is to correlate current SSTs to Mount Rainier's air temperatures in order to estimate paleo-air temperature at Mount Rainier from paleo-SSTs. The second goal is to assess spatial variability of snowpack around Mount Rainier which will be used to assess mass balance and glacier variation. Temperature and precipitation trends inferred from terrestrial proxies (average elevation 1,188 m) and SST, represent the climate variability at lower elevations, but to estimate the climate at higher elevations where glaciers are found, temperature and precipitation need to be adjusted. Temperatures at the Paradise Ranger Station (1,655 m elevation), Mount Rainier, are correlated with current SSTs for annual and seasonal (summer and winter) values. Summer temperatures will be used to estimate snow and ice ablation, while the winter temperatures will be used to estimate snow accumulation.

To define the relationship between paleo-SSTs and air temperatures on Mount Rainier, I chose a modern historic record for both. SSTs were obtained for a 2° cell from the gridded data set of SST's (1920-2006) (ICOADS, 2008). The cell is located about 250 km off the coast of Washington (Figure 19), is closer than the paleo-SST sites, and therefore should be the modern representation of my averaged paleo-SST. The SSTs were recorded on commercial maritime vessels and tallied monthly, an average of 680 records per month. Paradise monthly mean temperatures (1956-2006) were obtained from the Western Region Climate Center (National Weather Service coop station ID 456898, elev. 1,655 m) (WRCC, 2008).

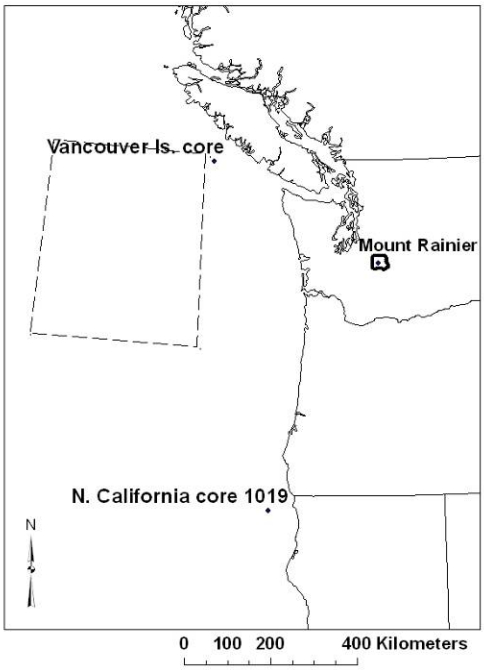

Figure 19. Subset of marine sea surface temperatures (dashed line) used to develop current SST-Paradise air temperature lapse rates (45N-49N, 127W-132W) (ICOADS, 2008). Ocean sediment cores that were used for paleo-SST are shown for comparison.

Regional warming is evident in the current marine record, but is inconclusive at the Paradise Ranger Station. Annual SST increased by 0.8°C (1920-2006) and is statistically significant *(R^2=0.19 p<0.01)*. General 20th century warming in the north Pacific Ocean has been confirmed with some limited cooling further west offshore around 40°N 150°W (Cane and others, 1997; IPCC 2007). Annual Paradise air temperatures increased by 0.6°C from 1956 to 2005 but the trend was not statistically significant *(R^2=0.06 p<0.1)* (Figure 20). However, the rate of increasing warmth is quite similar between records 0.01°C yr^{-1} for Paradise and 0.009°C yr^{-1} for the SST. The annual SST and Paradise air temperatures are significantly correlated *(R^2=0.33 p=0.01)* for years 1956-2005. Summer temperatures (May-September) and winter (October-April) correlate *(R^2=0.29 p=0.01, R^2=0.51, p=0.01)*. The season length was chosen

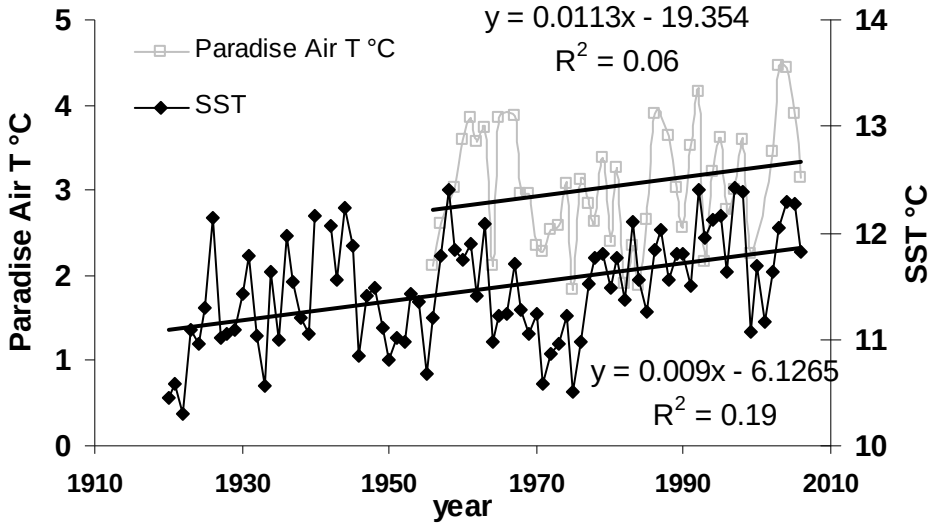

Figure 20. Paradise air temperatures (1956-2006) and annual SST (1920-2006) (ICOADS, 2008; WRCC, 2008).

based on the local ending of the ablation and accumulation seasons and the end of the water year (NWCC, 2008; Rasmussen and Wenger, 2009). I also calculated summer as June-August for later analysis using Leonard's (1989) model, which also offers correlations between average monthly SST and average monthly Paradise air temperature ($R^2=0.47$ $p=0.01$) for years 1956-2005 (Figure 21).

Air temperature lapse rates were calculated for estimating temperatures on the glaciers. Summer local air temperature lapse rate was calculated from Longmire Ranger Station (Western Region Climate Center coop station ID 454764, elevation 841 m) to Paradise (1979-2006) (Figure 2). SST-Paradise lapse rates, windward side of Mount Rainier, were compared to SST-White River Ranger Station temperature records, leeward side of Mount Rainier, (1967-1973) (coop station ID 459171, elevation 1,067 m) (WRCC, 2008). The annual, winter, and summer SST-Paradise temperature lapse rates are -5.1°C/km, -6.5°C/km, and -2.5°C/km respectively. The January and July mean lapse

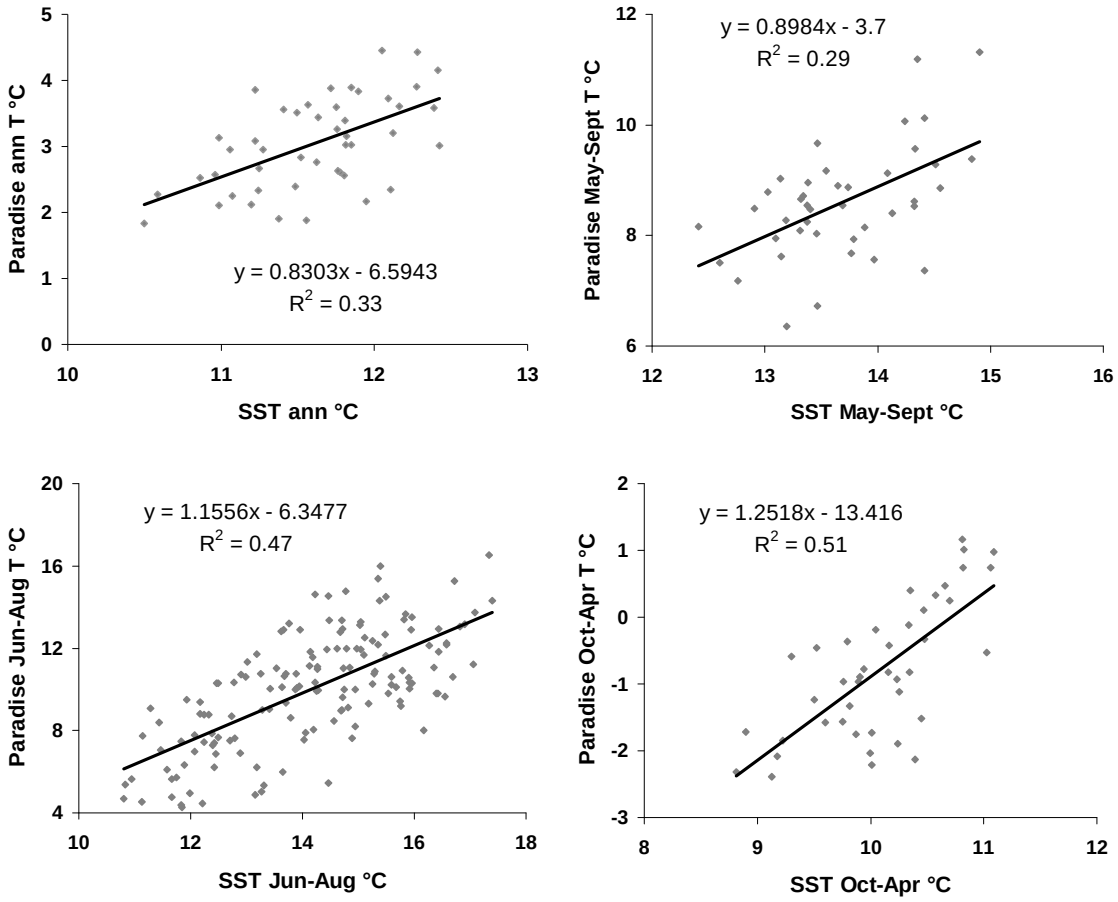

Figure 21. Relationships between annual, summer (May-September), monthly summer (June-August), and winter (October-April) Paradise air temperatures and SST.

rates are -6.7°C/km, and -2.7°C/km respectively (Greene and Klopsch, 1985). Similar lapse rates were found for the Cascade Mountains just north of Mount Rainier (Meyer, 1992). The local Longmire-Paradise annual, winter, and summer lapse rates are -4.9°C/km, -4.2°C/km, and -5.8°C/km respectively. This summer lapse rate is larger than the SST-Paradise lapse rate of -2.5°C/km (Figure 22) and is probably due to the relatively cold temperatures of the sea surface compared to warmer air temperatures at Longmire. By comparison, the winter air temperatures at altitude are much colder in winter and the Longmire air temperatures are probably close to the SST. Lapse rates around Mount

Rainier may differ due to moisture differences as leeward slopes immediately east of the Cascade Range have higher lapse rates than windward slopes (Wolfe, 1992). I presume the atmosphere is fairly well mixed around Mount Rainier so lapse rate differences may be small. Indeed, the annual SST- White River Ranger Station lapse rate showed no difference compared to SST-Paradise air temperature lapse rate.

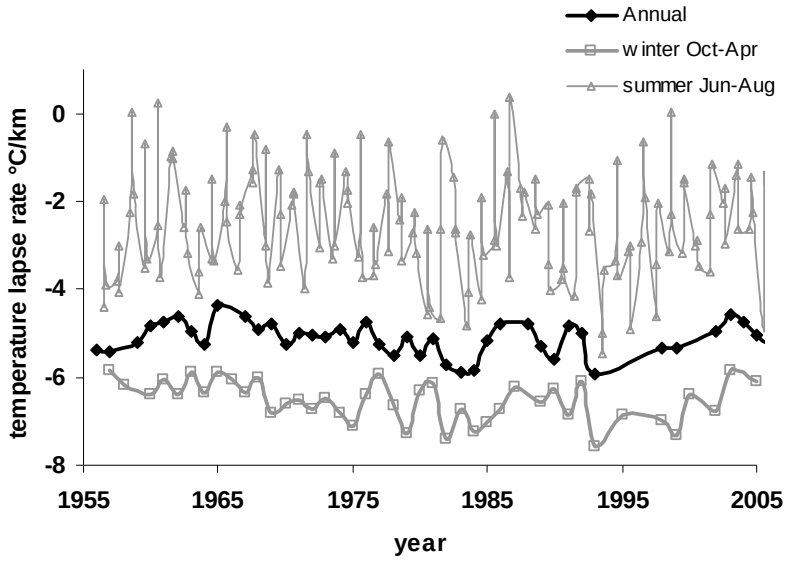

a.

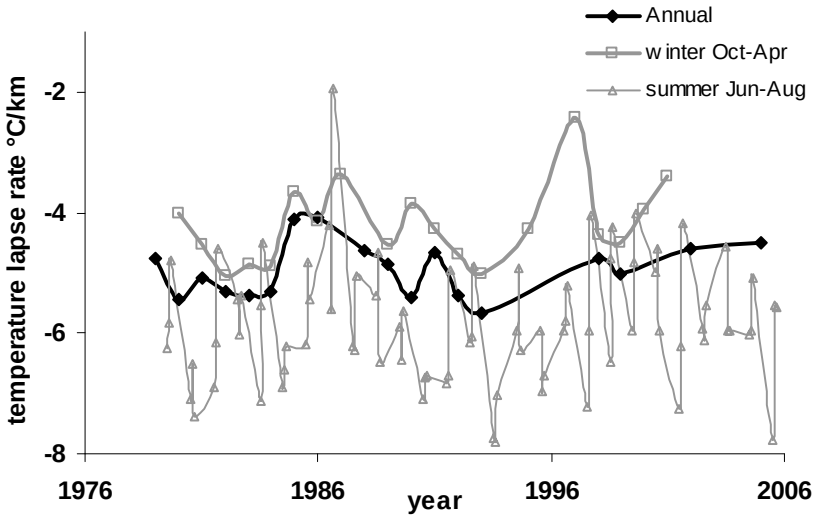

b.

Figure 22. Temperature lapse rates for a) SST- Paradise air temperature and b) Longmire-Paradise. The individual summer months of June-August are plotted. Note missing data from some years.

To estimate snow accumulation on the glaciers, I examine mass balance records from two glaciers and compare that to snowpack depths from nearby automatic weather stations, SNOTEL (NWCC, 2008), and gridded precipitation data for the region, PRISM (Daly and others, 1994; Daly and others, 2002). The SNOTEL data show broader-scale spatial variability than the mass balance record, and the PRISM precipitation data is used as a proxy for snow accumulation and fills in the data gaps of the other two records. The winter mass balance records are from the Nisqually and Emmons glaciers (2002-2007), southern and eastern aspects respectively(Rasmussen and Wenger, 2009).

Winter mass balance on the Nisqually and Emmons glaciers shows local orographic effects and spatial variability. The 2002-2007 end-of-winter mass balance for the measured sites on the Nisqually and Emmons glaciers average 2.54 m and 1.88 m respectively (Rasmussen and Wenger, 2009; Riedel, unpublished information). Winter mass balance was usually measured in May. The Nisqually Glacier average winter mass balance varied from 2.07 m weq at 1,761 m elevation to 3.4 m weq at 2,177 m elevation with sites ranging in elevation from 1,761 m to 3,382 m, 59% of the glacier's elevation range and largely below the ELA at about 3,180 m. Data above the ELA were not available as the highest site, 3,382 m, begins records in 2006. Mass balance gradients were +0.31 m/100 m weq < 2,200 m elevation and shrinks to -0.16 m/100 m >2,200 m elevation (Figure 23). This is called the diminished snow elevation (Harper and Humphrey, 2003) and is caused by wind scouring and/or a reduced water-carrying capacity of the clouds above this elevation. The Emmons Glacier winter mass balance varied from 0.81 m weq at the lowest site 1,561 m to 3.43 m weq at the highest site 3,115 m, 54% of the glacier's elevation range also largely below the ELA of 2,800 m. The

average winter mass balance gradient is +0.13 m/100 m and +0.35 m/100 m for sites above the ELA (Figure 23).

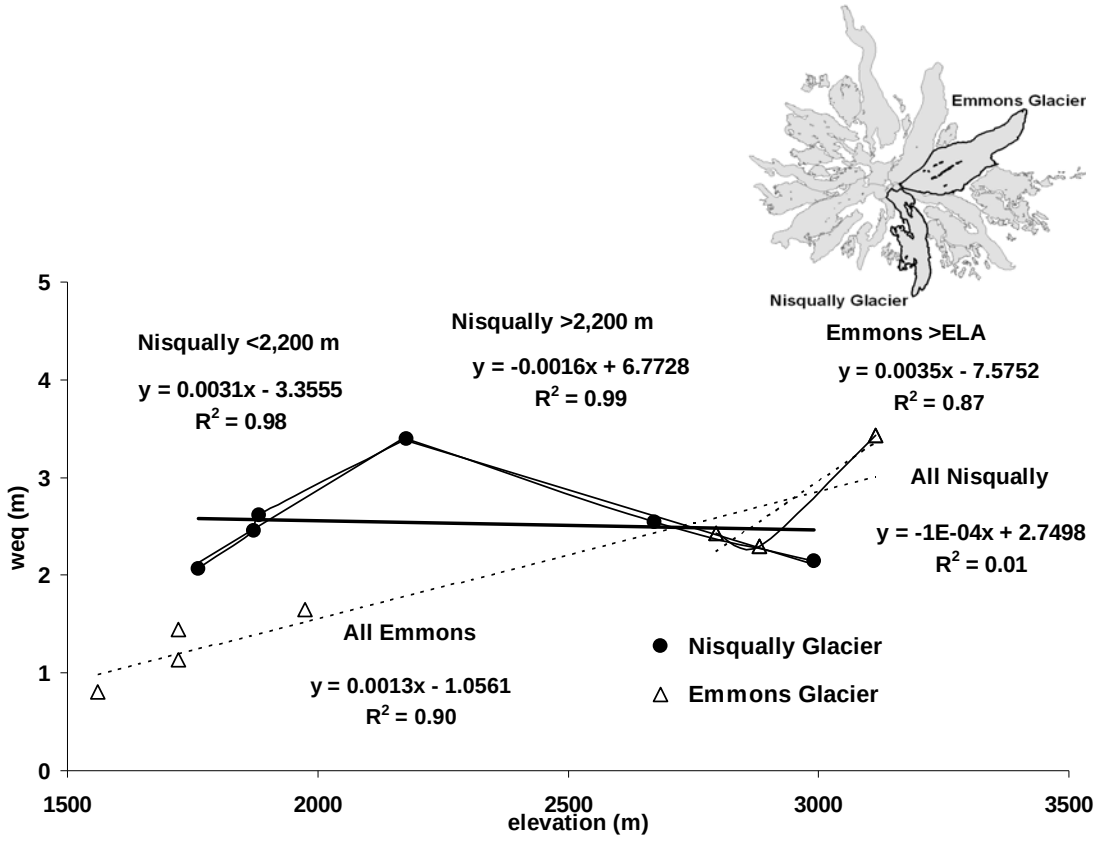

Figure 23. Snow accumulation on the Nisqually Glacier (ELA 3,180 m) and Emmons Glacier (ELA 2,800 m) 2002-2008 (Rasmussen and Wenger, 2009; Riedel, unpublished information).

To supplement the mass balance data for spatial variations, the highest monthly average snowpack data (1971-2000) from the SNOTEL sites was analyzed (Figure 24). The SNOTEL snowpack records are recorded on the first of the month and mid-month. The maximum monthly average water equivalent snowpack depths varied from 0.04 m at Mowich (960 m elevation, northwestern aspect) on March 1st to 1.9 m at Paradise (1,655 m elevation, southern aspect) on May 1st. Mowich is the lowest site and Corral Pass

(1,829 m elevation, northeast aspect) the highest. Paradise has the largest snowpack (weq) despite being at an elevation lower than other stations (Table 6). This may be explained by storms that generally arrive from southerly or westerly directions off the Pacific Ocean (Miller, 2002; Mote, 2003).

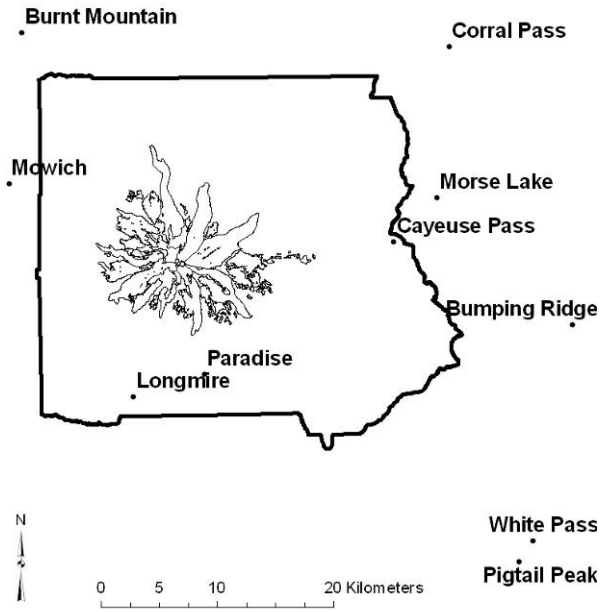

Figure 24. **Locations of SNOTEL sites in and around Mount Rainier National Park (boundary shown). Longmire Ranger Station is also shown for reference.**

Table 6. Maximum monthly average annual SNOTEL snowpack data for stations around Mount Rainier (1971-2000) (NWCC, 2008).

SNOTEL Sites	Aspect	Lat °N	Long °W	weq snowpack (m)	Elev (m)
Mowich	WNW	46.92	121.95	0.04	960
Burnt Mountain	NW	47.03	121.93	0.38	1,280
White Pass (east)	SE	46.63	121.37	0.61	1,372
Corral Pass	NE	47.02	121.45	0.91	1,829
Bumping Ridge	E	46.80	121.32	0.73	1,402
Pigtail Peak	SE	46.62	121.38	1.40	1,799
Cayeuse Pass*	ENE	46.87	121.52	1.40	1,598
Morse Lake	ENE	46.90	121.47	1.46	1,646
Paradise	S	46.77	121.73	1.90	1,560

* estimates based on 3/31/2008 snowpack

The four aspects of the mountain have differing snowpack accumulation-elevation gradients up to the elevation limit of the data, 1,829 m. Snow accumulation gradients for all sites are 16 cm/100 m, and separating the three sites west of Mount Rainier that are on the windward side of the mountain, 31 cm/100 m: Burnt Mountain, Mowich, and Paradise (Figure 25). The three westernmost sites have a similar snowpack accumulation gradient as the Nisqually Glacier mass balance sites below 2,200 m, 31 cm/100 m. The eastern sites (Corral Pass, Morse Lake, Cayeuse Pass, Bumping Ridge, White Pass, and Pigtail Peak,) record the rain-shadow effects of sites east of Mount Rainier, 12 cm/100 m. Northern and southern aspects were also analyzed, but the west-east aspects offer a distinct comparison evident on the gridded precipitation and elevation maps (Table 7) (Figure 26).

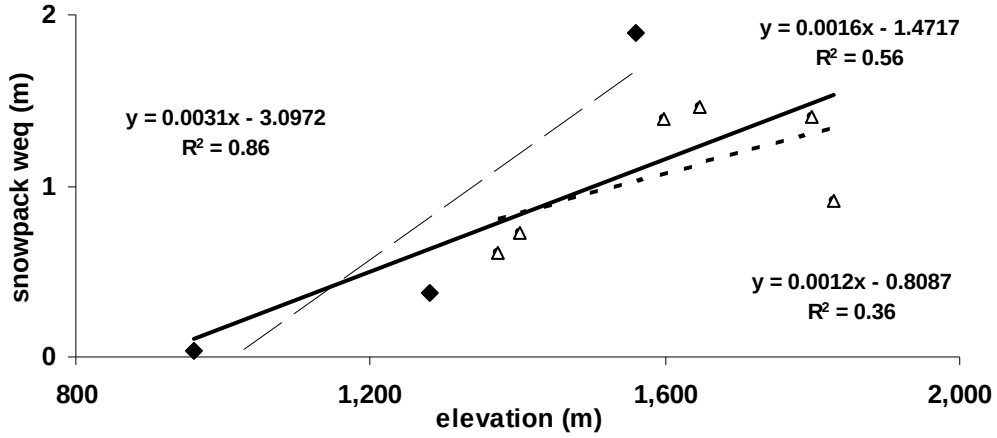

Figure 25. Snow accumulation versus elevation for all SNOTEL sites around Mount Rainier, 0.16 m/100 m (bold line, diamonds and triangles); the three western sites: Paradise, Burnt Mountain, Mowich 0.31m/100 m (dashed line and large diamond markers); the six eastern sites: Corral Pass, Morse Lake, Cayeuse Pass, Bumping Ridge, White Pass, and Pigtail Peak, 0.12 m/100 m

Table 7. Snow accumulation versus elevation for all aspects of Mount Rainier.

aspect	# of sites	accumulation-elevation cm/ 100m	R^2	*significance p*
all	9	16	0.56	0.05
western	3	31	0.86	NS
eastern	6	12	0.36	NS
northern	5	15	0.66	0.1
southern	4	20	0.42	NS

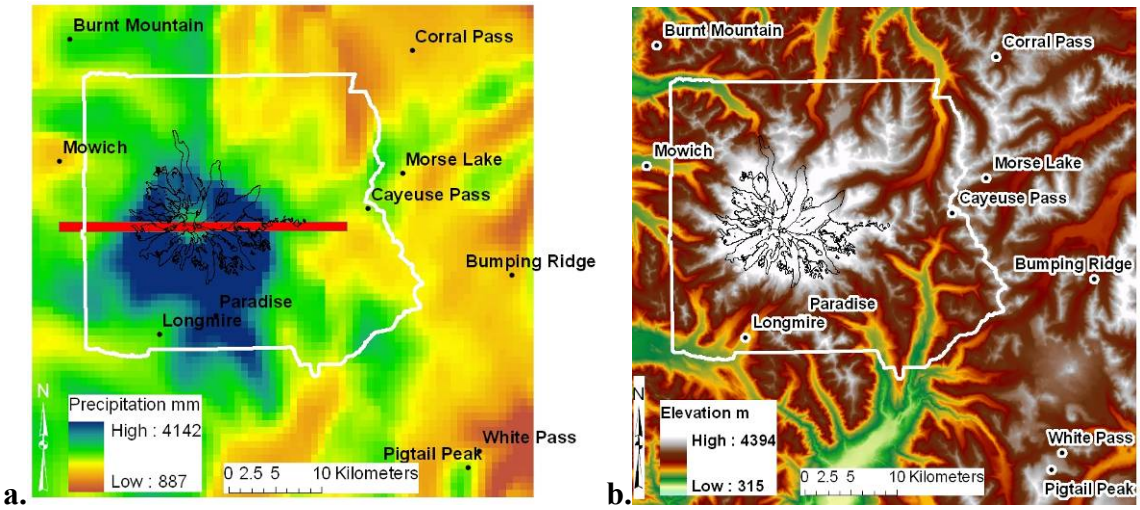

Figure 26. Mount Rainier National Park (boundary shown) and SNOTEL sites. Longmire Ranger Station is also shown for reference. a. PRISM precipitation data (1971-2000) (Daly and others, 1994). The highest precipitation falls on the south side of the mountain and dissipates high on the mountain. The red bar represents a west-to-east transect of precipitation in the next figure b. The topographic area encompassing the SNOTEL sites.

To further supplement the mass balance data that covers parts of Nisqually and Emmons glaciers, I assess the degree to which the mass balance data and the SNOTEL snowpack data represent modeled spatial trends of mass balance and snowpack conditions on the rest of Mount Rainier. Since winter mass balance is a function of precipitation, I compare gridded precipitation values, PRISM, (and its inferred snowfall) against winter mass balance data for Nisqually and Emmons glaciers and SNOTEL precipitation records. Annual precipitation values (1971-2000) were estimated for cells

800 m by 800 m (PRISM, 2007; Daly and others, 1994). The highest amount of precipitation falls on the southern slopes of Mount Rainier around Paradise Station and can be compared to the recent Paradise precipitation record (2002-2007 N=5, average 2.94 m weq) (WRCC, 2008). Also PRISM precipitation decreases on the mountain starting at an elevation of about 2,070 m for the Nisqually Glacier and 2,270 m for the Emmons Glacier (Figure 27 and Figure 28).

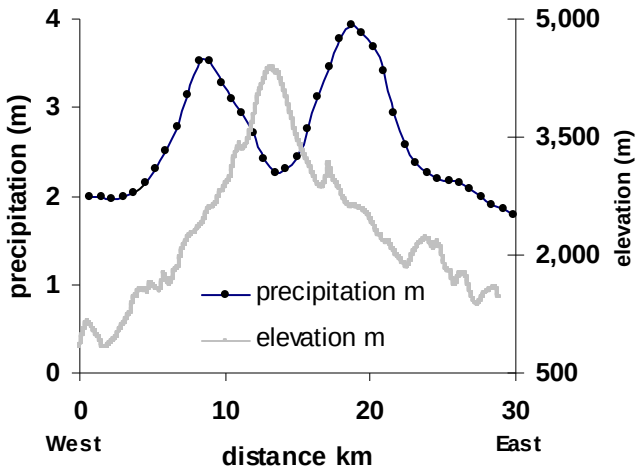

Figure 27. West-to-east transect of PRISM precipitation shown in red in the previous figure.

The general precipitation patterns depicted by PRISM are useful for visualizing spatial variations but are less useful for predicting winter mass balance. PRISM precipitation is a reasonable predictor of winter mass balance on the Nisqually Glacier, but is not useful for estimating winter mass balance on Emmons Glacier (Figure 28). PRISM data closely matches Paradise SNOTEL precipitation overall but overestimates the low elevation sites (Table 8). A good correspondence is expected because PRISM is partly based on SNOTEL (Daly and others, 2002).

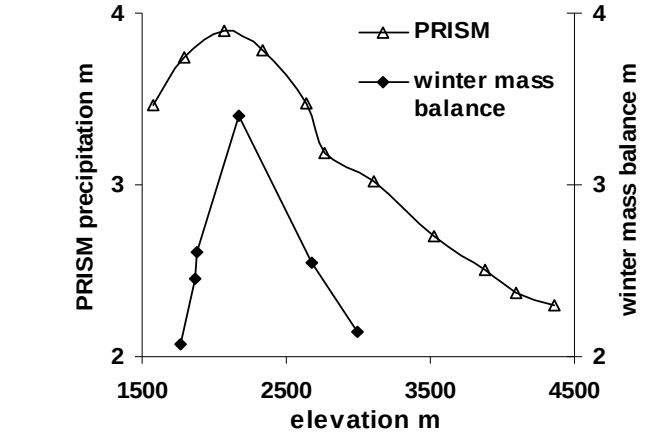

a.

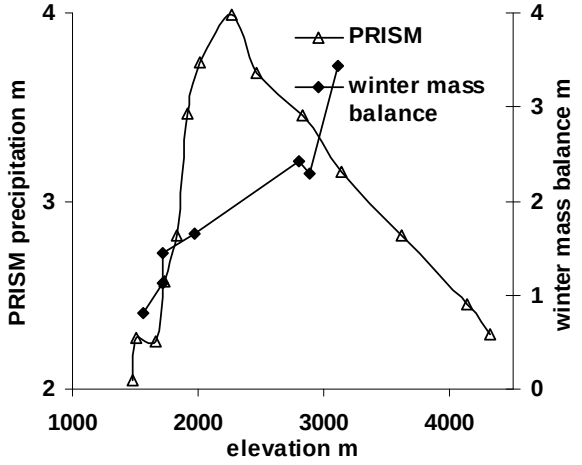

b.

Figure 28. PRISM precipitation (1971-2000) versus winter mass balance (2002-2007) for (a) Nisqually Glacier and (b) Emmons Glacier.

Table 8. Average annual precipitation comparing SNOTEL and PRISM (1971-2000).

SNOTEL Sites	Elev (m)	Yearly max. weq SNOTEL snowpack (m)	SNOTEL precip record years	SNOTEL precip (m)	PRISM precip (m)	Precip difference %
Mowich	960	0.04	99-07	1.37	1.59	16%
Burnt Mountain	1,280	0.38	00-07	1.84	2.07	12%
White Pass (east)	1,372	0.61	81-07	1.11	1.49	34%
Corral Pass 1940-2006	1,829	0.91	82-97	1.55	1.58	2%
Bumping Ridge	1,402	0.73	79-07	2.90	3.03	5%
Pigtail Peak	1,799	1.40	82-07	2.35	1.95	-17%
Cayeuse Pass*	1,598	1.40	2007	2.04	1.92	-6%
Morse Lake	1,646	1.46	79-07	2.01	1.88	-6%
Paradise	1,560	1.90	81-07	1.59	1.56	-2%
	Totals	8.83		16.74	17.05	38%
					Weighted difference	2%

* estimates based on 3/31/2008 snowpack

To investigate whether air temperature has an influence on snow weq, SSTs and historical snowpack at the Paradise SNOTEL were compared. Summer mass balance on Mount Rainier is roughly correlated to SST (Rasmussen and Wenger, 2009). A correlation exists between winter SST (October-April) and maximum annual weq snowpack at Paradise (1941-2000) *(R^2=0.36 $p<0.01$)*. Annual calendar year SSTs are less useful in predicting the maximum annual weq snowpack at Paradise (1942-2000) *(R^2=0.14 $p<0.01$)*, but adjusting to the annual hydrologic year (October-September) provides better results (1943-2000) *(R^2=0.20 $p<0.01$)* (Figure 29).

In summary, SSTs are a reasonable indication of air temperatures at Paradise. To represent spatial variability of mass balance I divide Mount Rainier in half and choose the mass balance data from the Nisqually and Emmons glaciers to represent the mass balance trends on the southern and northern halves of Mount Rainier respectively. SNOTEL is useful for assessing broader spatial variability around Mount Rainier, but there are an insufficient number of SNOTEL sites to capture snowpack patterns (and thus model winter mass balance) high on the mountain near glaciers. The PRISM precipitation data offer useful illustrations of spatial variability, but poorly models the Emmons Glacier winter mass balance and thus is not used for modeling mass balance. I choose historical SSTs the annual temperature relationship for modeling climate.

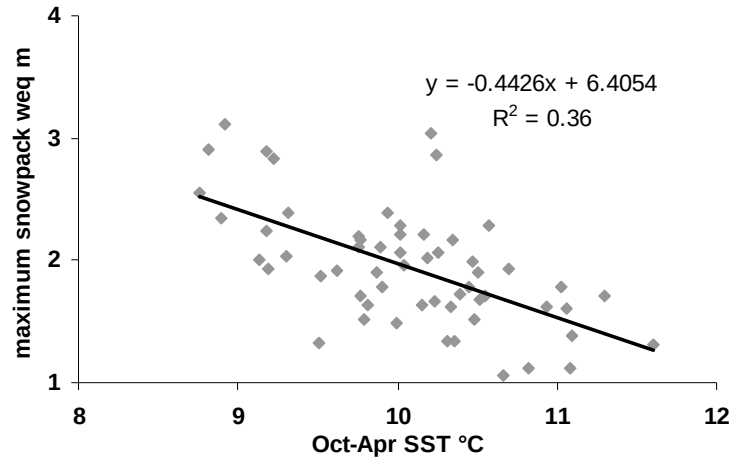

a.

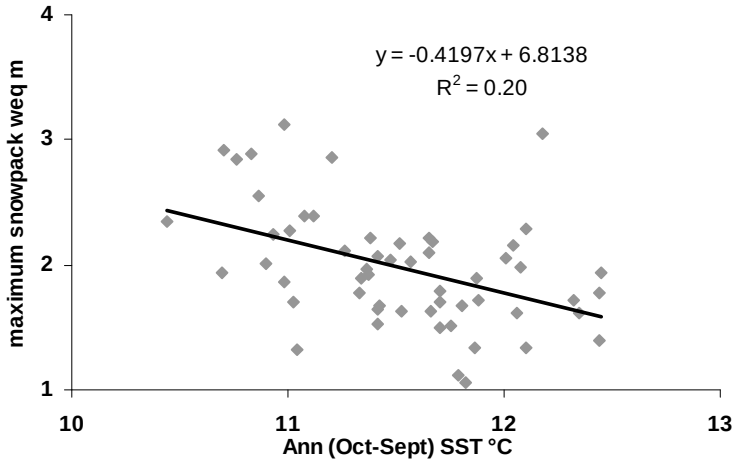

b.

Figure 29. Maximum weq snowpack at the Paradise SNOTEL versus SST (a) Winter (October-April) SST and (1941-2000) and (b) annual hydrologic year (October-September) (1943-2000).

4. RECONSTRUCTION OF PALEOGLACIERS

The goal of this chapter is to define the relation between current climate and the equilibrium line altitude of the glaciers on Mount Rainier, which defines glacial extent. Using the paleoclimatic variations of temperature and precipitation defined for Mount Rainier in Chapter 2, paleo-equilibrium lines are estimated and glacial extents through the Holocene are reconstructed.

The ELA is the elevation on the glacier at which the annual mass change is zero (Paterson, 1994). Above the ELA the glacier accumulates snow and is the mass recharge zone. Below the ELA the glacier ablates more than it gains through snow and is the mass discharge zone. The mass gained in the accumulation zone equals the mass lost in the ablation zone for a given time period, usually 1-5 years. The ELA is a climatically controlled variable as glacier motion plays no role. One can use the accumulation-area ratio (AAR), the ratio of accumulation zone area to total glacier, about 0.65 for alpine glaciers (Meier and Post, 1962), to estimate the ELA. This simple approach was applied to estimate past ELAs from past glacier extents in the Brooks Range, Alaska, (Balascio and others, 2005), and to the Colorado Rocky Mountains (Brugger and Goldstein, 1999; Leonard, 1989). Alternatively, the balance ratio method relies on hypsometric (area per elevation) bins and the ratio of the mass balance gradient in the accumulation zone to the ablation zone to reconstruct ELA (Benn and Gemmell, 1997; Furnbish and Andrews, 1984). The ratio (ablation gradient/accumulation gradient) averages 2:1 for temperate glaciers (Furnbish and Andrews, 1984). This latter method is particularly well suited for glaciers with complex area distributions.

Winter precipitation and summer temperature have varying influence on glacial mass balance depending on climate (Anderson and Mackintosh, 2006; Bitz and Battisti, 1999; Tangborn, 1980). In maritime conditions, like in western Washington, glacier mass balance in the Cascade Range is predominantly controlled by variations in winter precipitation (McCabe and Fountain, 1995), whereas continental glaciers are most affected by summer air temperature (Letreguilly, 1988; Pelto, 1989). Air temperature is an important an index of summer melt and mass loss (Anderson and Mackintosh, 2006; Tangborn, 1980). Leonard (1989) developed a relation between summer mean air temperatures and maximum winter water equivalent (weq) snowpack, deepest average water equivalent snowpack, at the ELA for glaciers in equilibrium.

At Mount Rainier, the ELA and mass balance for the Nisqually and Emmons glaciers were compared for years 2002-2007 (Rasmussen and Wenger, 2009; Riedel, unpublished information) (Figure 30). The Emmons Glacier, northeast facing, has a

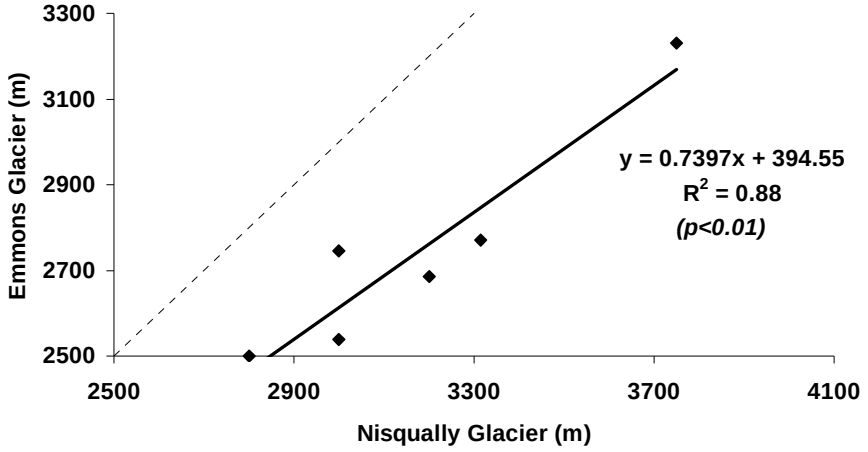

Figure 30. The relation between equilibrium line altitudes for Emmons and Nisqually glaciers. Dashed line represents 1:1 ratio.

lower average ELA (2,745 m) compared with the south-facing Nisqually Glacier (3,180 m). The 435 m difference in ELA represents spatial differences of climate including, differences in snow accumulation and solar radiation.

Mass balance gradients below and above the ELA are important for the balance ratio method (Furnbish and Andrews, 1984) and for use in numerical models of glacial extent (Harper and Humphrey, 2003). As mentioned, only one of the Nisqually Glacier measurements was above the average ELA, and only three on Emmons are measured above the average ELA. Since Nisqually data above the ELA are missing, and Emmons data below the ELA are anomalous (Figure 31), resulting in an ablation/accumulation ratio of -1.8:1, I derived a more reasonable value, the average overall ablation/average

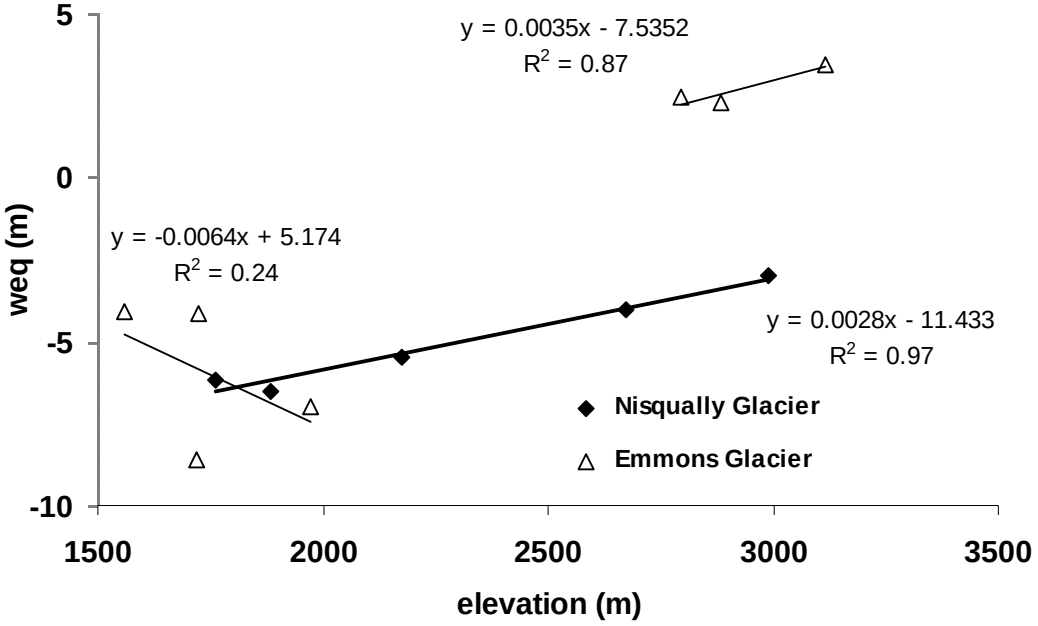

Figure 31. Accumulation above the ELA for Emmons and ablation below the ELA for Emmons and Nisqually. Data is not available for Nisqually accumulation data above the ELA.

overall accumulation (Emmons=2.3:1, Nisqually=1.8:1), close to the expected temperate glacier ratio of 2:1 (Table 9). The winter Nisqually Glacier accumulation gradient in the ablation zone is -1 cm /100 m elevation, compared to the Emmons Glacier over all stakes is 13 cm/100 m. The end-of-summer Nisqually Glacier ablation gradient is -26 cm/100 m similar to the Emmons of -29 cm/100 m (Figure 32).

Table 9. Ablation 2002-2007 and accumulation 2002-2008 data for Nisqually and Emmons glaciers (Rasmussen and Wenger, 2009; Riedel, unpublished information).

Nisqually elevation (m)	ablation (m)	accumulation (m)	Emmons elevation (m)	ablation (m)	accumulation (m)
3,382	2.39		3,115	1.71	3.43
2,991	3.00	2.14	2,882	2.51	2.30
2,673	4.05	2.55	2,794	2.20	2.43
2,177	5.47	3.40	1,974	7.01	1.65
1,883	6.51	2.61	1,721	8.61	1.44
1,872	4.13	2.45	1,722	4.16	1.13
1,761	6.16	2.07	1,561	4.12	0.81
average	4.53	2.54		4.33	1.88
ablation/accumulation		**1.79**			**2.30**

To compare the current glacial environment on Mount Rainier to the range of glacier environments for glaciers in equilibrium (Leonard, 1989), I plotted the maximum average yearly winter water equivalent snowpack and average summer temperatures at the ELA. Snowpack at the ELA for the Nisqually Glacier was extrapolated from the accumulation gradient above 2,200 m in Figure 23. The trend above 2,200 m was chosen over the overall accumulation (Figure 32) because the declining trend over 2,200 m better represents the highest site (2,991 m). Presumably, Nisqually would plot higher and further right with greater snowpack and higher temperatures if the ELA was around 2,200 m. For Emmons Glacier, the snowpack was extrapolated from the accumulation gradient

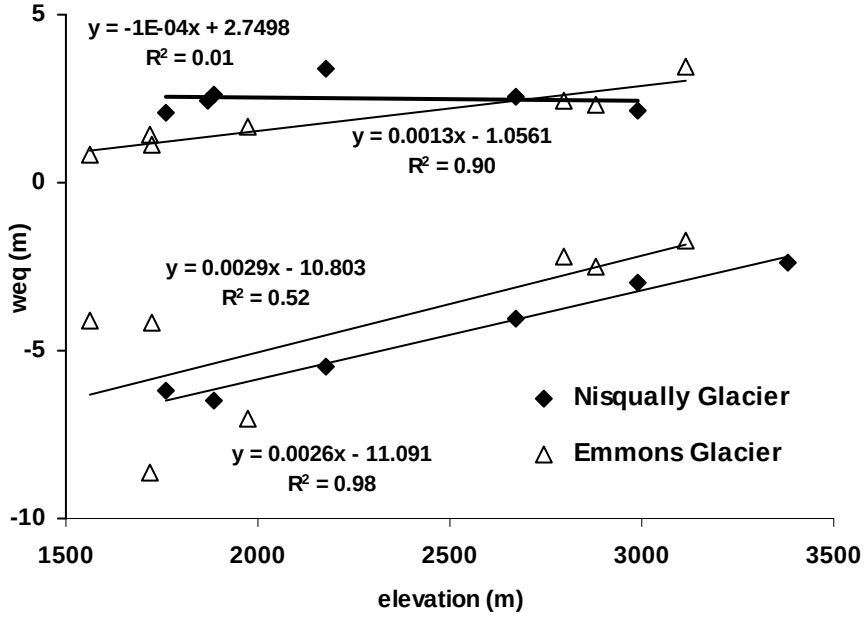

Figure 32. Nisqually Glacier (average ELA 3,180 m) and Emmons Glacier (average ELA 2,745 m) accumulation (2002-2008) ablation (2002-2007) data. The Nisqually Glacier stake at 3,382 m, above the ELA is for ablation only.

(13 cm/100 m) in Figure 32. Summer temperature data at the ELA for the Nisqually and Emmons glaciers were extrapolated from Paradise Station using the lapse rate defined by the Longmire-Paradise comparison. The estimated summer temperatures and maximum snowpack are 2.2°C, 214 cm weq at Nisqually Glacier and 4.8°C, 251 cm weq at Emmons Glacier respectively (Figure 33).

The values of winter accumulation and summer air temperature places Emmons within and Nisqually just outside the envelope defined by glaciers worldwide (Figure 33). Indeed, Emmons has been relatively stable 1971-1993 whereas Nisqually has been retreating (Nylen, 2001). However, that Nisqually plots to the left of the envelop, that is, in colder, snowier climate than equilibrium conditions is odd, because it suggests that under these conditions of more snow and colder temperatures the glacier should be

advancing. While it could be just an outlier as a few other points indicate, it may be the effective summer temperatures (solar radiation) are underestimated because of its southern exposure.

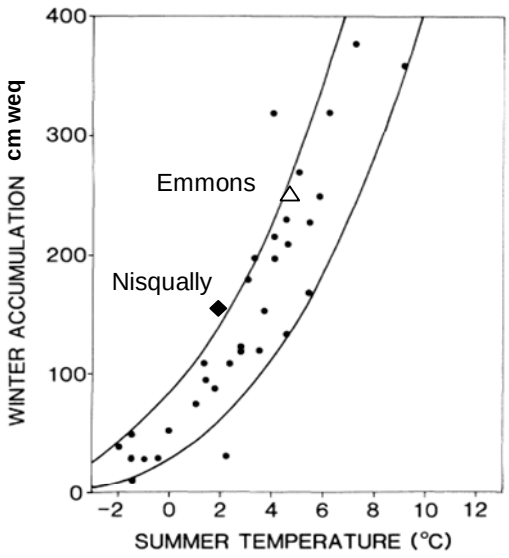

Figure 33. Current maximum snowpack and summer temperature (JJA) at the ELAs for Emmons and Nisqually glaciers compared with the climate envelope in which 32 worldwide glaciers have fallen (Leonard, 1989).

4.1 Glaciologically Reconstructed Climate

I reconstructed climate at the paleo-ELAs on the Nisqually and Emmons glaciers during the McNeeley II, Burroughs Mountain, and Garda advances. First since the ELAs of the Nisqually and Emmons glaciers are not separately reconstructed for the three advances but reconstructed uniformly on the mountain, I used their current elevation relationship to represent their elevation relationship in prior advances. Second, I define the current climate at the paleo-ELAs compared to that at the current ELAs addressed in

the previous section. We assume that snow and temperature lapse rates were constant throughout the Holocene.

The ELAs of the Nisqually and Emmons glaciers are based on the current ELA relationship as shown previously in Figure 30 which shows lower Emmons Glacier ELAs than for Nisqually Glacier. To remain within the elevation ranges specified by Burbank (1981) for Garda (1,943 ± 63 m) and Heine (1998) for McNeeley II (1,815 ±105 m), I established the Emmons Glacier ELA as the average ELA of McNeeley II (1,815 m) and the lowest end of the elevation range for Garda (1,880 m), and calculated the Nisqually ELAs. Although ELAs for the Burroughs Mountain advance have not been previously estimated, moraine extents are similar to Garda moraines (Crandell and Miller, 1974) suggesting a similar ELA of about 1,943 m (Table 10).

Table 10. Comparison of Holocene ELAs.

	current (m)	Garda /Burroughs Mtn (m)	difference Garda-current (m)	McNeeley II (m)	difference McNeeley II-current (m)
Nisqually ELA	3,180	2,008	-1,172	1,920	-1,260
Emmons ELA	2,745	1,880	-865	1,815	-930

To calculate climate at paleo-ELAs on the Nisqually Glacier, I computed an overall accumulation gradient for the western SNOTEL sites and Nisqually accumulation stakes (12 cm/100 m) *(R^2=0.48 $p<0.05$)* (Figure 34). The extrapolated snow accumulation rate on the Nisqually Glacier is negative (-16 cm/100 m) (Figure 23) at the current ELA (3,180 m), positive below 2,200 m (31 cm/100m), and accumulation would be higher at the Garda ELA (2,008 m). No adjustments were made to Emmons Glacier

snow accumulation rate (13 cm/100 m) since the trend is positive, linear, and is similar to the eastern SNOTEL sites (12 cm/100 m).

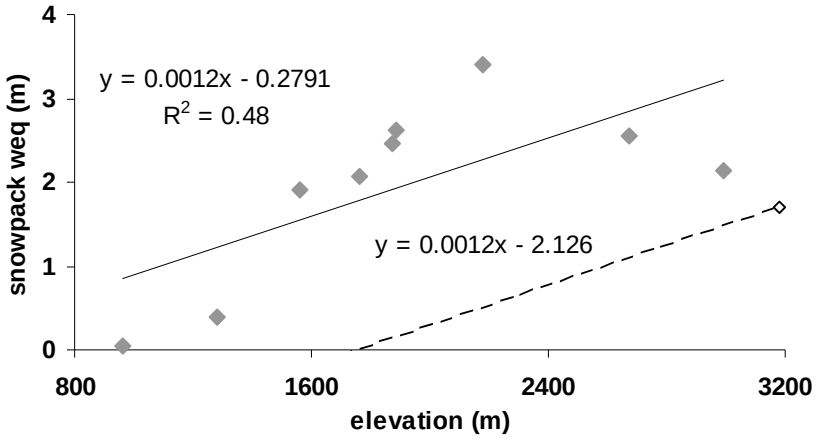

Figure 34. Snow depth from Mowich, Burnt Mountain, and Paradise SNOTEL stations and snow accumulation on the Nisqually Glacier. Dashed line indicates adjusted trend from the current ELA (3,180 m) used to compute relative climate changes.

Following Leonard (1989) I used temperature and snow accumulation lapse rates to infer differences in summer air temperature and winter precipitation at the paleo-ELAs. Compared to today, climate adjustments necessary to produce the Garda, Burroughs Mountain, and McNeeley II extents are notable. Minimum summer temperatures depressions and increased snowpack for the Garda/Burroughs Mountain and McNeeley II advances on the Nisqually Glacier are -4.7°C +94 cm weq, and -5.2°C +104 cm weq respectively (Table 11) (Figure 35). For Emmons Glacier, minimum summer temperatures depressions and increased snowpack for the Garda/Burroughs Mountain and McNeeley II advances are -3.6°C +74 cm weq, and -4.0°C +83 cm weq respectively.

Table 11. Former estimated differences in climate at the ELAs relative to current conditions.

	Garda & Burroughs Mountain			McNeeley II		
	ΔT only	Δ weq accumulation only	ΔT Δ weq accumulation	ΔT only	Δ weq accumulation only	ΔT Δ weq accumulation
Nisqually Glacier	-9.0°C	+310cm	-4.7°C, +94cm, -6.8°C, +141cm	-10.6°C	351cm	-5.2°C, +104cm, -7.3°C, +151cm
Emmons Glacier	-5.4°C	+278cm	-3.6°C, +74cm, -5.4°C, +112cm	-6.0°C	316cm	-4.0°C, +83cm, -5.8°C, +121cm

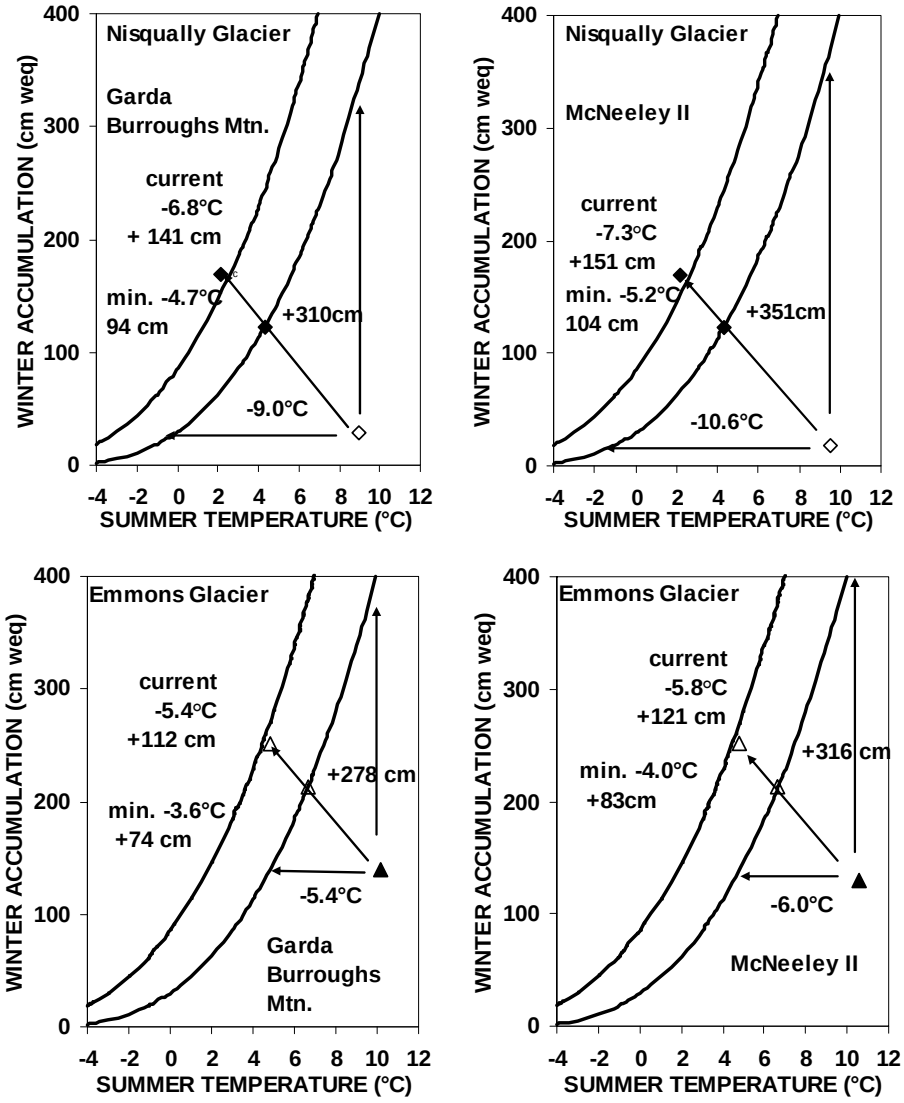

Figure 35. Current and former estimated differences in climate at the ELAs. Arrows and numbers indicate the minimum and maximum winter accumulation (snowpack) increases and summer temperature depressions necessary to produce the depressed ELAs of the prior Garda/Burroughs Mountain and McNeeley II advances.

4.2 Paleo-ELA Analysis & Reconstruction

The goal of this section is to use the historic and reconstructed ELAs to derive a continuous Holocene ELA model, and more specifically to model ELAs for periods where they are unknown. I estimated the ELA through the Holocene in two ways: a statistical model based on current ELA and climate conditions (Zemp and others, 2007); and a deterministic model, based on estimating melt and accumulation. The statistical model of ELA is a least squares multiple regression using two independent variables of mean annual Paradise air temperature and mean annual precipitation. The ten historic and paleo time periods are 2002-2007, Garda 160 cal. year B.P., Burroughs Mountain 2,790 cal. year B.P., and two periods for McNeeley II 10,170 and 10,990 cal years B.P. For air temperature, the historic and reconstructed paleo-SSTs were extrapolated to Paradise air temperature using the lapse rate of -5.1°C km^{-1} as determined earlier by the Longmire-Paradise temperature difference. For precipitation, I used the historic data at Paradise (2002-2007), and qualitative proxy data scaled by the 2002-2007 Paradise average of 2.94 m weq for the Garda, Burroughs Mountain, and McNeeley II advances (Table 12). Results showed a higher correlation for Nisqually Glacier *(R^2=0.93 $p<0.01$)* than for the Emmons Glacier *(R^2=0.86 $p<0.01$)*. I use the multiple regression for Nisqually Glacier to derive ELA (equation 1),

$$ELA = 734T + 82.9P + 53.9 \qquad (1)$$

where ELA is in meters, T is mean annual air temperature (°C), and P is annual precipitation (m).

Table 12. Known and reconstructed Nisqually ELA, and temperature (T) and precipitation (P) at Paradise.

Years	Nisqually Glacier ELA z (m)	Paradise T or f(SST) °C	Paradise P (weq m) or f(proxy P)
2007	3,000	3.9	2.68
2006	3,000	3.1	3.55
2005	3,200	3.9	2.81
2004	3,315	4.4	2.83
2003	3,750	4.5	2.98
2002	2,800	3.4	2.82
Garda ~160 cal yr. B.P.	2,008	2.3	3.48
Burroughs Mountain 2,800 cal yr. B.P.	2,008	2.5	3.98
McNeeley II 10,170 cal yr. B.P.	1,920	2.5	1.59
McNeeley II 10,900 cal yr. B.P.	1,920	2.2	1.55

Actual 2002-2007 and reconstructed Garda, Burroughs Mountain, and McNeeley II annual temperatures at Paradise were statistically significant *($t = 9.4$, $p < .01$)* but actual and reconstructed precipitation was not statistically significant *($t = 0.95$, $p > 0.1$).*

The deterministic model relies on the fact that at the ELA, ablation, essentially summer melt, equals the accumulation, essentially winter snowfall (Ahlmann, 1924). More specifically, the ELA *(z)* in meters, is the elevation on the glacier where the net annual balance b_n in meters weq is zero, and so to derive the ELA *(z)* the following equation must be solved:

$$bn(z) = Ac(z) - Ab(z) \qquad (2)$$

where the net balance is calculated by combining the accumulation A_c in meters weq and the ablation A_b in meters weq. Therefore, for a net balance $b_n = 0$ at the ELA, z_o, equation (2) becomes

$$bn(zo) = 0 = Ac(zo) - Ab(zo) \quad (3)$$

so, $$Ac(zo) = Ab(zo)$$

SST is the common dependent variable of both accumulation and ablation. Ablation is a function of summer air temperature (Leonard, 1989), which is related to elevation via the lapse rate. I chose mean annual SSTs as the unifying temperature variable for both accumulation and ablation. To calculate ablation as a function of temperature, I extrapolated annual SST to ablation stakes on the Nisqually Glacier (2002-2006) using the annual lapse rate of -5.1°C km^{-1} (Figure 36). SSTs are the annual averages computed from Chapter 2. The ablation equation is a regression equation (4) with an R^2 of 0.38 *($p<0.05$)*.

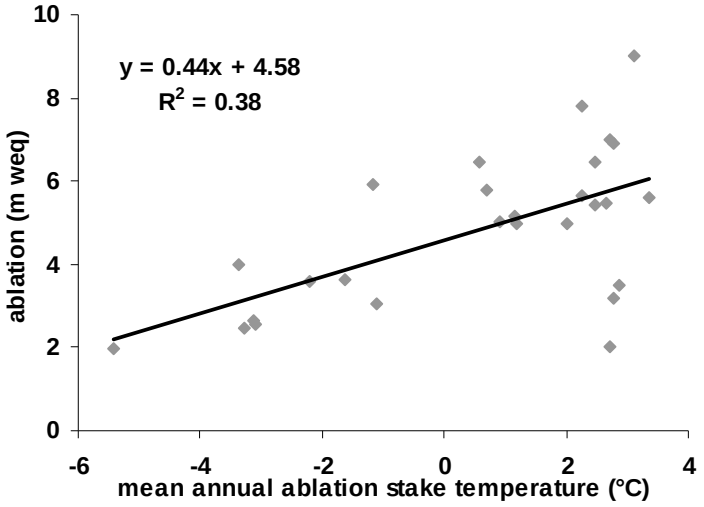

Figure 36. Temperature at Nisqually Glacier mass balance stakes 2002-2006 extrapolated from annual SST.

$$Ab(z) = 0.44T + 4.58 \quad (4)$$

$$T = -0.0051z + SST \quad (5)$$

where T is annual air temperature at elevation z, -0.0051°C km^{-1} is the temperature lapse rate, and SST is the mean annual May-April SST.

Accumulation is a function of SST and air temperature, elevation and precipitation. A large portion (65%) of average annual (2002-2007) precipitation (2.94 m) (WRCC, 2008) falls as winter snowfall and accumulates (1971-2000 1.9 m weq) (NWCC, 2008) at Paradise on Mount Rainier. The accumulation-elevation equation is a function of air temperature which is derived from annual May- April SST and annual May-April precipitation for period 1981-2005 (N=12 Table 13). An accumulation model

Table 13. Paradise snowpack and precipitation and SST data used in the accumulation equation. Missing years are due to the incomplete Paradise precipitation record.

Year	Snowpack weq (m)	SST (°C)	Paradise P (m)
1981	1.09	11.72	2.94
1983	1.83	11.61	2.74
1984	1.79	12.10	3.31
1985	1.90	11.37	2.67
1986	1.62	11.31	2.53
1987	1.58	12.14	2.71
1989	2.19	11.32	3.08
1991	2.14	11.66	3.84
1992	1.42	12.04	2.69
1993	1.73	12.04	2.44
2003	1.56	12.03	2.78
2005	1.00	12.49	2.80

was developed as a multiple regression (equation 6), has a goodness of fit *(R^2=0.49)*, and is statistically significant *(p=0.1)*. Residuals of the independent variables are shown in Figure 37.

$$Ac(z) = -0.55T(z) + 0.354P(z) + 7.17 \qquad (6)$$

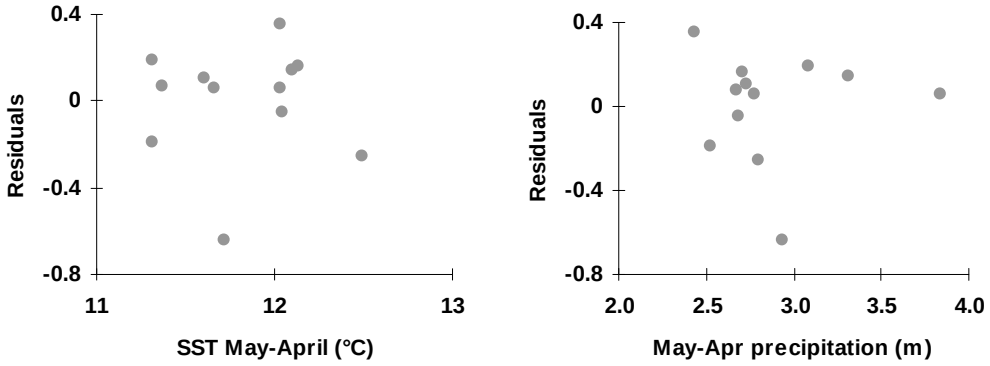

Figure 37. Residuals for the independent variables of the multiple regression of the accumulation equation: May-April SST, and May-April precipitation.

P, annual precipitation at elevation *z*, is a function of the precipitation at sea level P_{SL} plus a variable precipitation lapse rate δ (1.2 m weq km^{-1}) with a reasonable range of 0.3 to 1.7 m km^{-1} (equation 7). Drier periods as noted in the proxies yield lower lapse rates.

$$P(z) = PSL + z\delta \qquad (7)$$

P_{SL} is computed using the precipitation lapse rate *(δ)* and Paradise precipitation P_P (equation 8).

$$P_{SL} = -1{,}655 P_P \delta \qquad (8)$$

where 1,655 is the elevation (m) of Paradise, P_P is the quantitative value derived from qualitative precipitation proxy anomaly in Chapter 2 scaled to Paradise using the average annual 2002-2007 Paradise precipitation, 2.94 m. Precipitation at sea level was chosen as the starting point, z=0, for precipitation calculations. The result provides a reasonable range of precipitation-inferred snowpack (0.92 to 3.98 m weq).

To solve for $z_{o,}$ the ELA, equations (4) and (6) are set equal to each other in equation (9).

$$0.44T(z_o) + 4.58 = -0.55T(z_o) + 0.354P(z_o) + 7.17 \qquad (9)$$

and rearranging yields,

$$0.99T(z_o) - 0.354P(z_o) = 2.59 \qquad (10)$$

Equations (7) and (8), are substituted into equation (11) to yield,

$$0.99(-0.0051z_o + SST) - 0.354(P_{SL} + z_o\delta) = 2.59 \qquad (11)$$

$$-0.005z_o - 0.354z_o\delta = 2.59 - 0.99SST + 0.354P_{SL}$$

$$-z_o(0.005 + 0.354\delta) = 2.59 - 0.99SST + 0.354P_{SL}$$

Solving for z_o yields,

$$zo = -\frac{2.59 - 0.99\,\mathrm{SST} + 0.354 PSL}{0.005 + 0.354\delta} \qquad (12)$$

The result provides ELAs similar to reconstructed Garda and Burroughs Mountain (~2,008 m) with a Holocene range of 1,866 m to 2,652 m. The ELAs were extrapolated through the Holocene and compared to the reconstructed ELAs from the geologic record (Table 14).

Table 14. Reconstructed ELAs from statistical and deterministic models compared the reconstructed ELAs from the geologic record ((Burbank, 1981; Crandell and Miller, 1974; Heine, 1998)).

Calendar Years B.P.	Reconstructed geologic record	Statistical ELA	Deterministic ELA
Garda ~160	1,880-2,006	2038	2,008
Burroughs Mountain 3,442-2,153	1,880-2,006	1,664-2,189	1,842-2,069
McNeeley II 10,170	1,710-1,920	1991	2,213
McNeeley II 10,900	1,710-1,920	1768	2,134

Applying the two models to the paleoclimate record yielded similar but different results, with the statistical ELA generally lower than that for the deterministic (Table 15, Figure 38). Also the statistical model predicts a greater variability than the deterministic model. The statistical model shows significantly lower ELAs in the middle-Holocene 6,490 cal yr. B.P. (1,228 m) and 4,890 cal years B.P. (1,331 m) compared to the deterministic model, and much lower than any ELAs reconstructed from the geologic record. Time periods were chosen not on regular intervals but graphically from changes in the trends (positive or negative slope) in SST and/or precipitation shown on Figure 18.

Table 15. Climate data and results for statistical and deterministic ELA models.

cal yr. B.P.	Paradise (°C)	SST (°C)	Sea Level P (m)	P lapse rate mkm^{-1}	Calculated Proxy P (m)	Statistical ELA (m)	Deter-ministic ELA (m)
160	2.31	10.8	1.25	1.4	3.48	2,038	2,008
550	2.31	10.8	1.09	1.5	3.62	2,049	2,000
2,130	2.41	10.9	0.98	1.3	3.09	2,079	2,069
2,790	2.46	10.9	1.36	1.6	3.98	2,189	2,006
3,450	1.76	10.2	1.09	1.7	3.84	1,664	1,842
4,890	1.51	10.0	0.78	0.8	2.04	1,331	1,914
5,520	2.21	10.7	0.82	0.8	2.22	1,860	2,089
6,490	1.36	9.8	0.83	0.8	2.13	1,228	1,866
7,940	2.53	11.0	0.78	0.8	2.13	2,091	2,184
8,200	1.93	10.4	0.79	0.8	2.09	1,647	2,025
8,600	2.83	11.3	0.71	0.8	1.95	2,296	2,282
9,260	2.86	11.3	0.40	0.3	0.92	2,229	2,388
10,050	4.06	12.5	0.62	0.6	1.59	3,165	2,652
10,170	2.46	10.9	0.62	0.6	1.59	1,991	2,213
10,400	3.71	12.2	0.62	0.6	1.59	2,908	2,556
10,990	2.16	10.6	0.64	0.6	1.55	1,768	2,134
11,150	4.11	12.6	0.64	0.6	1.55	3,199	2,670
11,490	2.31	10.8	1.01	1.3	3.23	2,017	2,031

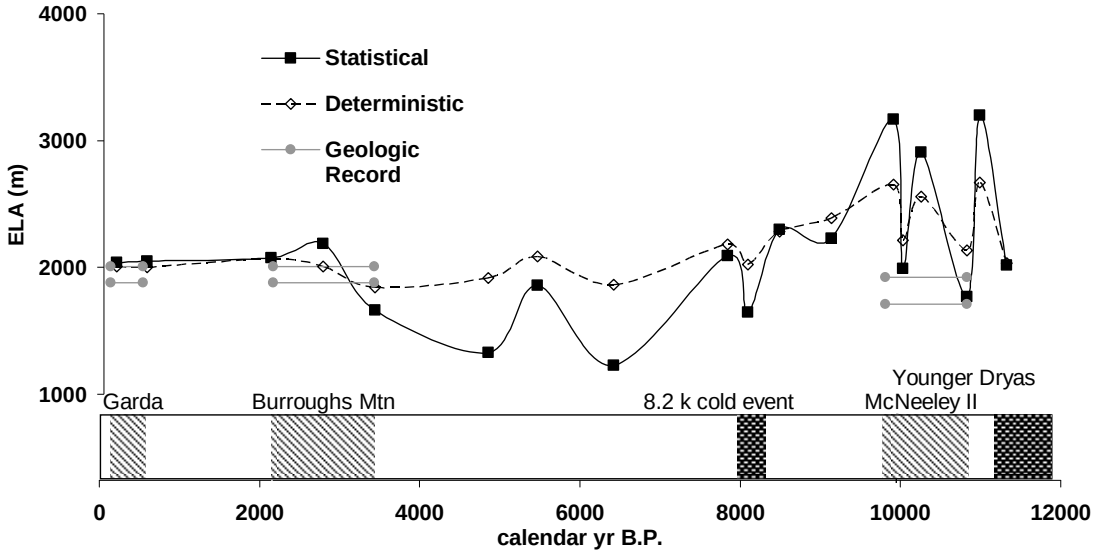

Figure 38. Reconstructed ELAs via a statistical approach using known ELAs and climate, and deterministic approach using melt and ablation models. Northern Hemisphere climate reversals (dark shaded areas on lower timeline) and glacial advances (diagonal shaded areas) on Mount Rainer: McNeeley II 10,900-9,950 cal yr B.P., Burroughs Mountain 3,442-2,153 cal yr B.P., Garda 500-90 cal yr B.P.

ELAs continue to descend through the Holocene until 3,450 cal yr. B.P. (1,842 m) which corresponds with the start of the Burroughs Mountain advance but is lower than the geologic record (Crandell and Miller, 1974). The model predicts decreasing ELAs over the last 2,000 years with a Garda ELA (2,008 m) within the range specified by Burbank (1981) (1,943 m ± 63 m).

I chose each approach based on its ELAs, instead of the weighting of temperature and precipitation. Temperature has a greater coefficient in the statistical approach but is more equal to precipitation in the deterministic approach. In the statistical approach *(1)*, results are nine times more sensitive to changes in temperature compared to precipitation whereas in the deterministic approach *(3)*, accumulation weights temperature by a factor of 1.6 higher than precipitation. I use a combination of the statistical approach in the early Holocene and the deterministic approach since 8,600 cal yr. B.P. to best fit the ELA estimates based on the geologic record. The statistical approach best captures the SST fluctuations of the early Holocene which produce McNeeley II ELAs similar to the geologic record, but the deterministic model best predicts ELAs of the Burroughs Mountain and Garda advances.

The ELA for the southern glaciers is assumed to equal that calculated for Nisqually. To estimate the ELA for the northern glaciers, I used the relation between ELAs of Nisqually and Emmons glaciers (Figure 30). Results are shown in Table 16 and Figure 39. The geologically-reconstructed McNeeley II ELAs, (1,710-1,920 m) (Heine, 1998), are close to the Emmons Glaciers ELAs I determined from the statistical model, 1,702-1,867 m.

Table 16. Holocene reconstructed equilibrium line altitudes (ELA) for Nisqually and Emmons glaciers, given in meters above sea level.

Time cal yr. B.P.	Nisqually Glacier ELA (m)	Emmons Glacier ELA (m)	Difference (m)	Average (m)
current	3,178	2,745	433	2,961
Garda 160	2,008	1,880	128	1,944
550	2,000	1,874	126	1,937
Burroughs Mountain 2,130	2,069	1,925	144	1,997
Burroughs Mountain 2,790	2,006	1,879	128	1,942
Burroughs Mountain 3,450	1,842	1,757	85	1,800
4,890	1,914	1,811	104	1,862
5,520	2,089	1,939	149	2,014
6,490	1,866	1,775	91	1,820
7,940	2,184	2,010	174	2,097
8,200	2,025	1,892	133	1,959
8,600	2,282	2,083	199	2,182
9,260	2,229	2,043	186	2,136
10,050	3,165	2,736	429	2,951
McNeeley II 10,170	1,991	1,867	124	1,929
10,400	2,908	2,546	363	2,727
McNeeley II 10,990	1,768	1,702	66	1,735
11,150	3,199	2,761	438	2,980
11,490	2,017	1,886	130	1,951

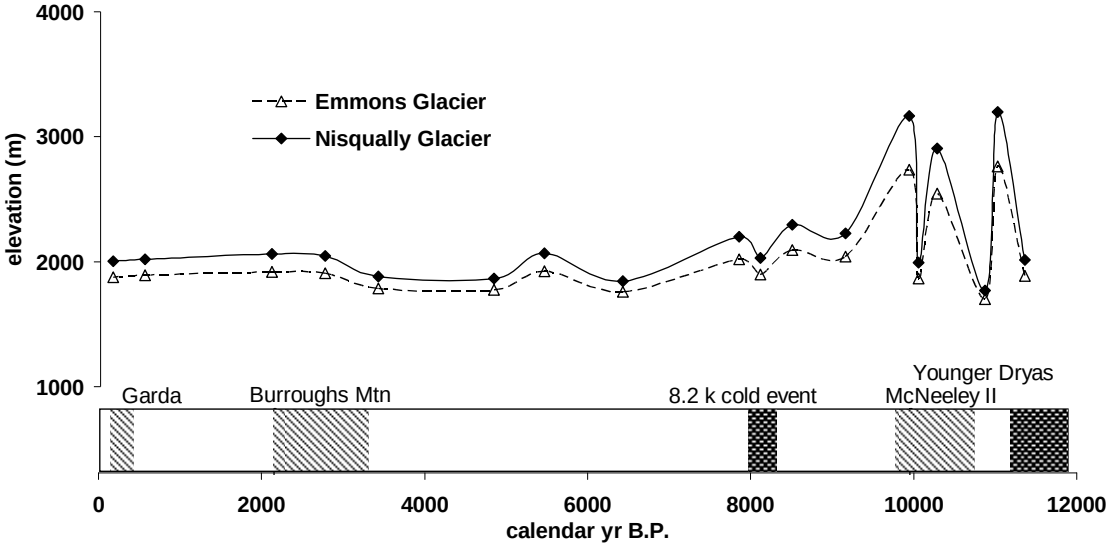

Figure 39. Variation in reconstructed equilibrium line elevation (meters above sea level) over the Holocene for the Emmons and Nisqually glaciers. Northern Hemisphere climate reversals (dark shaded areas on lower timeline) and glacial advances (diagonal shaded areas) on Mount Rainer.

The glaciological reconstruction of climate yields distinct temperature and precipitation changes while the climate changes for the statistical-deterministic methods of ELA reconstruction are less clear because the weighting of precipitation and temperature changes. For McNeeley II, temperatures depressed -4° to -7.3°C with an added +83cm to +121cm of added weq snow accumulation in the glaciological reconstruction, but based on the above weighting of temperature, I limited climate changes to temperature depressions of -6° to -10.6°C with little change in accumulation from added precipitation. For Burroughs Mountain and Garda, the climate changed -3.6°C to -6.8°C and +74 cm to +141 cm weq accumulation since the deterministic method weights temperature and precipitation more equally. For the Holocene, the most useful current climate variables in order of importance to the above methods are temperature, ablation and accumulation rates, and precipitation.

4.3 Spatial Analysis of Holocene Glaciers

To estimate the glacier extent around the mountain, the glacier area and extent were modeled using a steady state cellular automata model that incorporates ablation and accumulation data onto a digital elevation model (DEM) (Harper and Humphrey, 2003). This model uses simple rules to define the extent. Ice accumulates in each model cell according to preset gradients of ablation and accumulation. Once the basal shear stress (product of ice depth and surface slope of the cell) exceeds the critical shear stress for ice deformation the extra mass is transferred to the next cell downhill. Ice continues to move down slope until the ablation rate equals the rate of ice flow to the cell. The model

iterates until the ice extent no longer changes and equilibrium is reached, defined as <0.002 m/year. Because it is an equilibrium model it does not represent the rate of evolution from one period to the next period. Input variables include the ELA, the ablation rate gradient with elevation, the relationship between ablation rate with elevation and the accumulation rate with elevation. The no-snow elevation is set above the highest part of the DEM, the top of the mountain. I use a lower ELA for the northern half of the mountain based on Emmons relative to the southern half based on Nisqually. Although this represents a discontinuity in ELA across the direction separating north and south–facing glaciers, this difference is assumed small relative to the errors in the reconstructed data.

Two different models runs were used to reconstruct glacial extent: model parameters using current mass balance conditions, and a model that based on the best fit to the Garda extent 160 cal yr. B.P. For Model 1, the ablation rates and ratios of ablation to accumulation used for the Nisqually and Emmons glaciers (south and north halves of Mount Rainier) are 28 cm/100 m, 1.8:1; and 29 cm/100 m, 2.3:1 respectively as shown earlier and used in the deterministic method of ELA reconstruction. Because of insufficient data above the ELA, Emmons ablation rate represents all sites above and below the ELA on the north side, but the Nisqually ablation rate represents sites only below the ELA on the south side. Model 2 mass balance parameters were adjusted to fit the Garda moraines. Ablation rates were set at 200 cm/100 m, while the ablation/accumulation ratio was adjusted to 8:1. This ablation rate is an order of magnitude greater than rates on Mount Rainier, and the mass balance ratio is fourfold higher than temperate glaciers (Furnbish and Andrews, 1984), but the resulting

accumulation rate, 25 cm/100 m, is within the bounds of the Nisqually and Emmons glaciers. Nisqually ELAs were not changed from Model 1, but Emmons ELAs were adjusted to a constant 50 m lower than Nisqually ELAs for desired glacial extents.

The DEMs I used were downscaled (Gesch and others, 2002; Gesch, 2007) to a resolution of 120 m from 10 m for computer processing efficiency. Two different DEMs were used, one depicting current topography and adjusted to reflect a possible higher mountain prior to the Osceola lahar 5,600 cal yr. B.P. (Figure 40). I created a pre-Osceola lahar DEM, prior to 5,600 cal yr. B.P., by stretching or "layer caking" the upper flanks of the mountain (>3,900 m) until the summit increased by 500 m and the volume increased by 3 km^3 as estimated by the USGS (Kennard, Scott, Valance pers. comm.) (Scott and Vallance, 1995). Model 1 used both DEMs appropriate to the time period. Model 2 only used the modern topography.

The results for Models 1 and 2 show important differences with the current glacial extent. Using current mass balance measurements and current ELAs, Model 1 produced a combined glacial extent of 28.4 km^2, much smaller than currently exists (87.4 km^2) (Nylen, 2001) (Figure 41). Model 2 used current average ELAs and also produced much smaller glaciers (24.3 km^2). Possible explanations for the differences between the modeled results and current extent are the glaciers are not in equilibrium. Also, secondary effects are that the model does not explicitly account for snow redistribution, shading, or debris cover that has preserved glacial ice for decades on glaciers such as Emmons, Winthrop, and Carbon (Nylen, 2001). Also the DEM used already has glaciers on it therefore the modeled ice is much thinner than had the ice been removed from the DEM. The best representation of the current glacial extent used current mass balance

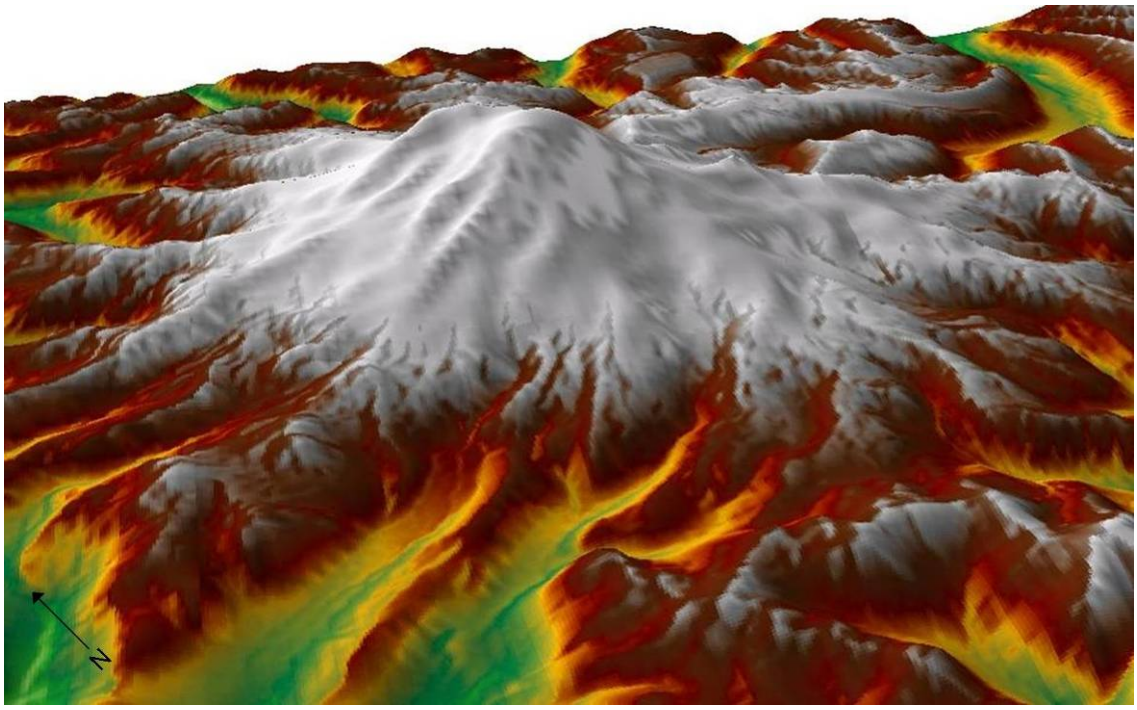

a.

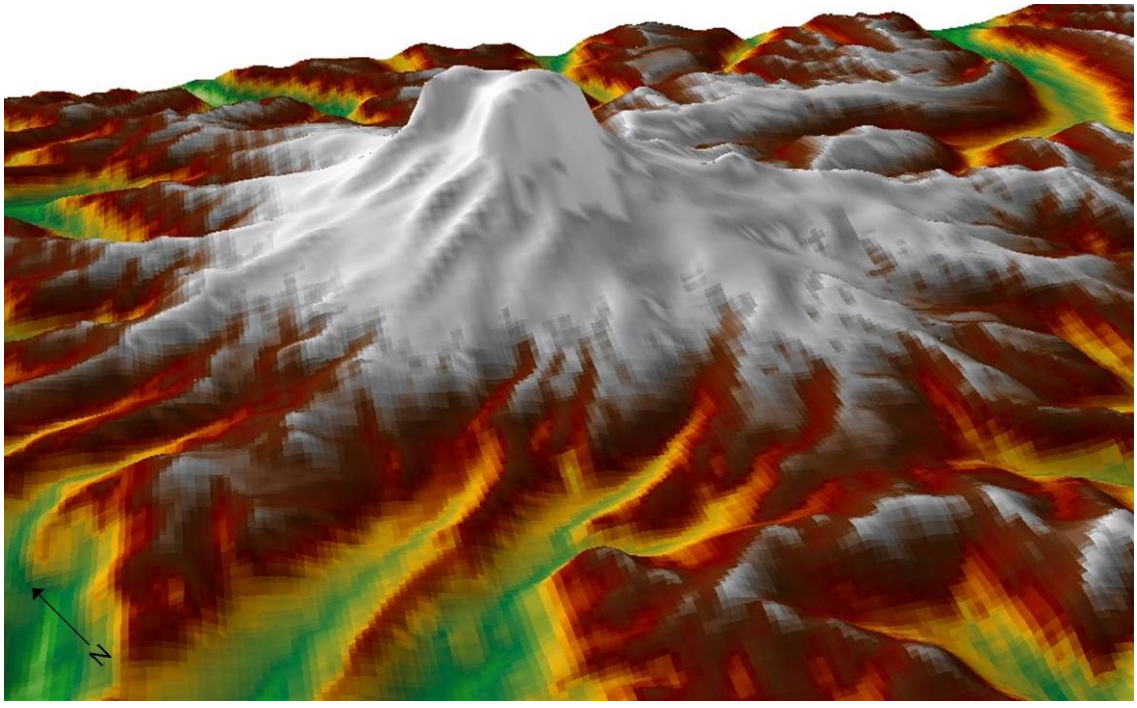

b.

Figure 40. a. Current DEM. b. Modified DEM to reflect pre-Osceola lahar on Mount Rainier 12,000-5,600 cal yr. B.P.

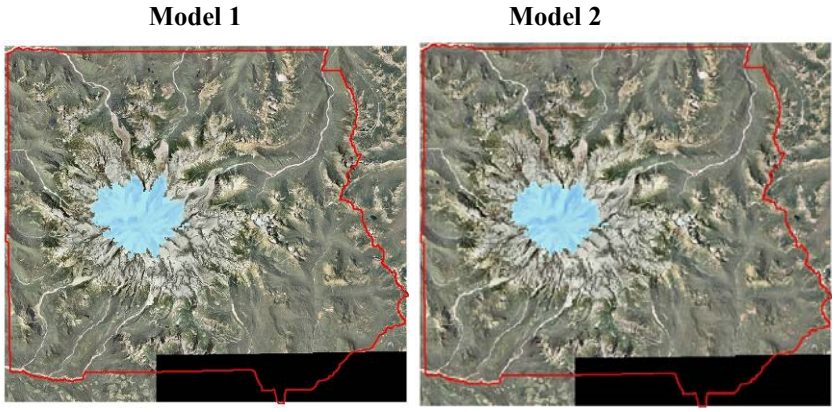

Figure 41. Modeled current extent using current mass balance measurements and current ELAs. The park boundary is shown for reference. Background image is a digital ortho quad from early 2000s.

measurements like Model 1 but with lowered ELAs and generally produced glaciers that matched mapped outlines (Figure 42). The southern ELA was lowered from 3,180 m to 2,700 m and the northern ELA from 2,800 m to 2,300 m.

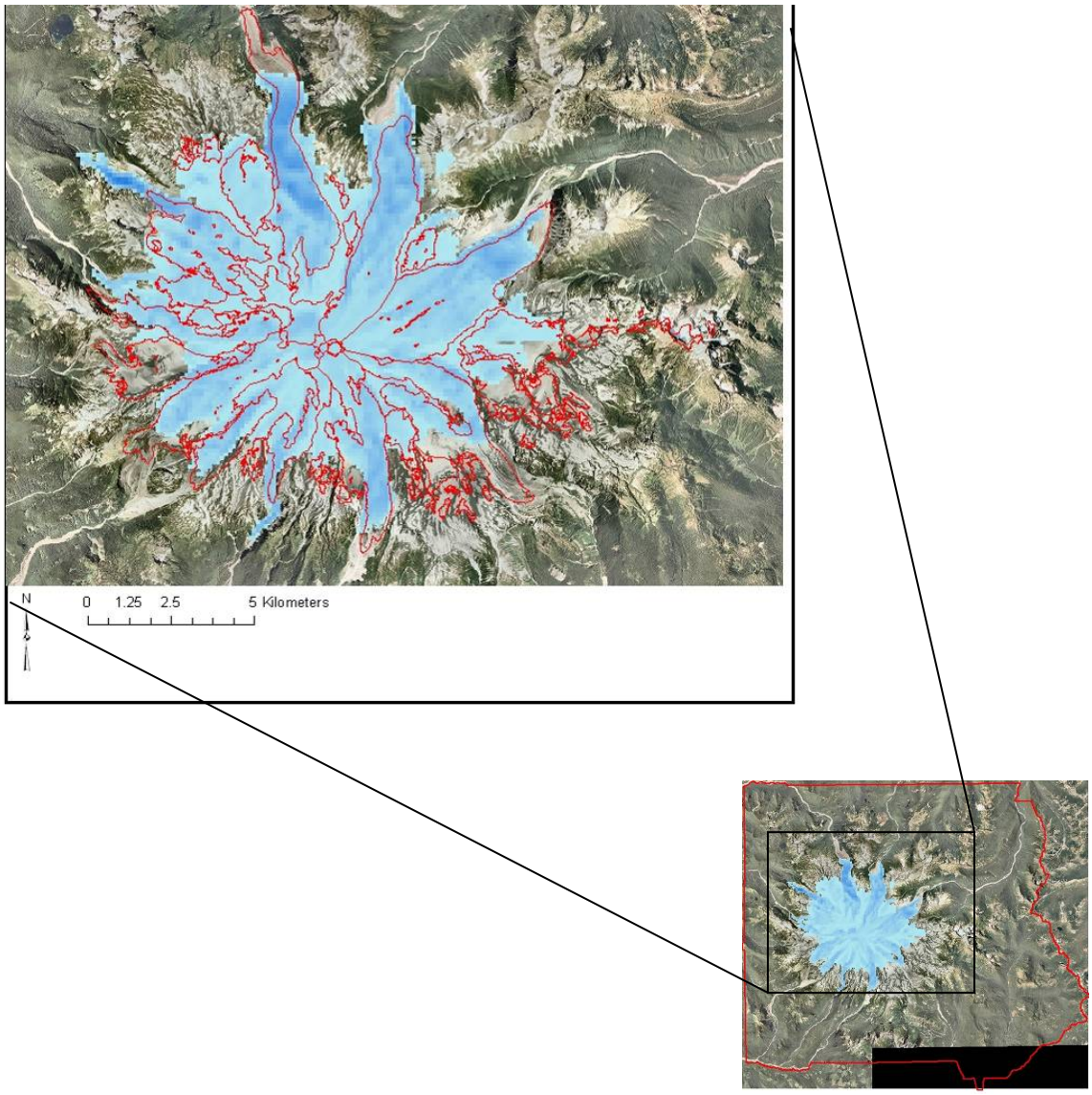

Figure 42. Best representation of current glacial extent (blue) with 1994 USGS outlines (red). The park boundary is shown for reference in the lower right.

Modeled McNeeley II extents, 10,990 cal yr. B.P., are compared with mapped moraines (Figure 43). In Model 1 the Nisqually Glacier extended to a McNeeley II moraine but results show glaciers extending beyond moraines in the rest of the park. Model 2 has more similarities with smaller glaciers than Model 1. Model 2 is arguably a better simulation of McNeeley II moraines in the northeast corner of the park for 10,990

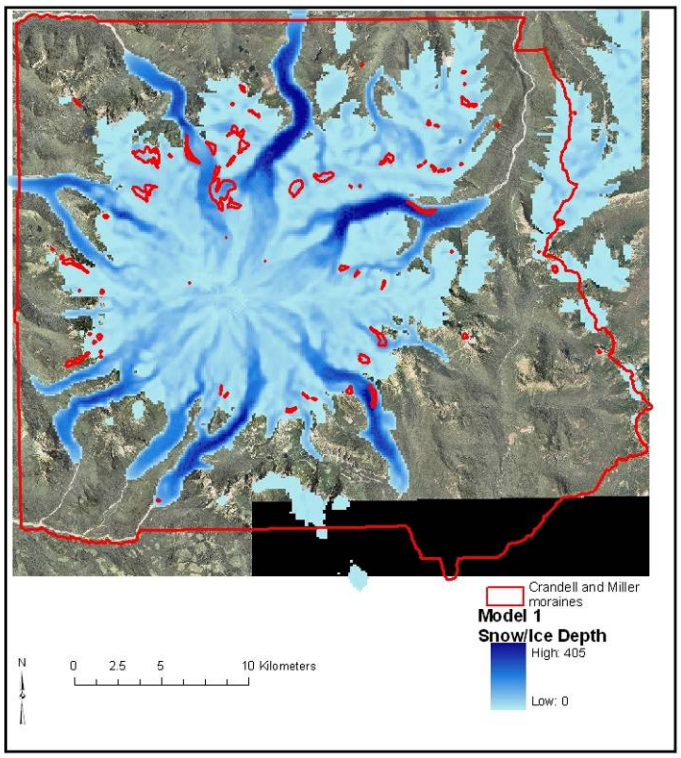

a.

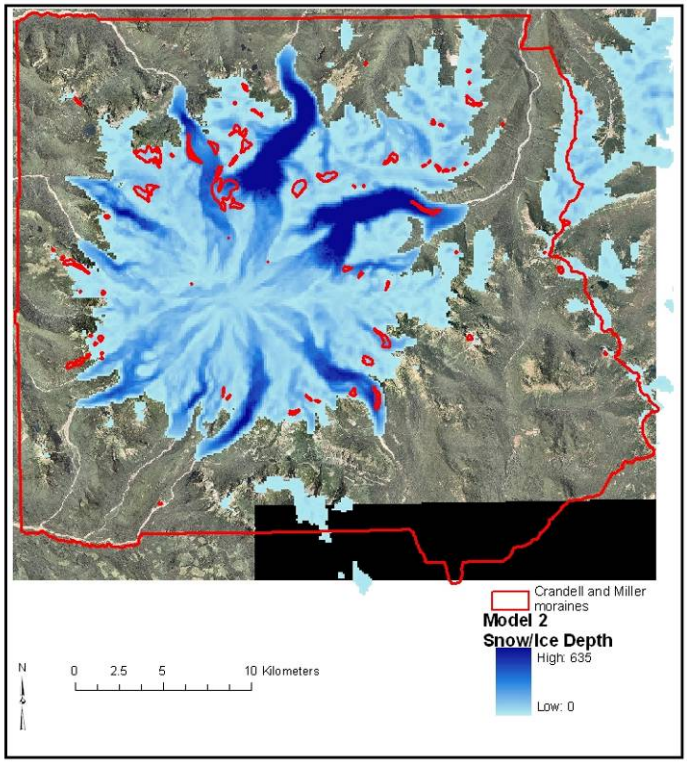

b.

Figure 43. McNeeley moraines and outer park boundary (red) (1974) **and modeled extents from 10,990 cal yr. B.P. for a) Model 1 and b) Model 2.**

cal yr. B.P. (Figure 44). To visualize only the thicker ice that could form moraines I removed the thinner "snow/ice," pixels (0-20 m depth) for both models for this time period only. I chose to shave the <20 m of ice from this time period only because it is the

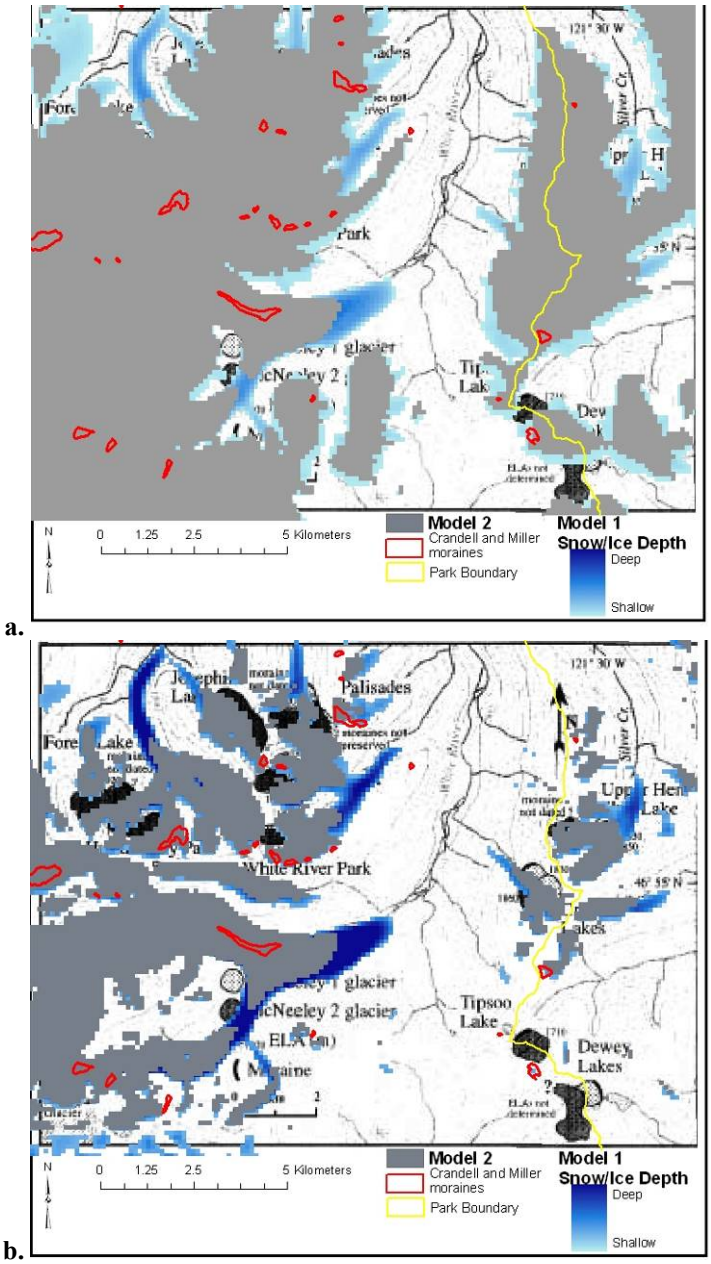

Figure 44. a) Model 1 (blue) and Model 2 (gray) extents from 10,990 cal yr. B.P. McNeeley moraines (red and black) (Crandell and Miller, 1974; Heine, 1998) overlaying Heine's (1998) map. b) Modeled results with depths <20 m removed.

largest modeled advance and has the highest density of radiocarbon-dated alpine (non-valley) moraines. Model 2 possibly best replicates the mapped moraines in Huckleberry Park, White River Park, Palisades, and Crystal Lakes (Heine, 1998) (Figure 44). However, the Tipsoo Lake and Dewey Lakes glaciers were more likely to have formed during the 10,990 cal yr. B.P. advance in Model 1 (no ice removed). (Refer to Figure 44b for the lakes locations). Heine (1998) noted a constant advanced state for glaciers during McNeeley II 10,900-9,950 cal yr B.P., but modeled results show two sustained advances 10,990 and 10,170 cal yr. B.P. intervened by a dramatic recession event 10,400 cal yr. B.P.

Modeling the second advance of McNeeley II, 10,170 cal yr. B.P. was smaller and, possibly Model 1 best represents some moraines on the east, northeast, and west sides of the mountain (Figure 45 and Figure 46). The McNeeley II moraines were likely formed by the larger 10,990 cal yr. B.P. advance, and later Holocene advances could have overridden the 10,170 cal yr. B.P. advance. Since the reconstructed climate during the McNeeley II time was very dry with sudden SST depressions (-1.95°C to -1.25°C), the advance was likely caused by air temperature depressions of -6.0°C to -10.6°C.

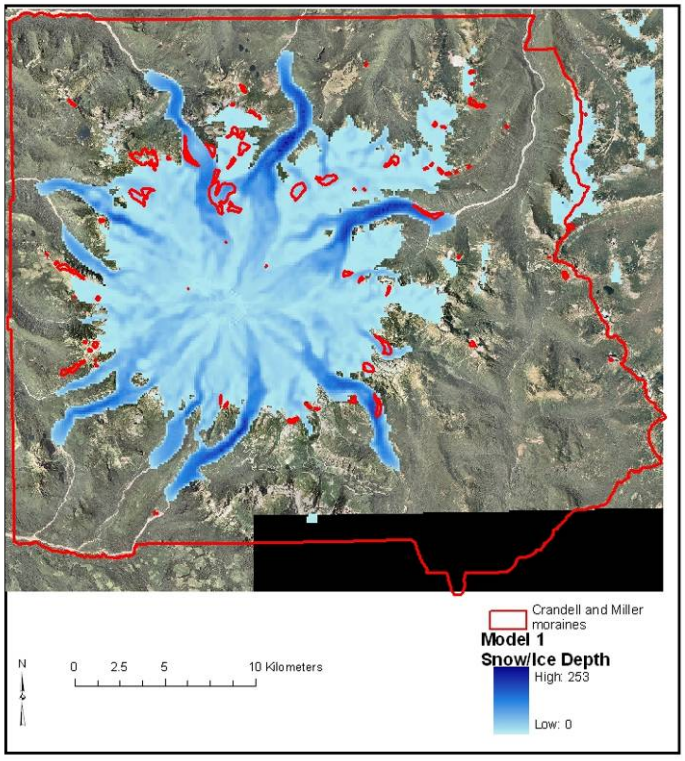

a.

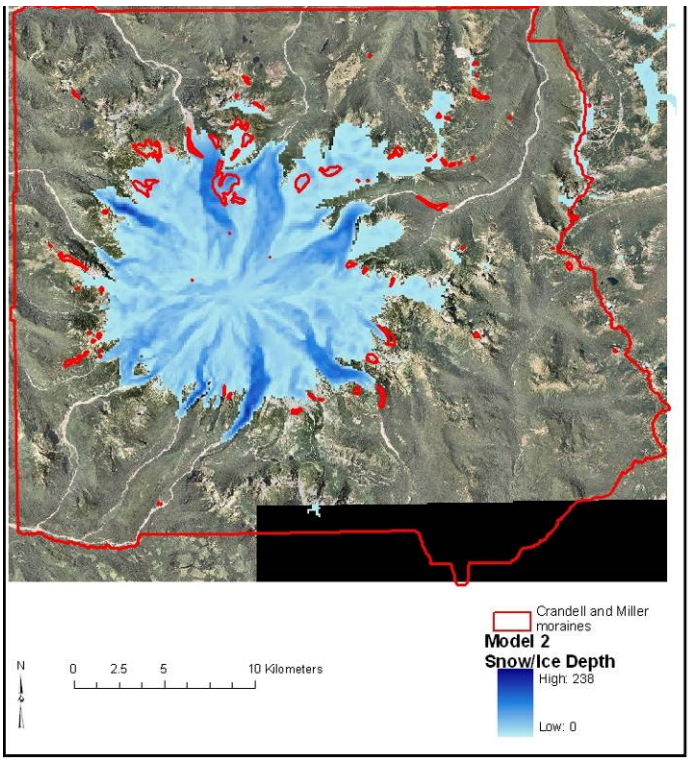

b.

Figure 45. McNeeley moraines (red) within the outer park boundary (1974) and modeled extents from 10,170 cal yr. B.P. for a) Model 1 and b) Model 2.

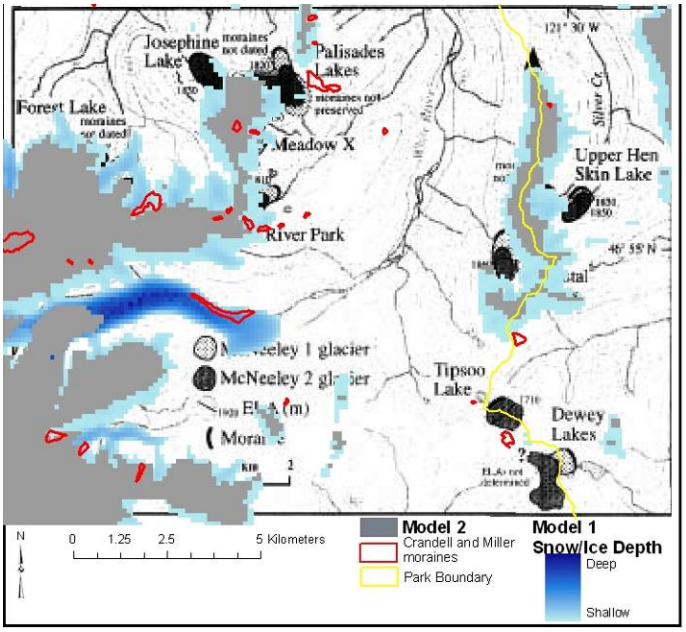

Figure 46. Model 1 (blue) and Model 2 (gray) extents from 10,170 cal yr. B.P. McNeeley moraines (red and black) (Crandell and Miller, 1974; Heine, 1998) overlaying Heine's (1998) map.

The modeled glaciers of Burroughs Mountain 3,450-2,790 cal yr. B.P. are larger than the limited moraine data suggest (Figure 47 and Figure 48). The Model 1 and 2 extents of 3,450 cal yr. B.P. are much larger, with much lower ELA than that inferred from the geologic data. The Model 2 extent of 2,790 cal yr. B.P. correlates best with the moraine data as expected since the Burroughs moraines are similar in extent to the Garda moraines, and the 2,790 cal yr. B.P. reconstructed ELAs match that of Garda. The SSTs were -0.55°C to +0.15°C compared to today while the precipitation was at its highest point of the Holocene, so the advance was caused by a combination of both temperature depression and increased precipitation, but the temperatures could be the same or higher. The climate changes necessary to produce the glacial advances were likely at the upper end or above the stated range since the 3,450 cal yr. B.P. modeled advance was the second largest of the Holocene. However the 3,450 cal yr. B.P. modeled extent is much larger than the geologic record.

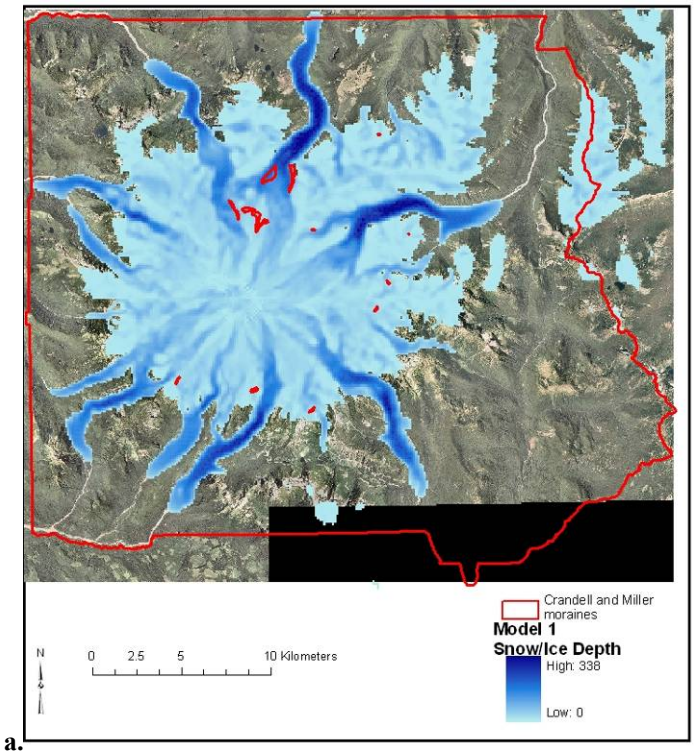

a.

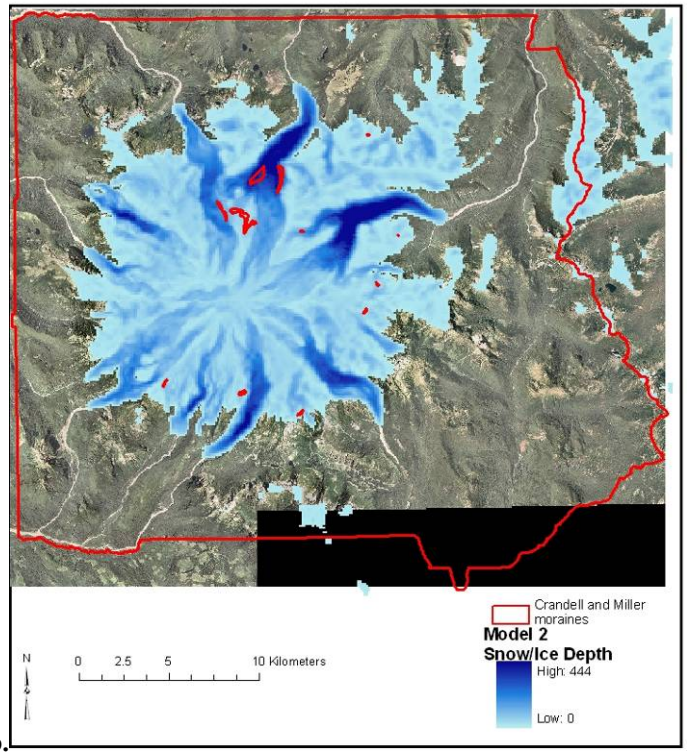

b.

Figure 47. Burroughs Mountain moraines (red) within the outer park boundary (1974) with modeled extent from 3,450 cal yr. B.P. for a) Model 1 and b) Model 2.

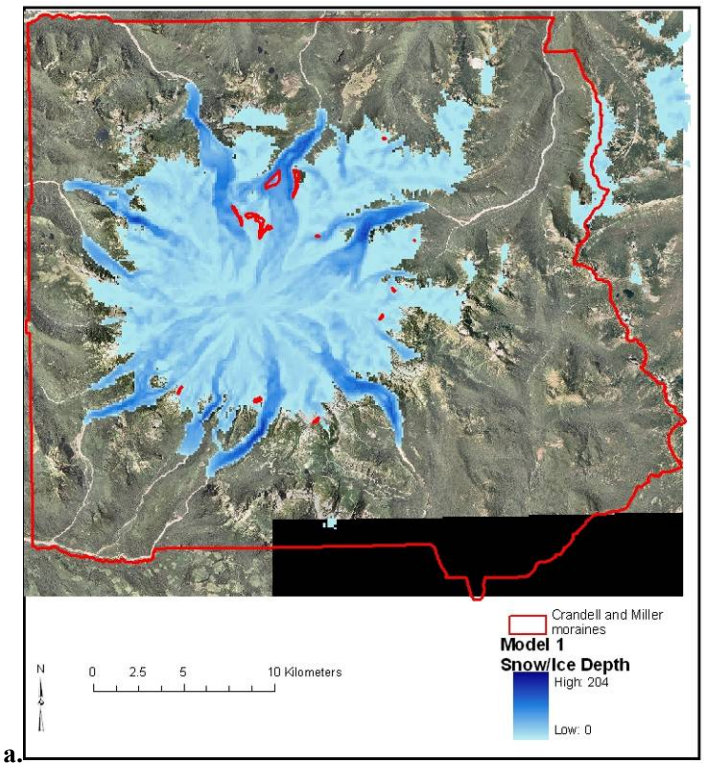

a.

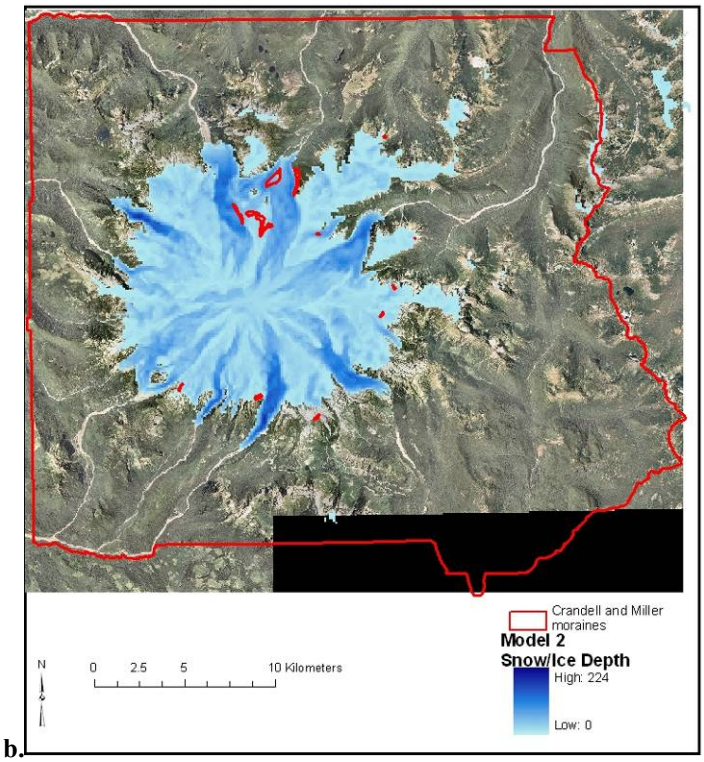

b.

Figure 48. Burroughs Mountain moraines (red) within the outer park boundary (1974) with modeled extent from 2,790 cal yr. B.P. for a) Model 1 and b) Model 2.

Since Model 2 was created specifically to match the mapped Garda moraines, Model 2 as expected, outperforms Model 1. The latter produces glaciers that extend past the moraines by 2.3-2.7 km (Figure 49). Model 2 also produced small glaciers on the ridges on the northeast flank of the mountain in the Burroughs Mountain area between the Winthrop and Emmons glaciers, but no Garda moraines have been mapped in this area. The SST was similar to today so the advance must have been caused mainly by the added snow accumulation.

The ELA and glacial extents of Model 1 and 2 are shown in Figure 50 and summarized in Table 17, and Figure 51, Figure 52, and Figure 53. Glacial extent, as expected, logically tracks the ELA with lower ELAs producing greater extents (Figure 51). Measured lengths of the modeled Nisqually and Emmons glaciers are shown in Figure 53 and Table 18. To show the accumulation of snow and ice above the ELA, I plotted an example time period shown in Figure 54.

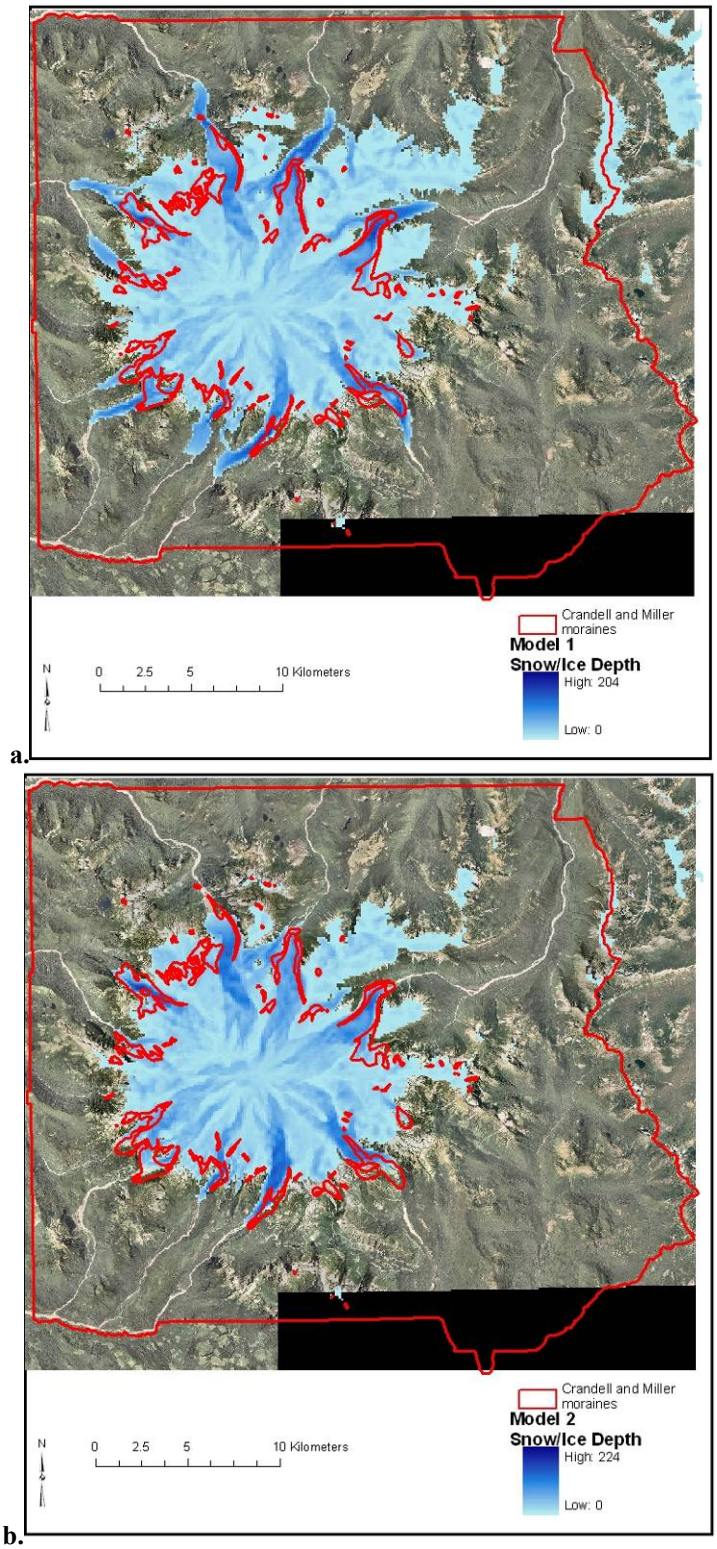

Figure 49. Garda moraines 750-100 cal yr B.P. and outer park boundary (red) (1974) with modeled extent for a) Model 1 and b) Model 2.

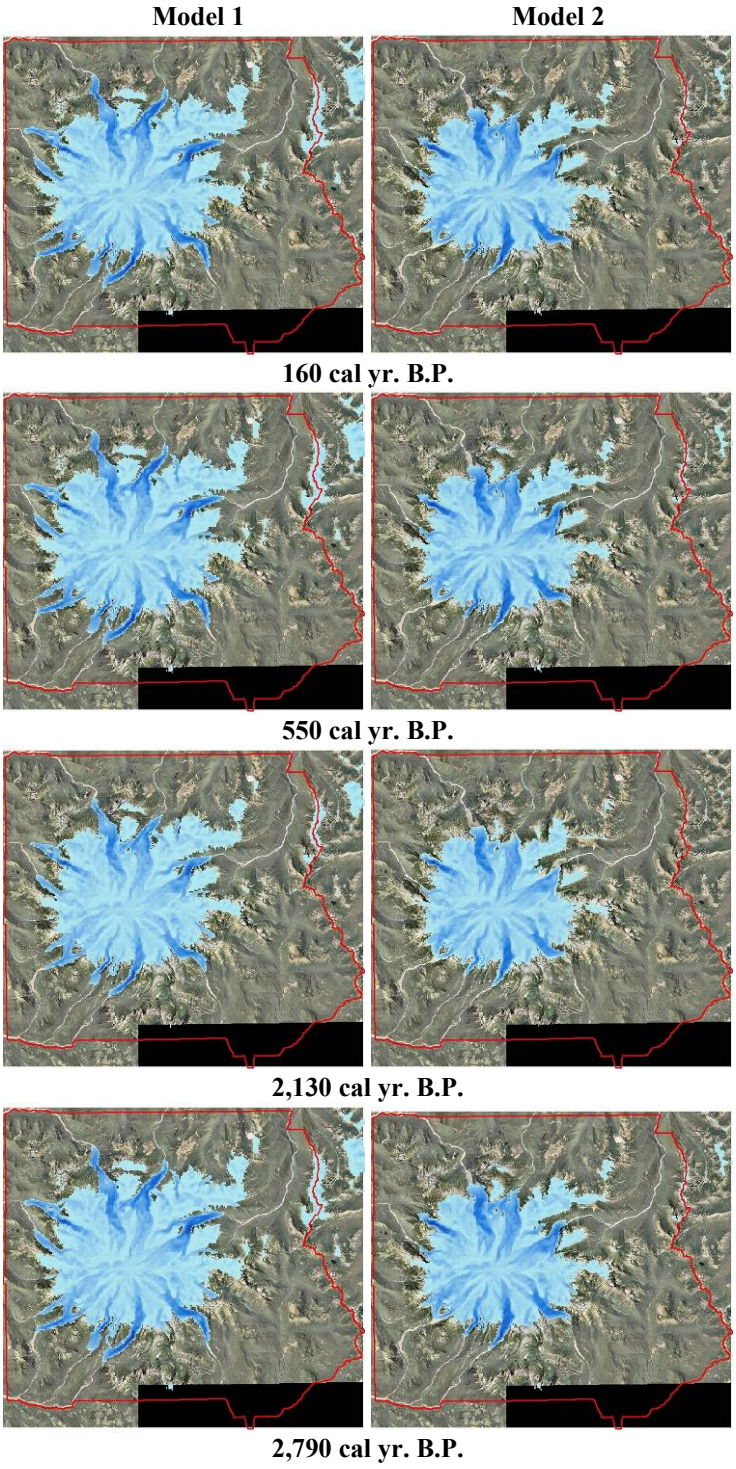

Figure 50. Spatial extents of Holocene Glaciers on Mount Rainer for Model 1 and 2. 160- 5,520 cal yr. B.P. are modeled with the current DEM. For Model 1 years 7,490-11,490 cal yr. B.P. are modeled with a DEM representing a taller Mount Rainier before the Osceola lahar 5,600 cal yr. B.P. Model 2 uses the current DEM throughout.

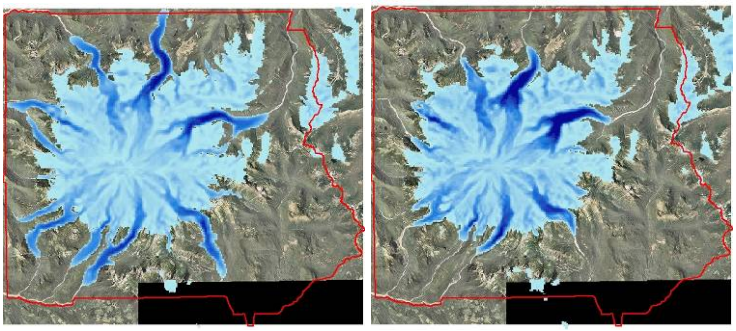

3,450 cal yr. B.P.

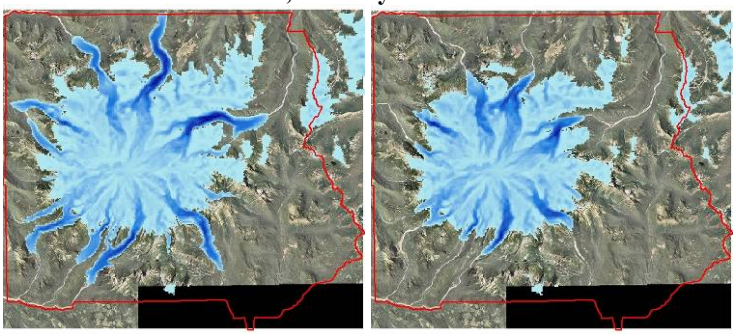

4,890 cal yr. B.P.

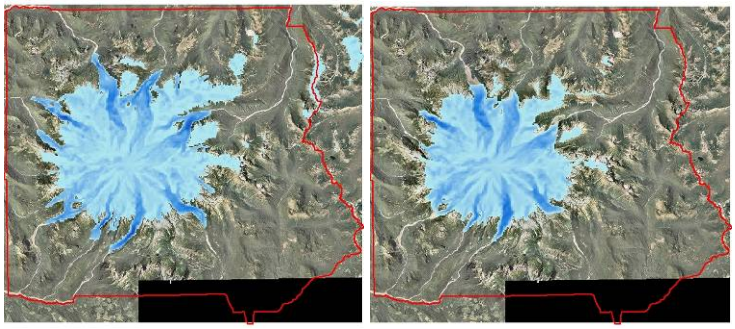

5,520 cal yr. B.P.

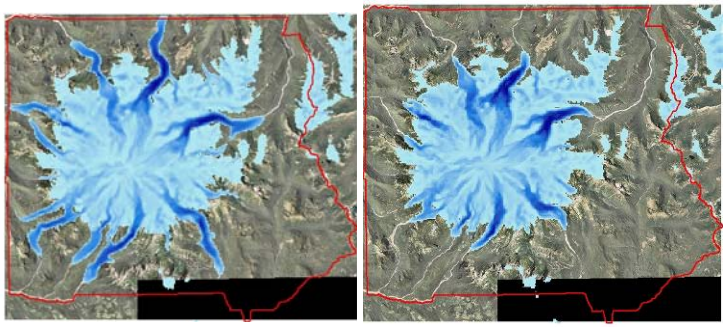

6,490 cal yr. B.P

Figure 50 cont'd. Spatial extents of Holocene Glaciers on Mount Rainer for Model 1 and 2. 160-5,520 cal yr. B.P. are modeled with the current DEM. For Model 1 years 7,490-11,490 cal yr. B.P. are modeled with a DEM representing a taller Mount Rainier before the Osceola lahar 5,600 cal yr. B.P. Model 2 uses the current DEM throughout.

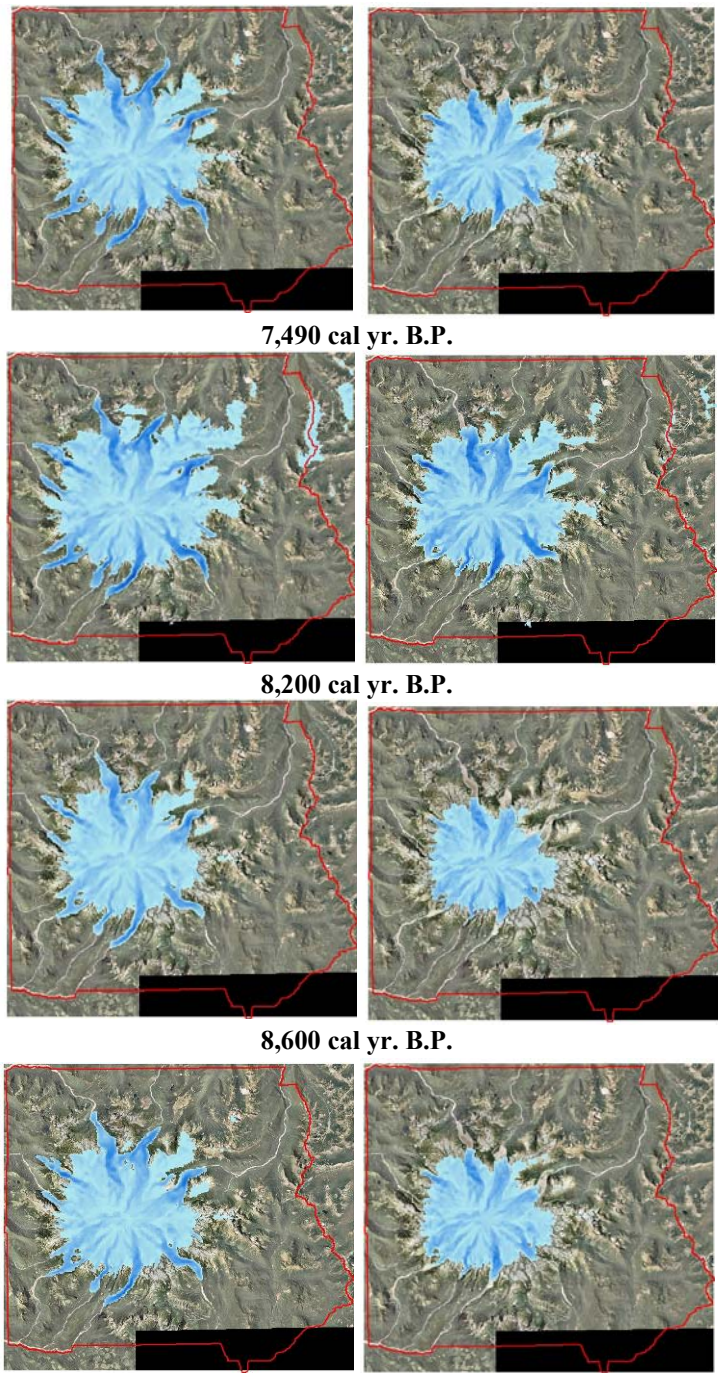

Figure 50 cont'd. Spatial extents of Holocene Glaciers on Mount Rainer for Model 1 and 2. 160-5,520 cal yr. B.P. are modeled with the current DEM. For Model 1 years 7,490-11,490 cal yr. B.P. are modeled with a DEM representing a taller Mount Rainier before the Osceola lahar 5,600 cal yr. B.P. Model 2 uses the current DEM throughout.

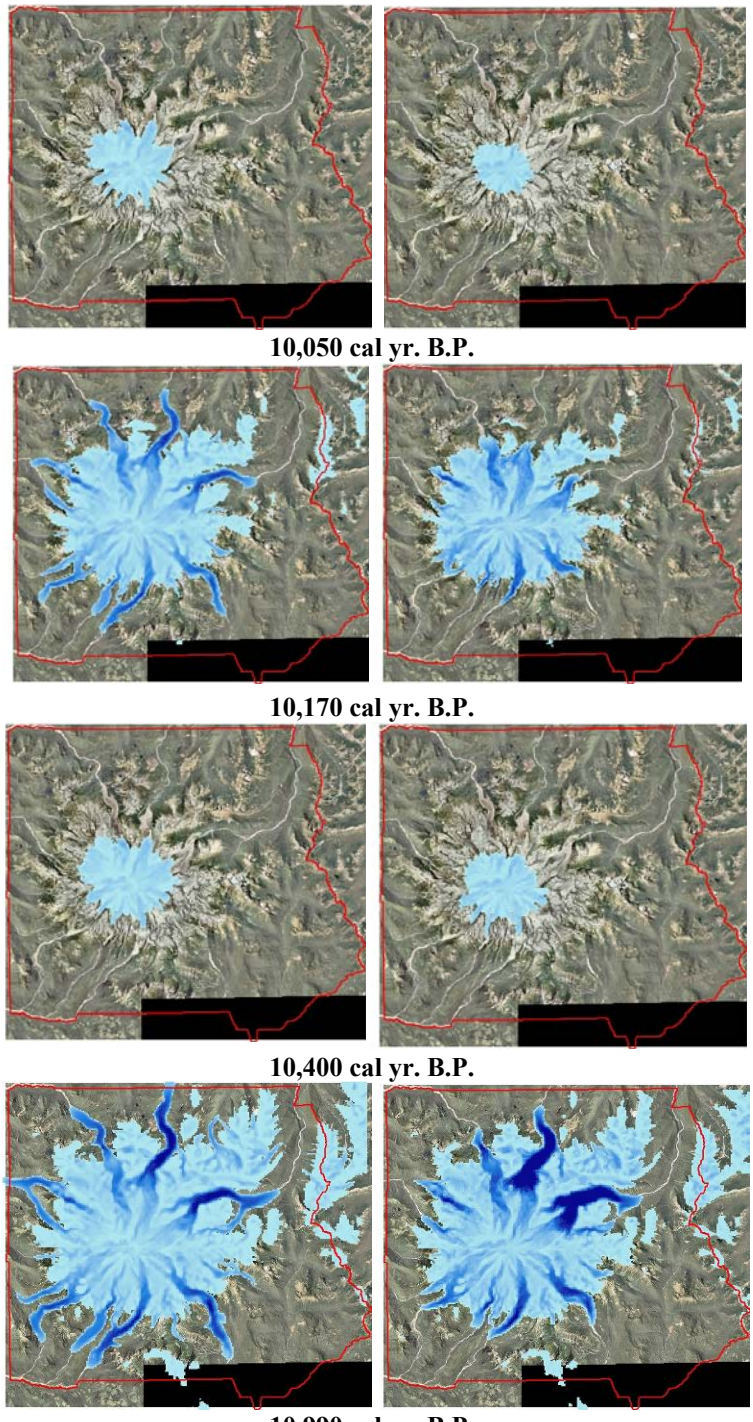

10,050 cal yr. B.P.

10,170 cal yr. B.P.

10,400 cal yr. B.P.

10,990 cal yr. B.P.

Figure 50 cont'd. Spatial extents of Holocene Glaciers on Mount Rainer for Model 1 and 2. 160-5,520 cal yr. B.P. are modeled with the current DEM. For Model 1 years 7,490-11,490 cal yr. B.P. are modeled with a DEM representing a taller Mount Rainier before the Osceola lahar 5,600 cal yr. B.P. Model 2 uses the current DEM throughout.

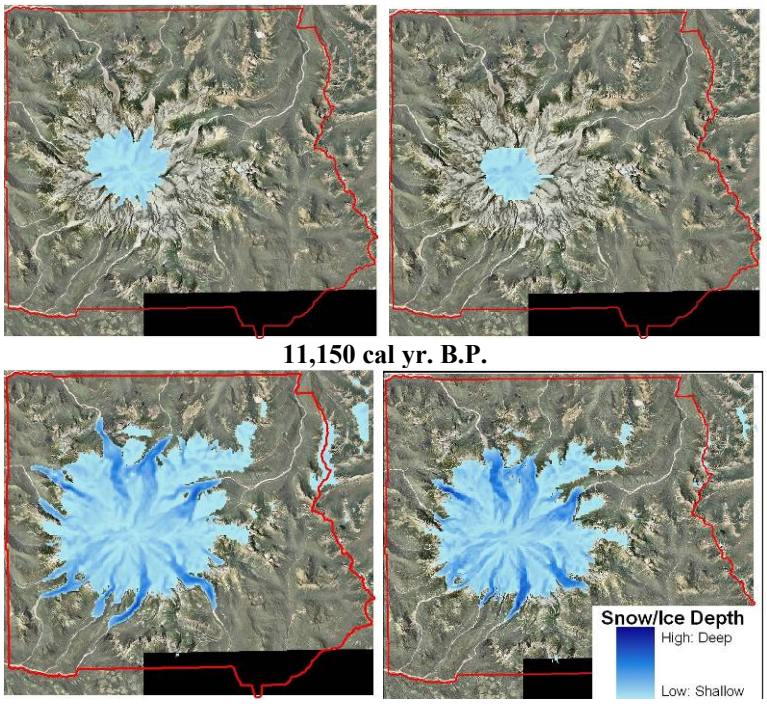

Figure 50 cont'd. Spatial extents of Holocene Glaciers on Mount Rainer for Model 1 and 2. 160-5,520 cal yr. B.P. are modeled with the current DEM. For Model 1 years 7,490-11,490 cal yr. B.P. are modeled with a DEM representing a taller Mount Rainier before the Osceola lahar 5,600 cal yr. B.P. Model 2 uses the current DEM throughout.

Table 17. Modeled glacier extents for Mount Rainier for the Holocene.

		Model 1				Model 2				
cal yr. B.P.	Advance Name	Nisqually Glacier ELA m	Emmons Glacier ELA m	ELA Avg. m	Area km^2	Nisqually Glacier ELA m	Emmons Glacier ELA m	ELA Avg. m	Area km^2	Difference Area km^2
modeled current		3,178	2,745	2,962	28.4	3,178	2,745	2,962	24.3	4.1
best current represent.		2,700	2,300	2,961	63.1					
160	Garda	2,008	1,880	1,944	192.7	2,008	1,958	1,983	123.8	68.9
550		2,000	1,874	1,937	192.7	2,008	1,958	1,983	123.8	68.9
2,130	Burroughs Mtn.	2,069	1,925	1,997	161.5	2,069	2,019	2,044	99.1	62.4
2,790	Burroughs Mtn.	2,006	1,879	1,942	192.7	2,008	1,958	1,983	123.8	68.9
3,450	Burroughs Mtn.	1,842	1,757	1,800	265.8	1,842	1,792	1,817	233.9	32.0
4,890		1,914	1,811	1,862	253.0	1,914	1,864	1,889	176.0	77.0
5,520		2,089	1,939	2,014	161.5	2,089	2,039	2,064	92.3	69.2
6,490		1,866	1,775	1,820	265.8	1,866	1,816	1,841	212.3	53.6
7,940		2,184	2,010	2,097	118.5	2,184	2,134	2,159	71.5	47.0
8,200		2,025	1,892	1,959	173.2	2,025	1,975	2,000	115.7	57.5
8,600		2,282	2,083	2,182	67.8	2,282	2,232	2,257	58.7	9.1
9,260		2,229	2,043	2,136	73.5	2,229	2,179	2,204	64.7	8.8
10,050		3,165	2,736	2,951	29.4	3,165	3,115	3,140	12.4	17.0
10,170	McNeeley II	1,991	1,867	1,929	193.7	1,991	1,941	1,966	131.5	62.2
10,400		2,908	2,546	2,727	36.3	2,908	2,858	2,883	20.1	16.2
10,990	McNeeley II	1,768	1,702	1,735	327.3	1,768	1,718	1,743	303.8	23.4
11,150		3,199	2,761	2,980	26.7	3,199	3,149	3,174	11.8	14.9
11,490		2,017	1,886	1,951	173.2	2,017	1,958	1,987	123.8	49.4
									average	44.8
									Std Dev	24.2

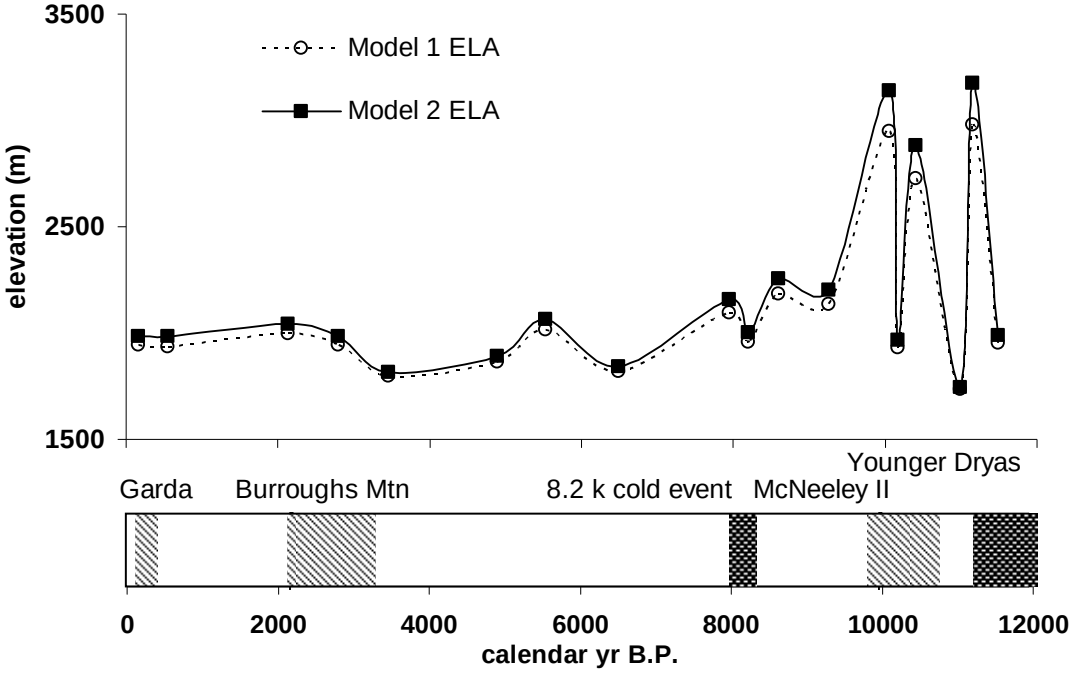

Figure 51. Average ELAs for combined Nisqually and Emmons glaciers for Models 1 and 2.

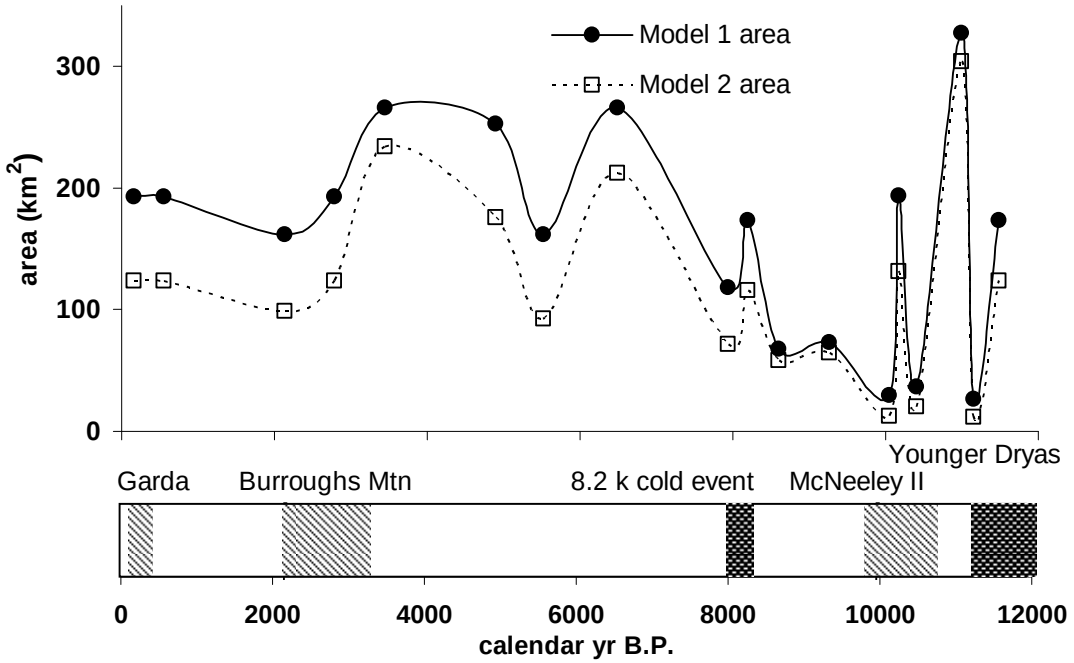

Figure 52. Modeled area of Mount Rainier glaciers.

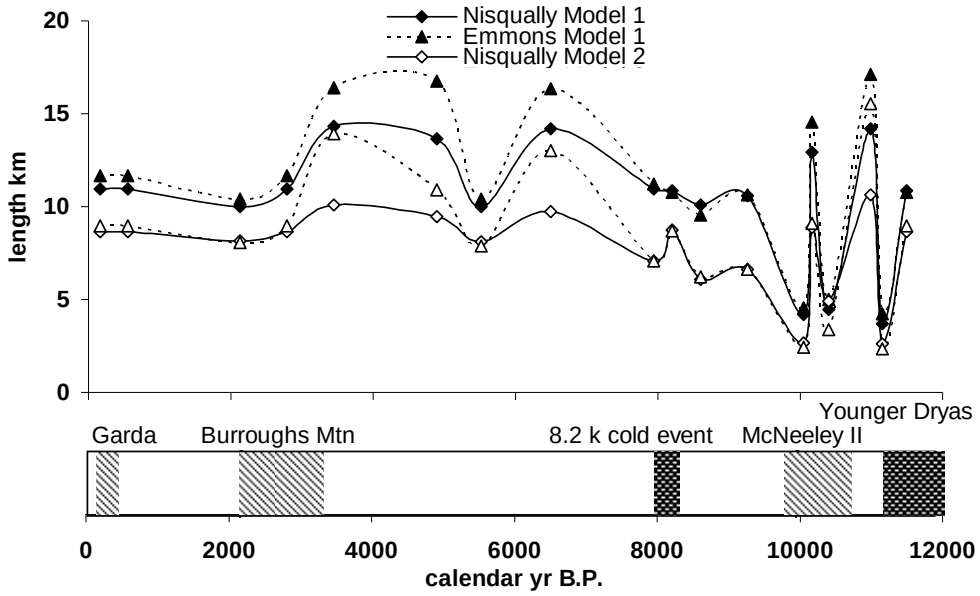

Figure 53. Modeled glacial lengths for the Nisqually and Emmons glaciers.

Table 18. Modeled glacier lengths for the Nisqually and Emmons glaciers with the noted Garda, Burroughs Mountain, and McNeeley II advances.

cal yr. B.P.	Advance Name	Nisqually Glacier length km	Emmons Glacier length km	Nisqually Glacier length km	Emmons Glacier length km
160	Garda	11.0	11.7	8.6	9.0
550		11.0	11.7	8.6	9.0
2,130	Burroughs Mtn.	10.0	10.4	8.2	8.1
2,790	Burroughs Mtn.	11.0	11.7	8.6	9.0
3,450	Burroughs Mtn.	14.3	16.4	10.1	13.9
4,890		13.6	16.8	9.5	10.9
5,520		10.0	10.4	8.1	7.9
6,490		14.2	16.4	9.8	13.0
7,940		11.0	11.2	7.1	7.1
8,200		10.8	10.8	8.7	8.7
8,600		10.1	9.6	6.1	6.2
9,260		10.6	10.6	6.6	6.6
10,050		4.2	4.6	2.6	2.4
10,170	McNeeley II	12.9	14.5	8.9	9.1
10,400		4.5	5.0	4.9	3.4
10,990	McNeeley II	14.2	17.1	10.6	15.5
11,150		3.7	4.2	2.6	2.3
11,490		10.8	10.8	8.6	9.0

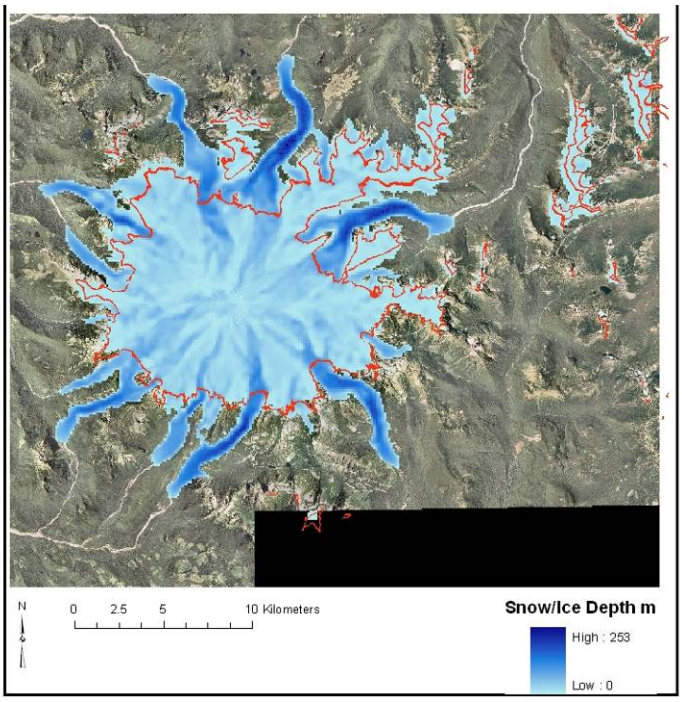

Figure 54. Model 1 glacial extent 10,170 cal yr. B.P. with average ELA 1,929 m (red) showing that snow/ice above the ELA is ubiquitous.

The evolution of the glacier extents over the Holocene shows great variability, especially early in the Holocene. Figure 50 shows glaciers dramatically shrinking 6.0-6.6 km in 340 years (18-20 ma^{-1}) from 11,490 to 11,150 cal yr. B.P. Length changes are for Nisqually and Emmons glaciers for Model 2. Glaciers then advance 8.0-13.2 km in 160 years (50-83 ma^{-1}) by 10,990 cal yr. B.P. and retreat again 5.7-12.1 km by 10,400 cal yr. B.P. (10-21 ma^{-1}). Over the next 230 years, glaciers advance again 4.0-5.7 km (17-25 ma^{-1}). By 10,050 cal yr. B.P., 120 years later, Nisqually and Emmons retreated 6.0-6.6 km (52-56 ma^{-1}). Average glacier length change rates for the remaining Holocene were 3.0-3.6 ma^{-1}. Figure 51 and Figure 52 show sensitivity of glacier area to small changes in ELA.

In summary, reconstructing glacial extents proved to be problematic but was met with some success. Modeling glacial extent is a compounding of errors in the paleoclimate model, the ELA models, and the cellular automata-based glacier extent model yet the results are mostly satisfactory. The results-based Model 2, matched to Garda glaciers, performed better overall than current based Model 1 at modeling McNeeley II and Burroughs Mountain advances. Replicating the broad reach of McNeeley II glaciers to the moraines on the ridge tops of the northeast corner of the park produced reasonable results. However, regardless of model, the ELAs of the Burroughs Mountain advance created a much larger modeled extent than the limited moraine data suggest. This implies perhaps, that the ablation/accumulation gradients changed over time if we assume the geologic data are correct.

The modeling indicates four new glacial advances not seen in the geologic record with glaciers being in advanced positions eight times through the Holocene. Holocene advances not seen in the geologic record first occurred 11,490 cal yr. B.P. McNeeley II had possibly two distinct advances 10,990 and 10,170 cal yr. B.P., the first one, largest of the Holocene, overriding the earlier advance. A smaller advance occurred 9.260 cal yr. B.P., and then glaciers readvanced to greater extents during the 8.2 k cold event. The mid-Holocene saw the third largest advance 6,490 cal yr. B.P. which would have been overridden by the Burroughs Mountain advance, 3,450 cal yr. B.P. Modeling shows Garda moraines started forming 550 cal yr. B.P. and continued through 160 cal yr. B.P.

5. DISCUSSION AND CONCLUSIONS

Mount Rainier's glacial activity is mostly correlated with its southern neighbors, the Wallowa Mountains, Oregon (390 km SE) and the Three Sisters, Oregon (300 km S), based on the moraines. The first evidence of a Holocene advance is the McNeeley II 10,900-9,950 cal yr B.P., which matches that of both sites (Licciardi and others, 2004; Marcott and others, 2009). To the north, however, this early advance is not found at Enchantment Lakes (100 km NE) (Bilderback, 2004) and Mount Baker (215 km N) (Thomas, 2000). The second Holocene advance on Mount Rainier, Burroughs Mountain, was synchronous with an advance on the Three Sisters in Oregon (Marcott and others, 2009) and a site in the southern Coast Mountains of British Columbia (Osborn and others, 2007) but not elsewhere. Finally, the Garda advance was synchronous with most LIA sites in the region.

The marine and terrestrial paleoclimate proxies each have their strengths and weaknesses. The strengths of the SST records are their temporal and temperature resolution. A weakness is that the SST could be influenced by a changing currents such as migrations of cold waters of the Bering Sea Gyre and Pacific subarctic Gyre, strengthening and weakening of the California Current, or enhanced coastal upwelling (Barron and others, 2003; Kienast and McKay, 2001). These influences may have affected the two sites differently causing the two SST records to diverge in the late Holocene. Strengths of the terrestrial records include close proximity and large sample size, fourteen spatially diverse terrestrial records that comprise a general picture of Holocene climate for the Pacific Northwest. Weaknesses include poor temporal and temperature/precipitation resolutions. Another weakness is that it mostly records only the

summer climate (Walsh and others, 2008; Williams and others, 1998). And great variation can exist between terrestrial proxies. Finally, the terrestrial proxies also express climatic differences qualitatively "different than present" making quantitative inferences difficult. Neither terrestrial nor oceanic proxies directly reflect climate at glacial elevations, however the terrestrial proxies are much closer at an average elevation of 1,188 m.

Comparing the reconstructed climate to other records yields some interesting results. The early Holocene SST fluctuated wildly and warmed which agrees generally with the GISP2 air temperatures until 10,100 cal yr. B.P. at which time the SSTs cool while the GISP2 air temperatures remain relatively constant (Alley, 2000). In contrast, North America pollen-derived air temperatures show slow warming until peaking 3,300 cal yr. B.P. (Alley, 2000; Viau and others, 2006), and warmer than present on the Pacific northwest coast (Moss and others, 2007). The SST is cooler than current until 2,790 cal. yr. B.P. Notably absent from my results is the mid-Holocene Hypsithermal warm period others noted (Burtchard, 1998; Thompson and others, 1993). Tweiten (2007) shows that the Hypsithermal was not monolithically warm and dry on Mount Rainier. It is not clear how others reached the conclusion that the mid-Holocene was the warmest and driest period, but as can be seen amongst the individual terrestrial climate summaries, there is some local variability e.g. (Dunwiddie, 1986; Gavin and others, 2001). The benefit of averaging the records is that regional trends outweigh local anomalies. For the late Holocene, GISP2, the North American pollen record, and SSTs show cooling from above normal temperatures to normal temperatures while the regional reconstructed terrestrial temperature record shows below normal cooling (Alley, 2000; Viau and others, 2006).

Heine (1998) directly addresses the discrepancy between the warm, dry summer climate at Mount Rainier as inferred by the early Holocene pollen data and the McNeeley II glacier advance, by postulating greater seasonality -high summer insolation and low winter insolation -and presumably winter temperatures that would support glacier growth. Heine (1998) and Bartlein (1998) agree that the low winter insolation would create greater seasonality and produce colder and wetter winters favorable to glacier growth despite warm SSTs and terrestrial proxy temperatures. Such colder-than-present winter temperatures combined with dry conditions could have caused higher adiabatic lapse rates (Barnosky and others, 1987) and therefore lower winter temperatures at high elevations. Such conditions would be favorable to the McNeeley II advance and may have sustained the advance from 10,990 to 9,950 cal yr. B.P. My numerical reconstructed glacial extents do not directly account for seasonality and therefore each recession (10,400 and 10,050 cal yr. B.P.) caused by warm SSTs. Lie (2006) suggests that seasonality effects (reduced winter temperatures) would be attenuated by decreases in winter precipitation. Unlike the McNeeley II advance, the Burroughs Mountain glacial advance has obvious paleoclimatic conditions that aid a glacial advance, mostly cool temperatures and increased precipitation. The conditions also occur during the Garda advance but to a lesser degree.

The data available from weather stations and sea surface temperatures in Chapter 3 offers a good climate record but high altitude, spatially-diverse aspects on the mountain are absent as the automatic weather stations and SNOTEL sites are located mostly on the northeastern. There is a lack of temperature and snowfall data on the major glacial covered faces of the mountain with the exception of the south side, Paradise. The rain

shadow likely produces significantly less snowfall on the eastern and northern aspects of the mountain (Figure 2) and the only site, White River Ranger Station, is too low capture the orographic trends at glacial levels.

The accumulation rates on Mount Rainier are similar to other Washington glaciers, but the ablation rates are much lower. The accumulation rate on the lower Nisqually Glacier (30 cm/100 m) is similar to calculations for the east side of Three Sisters, OR (32 cm/100 m), and inferred from South Cascade Glacier, WA (34 cm/100 m) (Marcott, 2005; Rasmussen and Conway, 2001). The overall accumulation rate for the Nisqually Glacier that I used that included the western SNOTEL sites (12 cm/100 m), and the accumulation rate for Emmons (13 cm/100 m), are similar to the accumulation rate for the Blue Glacier, WA (13 cm/100 m) (Rasmussen and others, 2000). The accumulation peak at 2,200 m on Nisqually Glacier seems to substantiate the hypothesis of diminished snowfall with elevation on high mountains (Harper and Humphrey, 2003). The diminished snowfall elevation is not seen on Emmons Glacier because perhaps the measurement sites are not high enough. The ablation rates on Mount Rainier of -26 to -28 cm/100 m are lower than rates for South Cascade and Blue glaciers which are -88 cm/100 m and -108 cm/100 m respectively (LaChapelle, 1960; Rasmussen and Conway, 2001).

In Chapter 4.1, the glaciological reconstruction of climate for the three known advances provides an interesting comparison to other areas. The McNeeley II ELAs were depressed -930 m to -1,260 m from the average of 2002-2007 ELAs to those reconstructed by Heine (1998) and would have required a -4.0°C to -7.3°C temperature depression with +83 cm to +151 cm of additional winter water equivalent snowpack. The

similarly dated post-LGM advance on Three Sisters, OR required an ELA depression of -160 m to -360 m from 1995 data and a temperature decrease of -0.9°C to -1.9°C and a winter precipitation increase of + 50 to +120 cm (Marcott and others, 2009). Although climates and topographies for Mount Rainier and Three Sisters are different, to equate the two ELA depressions, a threefold increase in the ELA depression of Three Sisters would have necessitated a -2.7°C to -5.7°C temperature depression, partially within the range specified on Mount Rainier; and +150 to +360 cm of added accumulation, above the range specified by Mount Rainier. The timing of the Burroughs Mountain advance overlapped in time with two advances found elsewhere in the region, the Coast Mountains, B.C. and possibly the Three Sisters, OR, but no estimates of temperature depression and added winter accumulation were available (Marcott, 2005; Marcott and others, 2009; Osborn and others, 2007; Osborn and others, 2007).

Based on the current (2002-2007) average ELA (Rasmussen and Wenger, 2009), I estimated an -865 m to -1,170 m ELA depression for Garda (-420 m to -692 m relative to my best modeled fit for current glaciers) which would be caused by -3.6°C to -6.8°C temperature depression and +74 cm to +141 cm weq accumulation. As an earlier study estimated, the glaciological reconstruction of climate for Garda would require a 160 m ELA depression from the ~1980 ELA of 2,125 m, temperature depression of -0.77°C to -0.92°C, and a corresponding increase in precipitation 0-20% (Burbank, 1982). To equate the ELA depressions, a five to sevenfold increase in temperature depressions for Burbank's (1982) estimate would be -3.8°C to -6.4°C, similar to my estimate. A five to sevenfold increase in precipitation would yield 0-140%. On Three Sisters the LIA advance had ELAs 70-150 m lower than current ELAs and were caused by +20 to +50

cm increase in precipitation and -0.4°C to -0.8°C temperature depression (Marcott and others, 2009). Equating that to ELA changes on Mount Rainer, a seven to twelvefold increase would yield temperature depressions of -2.8°C to -9.6°C and +140 cm to + 600 cm of increased precipitation. Mount Baker's glaciers required a -285 m ELA depression from circa 1999 ELA of 2,095 m to 1,810 m which was forced by a temperature depression of at least -0.5°C (excluding accumulation changes) (Thomas, 2000). To put it in perspective of Mount Rainier's ELA changes, a three to fourfold increase would be a -1.5°C to -2.0°C temperature depression, which is lower than estimated on Mount Rainier.

Of the variables that define the glaciological reconstruction of climate- change in ELA, temperature lapse rate, and snow accumulation rate- the change in ELA at Mount Rainier is larger than computed by Burbank (1982) for Mount Rainier and Three Sisters, which is thereby increasing the computed climate changes (Burbank, 1982; Marcott and others, 2009). The magnitude of ELA depressions on Mount Rainier is much greater than for Three Sisters and Mount Baker. This implies that glaciers on Mount Rainier are more sensitive to climate changes than Three Sisters and Mount Baker. The high ELA depressions are likely a product of more current (2002-2007) end-of-summer field data showing higher average ELAs for Mount Rainier (2,745 to 3,178 m) compared with Three Sisters 1995 data (2,540±20 m) and much lower ELAs for Garda (1,943±63 m) and McNeeley II (1,815± 105 m) on Mount Rainier than for the LIA (2,420±20 m) and post-LGM (2,250±30 m) respectively on Three Sisters (Burbank, 1982; Heine, 1998; Marcott and others, 2009; Rasmussen and Wenger, 2009). Also the method of determining the ELAs for Mount Rainier was based on mass balance data (Riedel, unpublished

information) while the Three Sisters ELAs were determined by the balance ratio method (Marcott and others, 2009) and Mount Baker the AAR method (Thomas, 2000) which could produce varying results.(Rasmussen and Wenger, 2009)

Neither the statistical ELA model nor the deterministic model match the reconstructed ELAs of the geologic record through the entire Holocene, but each is appropriate at certain times. The statistical ELA model provides highly variable glacial record while the deterministic model produces much less variability. Despite differences in the predicted ELAs, statistical models of ELA relationship to temperature and precipitation (Ohmura and others, 1992) have been shown to agree well with other analytical glacial-meteorological models (Kerschner and Ivy-Ochs, 2008) which supports my use of modern climate data in the statistical model and glaciological reconstruction of climate. Interannual variability in air temperature is the determining climate factor of melt-dominated (high precipitation) glaciers (Rupper and Roe, 2008), which supports these results that temperature is more significant than precipitation at predicting ELA. The statistical model captures the McNeeley II advance (ELA) although it predicts variability that was not seen by Heine (1998). After 8,600 cal yr. B.P., the predicted ELAs of the middle Holocene produce ELAs much lower than reconstructed from the geologic record.

The deterministic model predicts higher McNeeley II ELAs and therefore was not employed until 8,600 cal yr. B.P. from which time it predicts ELAs lower than the reconstructed Burroughs Mountain ELAs but within the range of ELAs for the Garda advance. The deterministic model generally works well (Ohmura, 2001), however for simplicity of modeling prehistoric temperatures this model uses annual temperatures.

One limitation of the deterministic model is one has to proscribe ablation and accumulation gradients, which may change with time (Kerschner and Ivy-Ochs, 2008).

My statistical and deterministic models are certainly simplifications. Solar radiation plays a large role in ablation on southern aspects like Nisqually Glacier but is minimized where shading and debris cover shelter ice (Nylen, 2001). On South Cascade Glacier, WA, which has a northern aspect, solar radiation is the dominant summer energy source for ablation followed by sensible heat, latent heat, and longwave radiation (negative) (Anslow and others, 2007). Mount Rainier likely has similar energy balance components but with variability due to aspect, shading, etc. Other energy balance factors not addressed here, such as wind could have a significant effect by either lowering freezing heights during lower wind speeds (Betts and Ridgeway, 1992) and/or by scouring or depositing snow.

The final ELA model, early Holocene-statistical and remaining Holocene-deterministic, is useful but difficulty remains in capturing climate anomalies. Heine (1998) hypothesizes that McNeeley II was a sustained advance that lasted approximately 1,000 years but my ELA reconstruction shows at least two recessions between the two advances 10,990 and 10,170 cal yr. B.P., caused by fluctuating SST. The extreme dryness at 9,000 cal yr. B.P. (Figure 18) had little effect on modeled ELAs. In contrast, the wettest period combined with low temperatures, 3,000 cal yr. B.P., produced modeled ELAs lower than Burroughs Mountain advance. Modeled Garda ELAs match the geologic record.

Modeled glacial advances, shown by the ELA model, are coeval with other glacial advances in the region (Table 19). Early Holocene advances on Mount Rainier were

similar to advances in the Wallowa Mountains 10,200 cal yr B.P. (Thomas, 2000) and the Oregon Cascades 11,100-10,900 cal yr. B.P. (Marcott and others, 2009). The modeled advance at 8,200 cal yr. B.P., which was likely overridden by later advances and not found in the geologic record, is coeval with advances in the Southern Coast Ranges of British Columbia (Menounos and others, 2004; Osborn and others, 2007). Two other advances not found in the geologic record, 6,490 and 3,450 cal yr. B.P., were coeval with advances in the Fitzsimmons and Spearhead ranges of southern Coast Range of British Columbia (Osborn and others, 2007). The timing of the 3,450 cal yr. B.P. advance places it within the Burroughs Mountain advance but earlier than the advance in the Three Sisters, Oregon Cascades 2,500-1,700 cal yr. B.P. (Marcott and others, 2009). Modeled ELAs would have risen by 150-200m when the Three Sisters advanced occurred thus correlations of simultaneous advances are unlikely.

Climate anomalies are used to explain other paleoglacier activity elsewhere in the Northwest. Glaciers on Mount Baker exhibited a glacial advance 9,450-8,400 cal yr. B.P. that was not supported by pollen proxies (Barnosky and others, 1987) and wood and peat proxies (Clague and Mathewes, 1989) but could be supported by temperature depressions found in higher resolution SST changes (Thomas, 2000). In the Wallowa Mountains, the absence of a glacial advance during the Younger Dryas and the presence of the possible 10,200 cal yr B.P. advance were explained as precipitation anomalies or at least a local sensitivity to precipitation changes (Licciardi and others, 2004) which could also be the case with Mount Rainier.

Table 19. Summary of glacial advances for western Pacific North America compared with modeled Mount Rainier advances (k= thousands of calendar years B.P.) Hemispheric cold periods are shown in gray: * Little Ice Age 50-450 years B.P., **8.2k cold event 8,000-8,200 years B.P, ***Younger Dryas 11,600-12,900 B.P.

Location	0k*	1k	2k	3k	4k	5k	6k	7k	8k**	9k	10k	11k***	12k***	Reference
Canadian Rockies												11.5		Reasoner and others, 1994
	0.25±0.2													Luckman, 2000
					4.0 ± 0.2									Menounos and others, 2008
S. Coast Mountains, B.C.				3.2 ± 0.3	4.2 ± 0.2[1]		6.8 ± 0.1		8.3 ± 0.3					Osborn and others, 2007
									8.3 ± 0.3					Menounos and others, 2004
	0.25-0.9													Koch and others, 2007
													12.7 ± 0.2	Friele and Clague, 2002
Mount Baker, WA	undated								8.9 ± 0.5					Thomas and others, 2000
Enchantment Lakes, WA	0.8-0.47+											> 11.3		Bilderback, 2004
Mount Rainier, WA	**0.4 ± 0.3**		**2.8 ± 0.6**								**10.4 ± 0.5**			Heine, 1998;
														Crandell and Miller, 1974
modeled Mount Rainier	**0.3 ± 0.2**			**3.4**			**6.5**		**8.2**	**9.3**	**10.1**	**11.0**		
Wallowa Mountains, OR											10.2 ± 0.6			Licciardi and others, 2004
	0.21 ± 0.13													Kiver, 1974
Three Sisters, OR	0.2 ± 0.1		2.1 ± 0.4			5.5 ± 1.0						11 ± 1[2]		Marcott, 2009
Mount Thielsen, OR	0.2 ± 0.1													Lafrenz, 2001
Sierra Nevada, CA	0.2 ± 0.1													Clark and Gillespie, 1997

[1] Authors noted as a probable glacier advance because of limited datable material

[2] Fountonnour advance late Pleistocene or early Holocene

The modeled glaciers for the southern half of Mount Rainier are more sensitive to climate, which produce higher ELAs, at least during periods of warmth and dryness that causes recession; than the northern half of the mountain (Table 16). Spatial variations probably result from solar radiation, which is greater on the south side compared to the north side, and causes thinner snowpacks due to melting despite higher precipitation (Daly and others, 1994) on the south side (Figure 2). Based on the 2002-2007 record (Rasmussen and Wenger, 2009), ELAs are more similar during colder and or wetter periods and presumably during glacial advances like most of the Holocene record shows (Figure 30) which may reduce the relative impact of solar radiation on the net annual surface energy balance. Other geomorphic variables such as greater fluxes of rock fall on the Emmons, Carbon, and Winthrop glaciers blanket the ice, insulating it from the sun and warm air temperatures thus reducing ablation (Nylen, 2001). This is also observed on other glaciers and other Cascade mountains (Jackson and Fountain, 2007; Pelto, 2000). The degree to which Holocene glaciers were debris-covered is unknown, but volcanic activity and edifice changes likely affected all glaciers periodically.

On-site and global evidence exists to support high retreat rates (10-56 ma^{-1}) after early Holocene modeled glacial advances on Mount Rainier. In light of worldwide glacial retreat since the LIA, most measurements are of retreat with few estimations of annual paleo-retreat. On Mount Rainier, South Tahoma and Nisqually glaciers retreated 33-36 ma^{-1} from 1950-1994 (Nylen, 2001). Elsewhere, the fastest retreat rates for the continental Tibetan glaciers at the headwaters of the Yellow and Yangtze are 41-57 ma^{-1} (1966-2000) and post LGM glaciers in southwestern Colorado retreated an average 15 ma^{-1} (Guido and others, 2007; Jianping and others, 2003). Little (or no) information

exists to support the fast early Holocene advance rates (17-83 ma^{-1}). The possibility exists that modeling overestimated the ablation and retreat because of unaccounted shading, debris cover, etc., and that advance rates are thereby overestimated.

The simple cellular automata model used to recreate glacial extent was problematic but produced satisfactory results. Holocene Models 1 and 2 both produced glaciers smaller than currently exist likely indicating that current glaciers are out-of-balance. Replicating the current glaciers produced some larger (N. Mowich) while others are smaller (Carbon, Cowlitz-Ingraham), and the discrepancies in the areas are difficult to explain (Figure 42). One possible explanation is that the DEMs contain glaciers, do not reflect the subglacial topography, therefore they partially fill the valleys and cirques and would presumably provide a higher, wider, and smoother surface on which glaciers would flow more easily and probably farther than they would otherwise.

Model 1 with the higher DEM used prior to the Osceola lahar, produced a less reasonable, surprising result, glaciers that were 1-11% greater in extent (not shown) than those produced by a higher DEM of scenario 1. One possible explanation is that the higher “layer caked” peak accumulates less ice on its steeper flanks, thus moving thinner ice to lower reaches in the ablation zone quicker similar to a steep alpine headwall that continuously sloughs any accumulated snowfall.

Paleo-glaciers and future glacier extents have been modeled for numerous locations and are based on different climate and model parameters e.g. (Coleman and others, 2009; Coleman and others, 2009; Hall and Fagre, 2003; Hall and Fagre, 2003; Hall and Fagre, 2003; Harper and Humphrey, 2003; Harper and Humphrey, 2003; Harper and Humphrey, 2003; Jouvet and others, 2008; Laabs and others, 2006). Laabs and

others (2006) used a coupled 2-D mass balance and ice-flow numerical modeling approach to reconstruct Last Glacial Maximum glaciers in the Wasatch and southern Uintah Mountains of Utah. Glacial extent was a function of mass balance (accumulation/ablation) and ice flow and is similar to thesis Model 2 in that climate is adjusted until glacier extent reaches physically based features (moraines) (Laabs and others, 2006). Laabs and others (2006) use local climate data (SNOTEL) to get a spatial representation of temperature and precipitation for three glacier basins, while I use southern and northern halves of Mount Rainier to represent spatial variations of the mass balance parameters of accumulation, ablation, and ELA (Model 1) and ELA (Model 2). Laabs and others (2006) also tune their model with local snowpack data from two small snow fields and modeled winter accumulation compared to SNOTEL data. Ice flow assumptions were similar to the cellular automata model used here (Laabs and others, 2006). Laabs and others (2006) concluded that their physically based model, similar to thesis Model 2, was useful for estimating precipitation and temperatures at the colder end of the temperature depressions while other paleoclimate proxies were useful for the warmer end of the range. Harper and Humphrey (2003) use a physically based cellular automata model, upon which these thesis models are based, and initiate glaciers above their diminished snowfall elevation (DSE), while I placed glaciers below that threshold for modeling simplicity, which likely produced different results.

Future glacial extents in Glacier National Park were modeled with satisfactory results using parameters similar to the ELA parameters of Model 1 of this thesis, July-August mean temperature and mean annual precipitation (Hall and Fagre, 2003). While the thesis uses a DEM as topographic control, Hall and Fagre (Hall and Fagre, 2003)

found that of three topographic factors- elevation, slope, and aspect- elevation was the most significant for explaining probability of melt for each cell, and overall glacial extent in their GIS model.

Numerically modeled glacial extents from the Vadret Muragl, Swiss Alps, show the glacier was larger in volume than the geomorphological evidence suggests, and that the geomorphological evidence was likely not a maximum but a transient retreat state which could support results from Model 1 where glaciers extended beyond mapped moraines (Jouvet and others, 2008). This could suggest that some of the mapped moraines on Mount Rainier (Crandell and Miller, 1974; Heine, 1998) could be left by transient retreat states. Further modeling and field analysis of individual moraines would be required to reach such conclusions and is beyond the scope of this thesis. Like Model 2, Jouvet and others (2008) also solved the "inverse problem" of matching a modeled glacier to given tongue position, but they found lateral moraines would be useful to further define the shape of the glacier and thus its overall volume. As they point out, there may be an infinite number of mass balance variables that produce a given glacier length, and within realistic precipitation and temperature parameters, a high degree of resulting variability exists- the ELAs varied 100-220 m and volumes as much as 40% (Jouvet and others, 2008). Model 2 is an example of the variability that Jouvet (2008) presents as mass balance parameters are unrealistic, but the resulting glacier lengths and widths (where lateral moraines were identified) were mostly satisfactory for the Garda Stade.

The periglacial environments that early humans would have used varied in elevation over the Holocene. Early humans likely used elevations in the alpine and

subalpine below the snow line or adjacent to and above the terminus positions of large valley glaciers (Burtchard, 1998), 1,730-2,980 m, as above this elevation winter snows would likely exist at summer's end. Early Holocene glacial extent 11,150 cal yr. B.P. would have permitted access to the highest Holocene reaches on the mountain 2,980 m. One hundred sixty years later the largest Holocene glacial advance would have limited human activity to below 1,730 m. The following 900 years would have twice permitted snow-free access to the mountain's higher reaches 2,720 and 2,950 m. Encroaching snow and ice would have forced users to access lower elevations through the middle Holocene culminating in 6,490 cal yr. B.P. at 1,820 m. After a slight reprieve of higher elevation snow and ice extents, another similar advance would have affected humans 3,450 cal yr. B.P. From that time and until the historic era, snow and ice-free areas rose to approximately 2,000 m. The glaciers and snowfields provided a vegetation boundary that would have affected humans gathering resources, but the major valleys also would have proven to be dangerous with flooding and outburst flooding events.

In conclusion, the reconstructed Holocene climate and glaciers paint a picture of great variability. The geologic record shows three glacial advances, McNeeley II 10,900-9,950 cal yr. B.P., Burroughs Mountain 3,442-2,153 cal yr B.P., and Garda 500-90 cal yr B.P. The scientific literature shows that paleoclimate was highly variable in the early Holocene when the air temperatures were much warmer than current while staying consistently dry. The environment became more moist through the mid-Holocene while temperatures slowly varied below current temperatures. The late Holocene was marked by moist conditions and temperatures that warmed before cooling to current temperatures.

The glaciers on Mount Rainier are highly sensitive to climate changes as the ELAs respond wildly, more so than other lower elevation glaciated peaks in the region possibly due to its large size and other unknown climate variables. For coeval glacial advances as seen in the geologic record, the ELA depressions on Mount Rainier are three to fourfold larger than Three Sisters, OR (Marcott and others, 2009) and Mount Baker, WA (Thomas, 2000) thus producing unreasonable temperature depressions and added winter accumulations when using conventional glaciological reconstruction of climate methods. The reconstructed paleoclimatic variables, SST and the qualitative precipitation proxy, were the climate variables initiating the large ELA changes on Mount Rainier and its inferred larger glaciologically computed climate changes. Although the resulting temperatures are similar to today, the sudden SST declines of -1.2°C to -2.0°C in the early Holocene were amplified on Mount Rainier and produced the McNeeley II glacial advance with an ELA depression of 1,260 m. The Burroughs Mountain advance was initiated by a SST decline of -0.6°C from today and was continued by the wettest climate of the Holocene thus producing an ELA depression of 1,170 m. With similar ELA depressions to Burroughs Mountain, the Garda advance was caused by higher precipitation and SSTs similar to today, which is in contrast to most worldwide literature that supports both added precipitation and lower temperatures for the Little Ice Age (Oerlemans, 2005).

My modeled ELAs and glacial extents, Models 1 and 2, show seven Holocene advances: 10,990, 10,170, 9,260, 8,200, 6,490, 3,450-2,790, and 550-160 cal yr. B.P. and ELAs ranging from 1,730-2,980 m. With the same Nisqually Glacier ELAs between the two models, Model 1 postdicts larger glaciers while Model 2 (tuned to Garda moraines)

best fits the McNeeley II moraines. North-south spatial variations in glacial extent seem to occur during periods of glacial recession but to a lesser degree during periods of advance. The first two advances (10,990, 10,170 cal yr. B.P.) are similar to the ELAs and extent of the McNeeley II data. The modeled advances at 9,260, 8,200, and 6,490 were not found in the geologic record. Yet, the worldwide 8,200 cal yr. B.P. cooling event was recorded elsewhere in the region (Menounos and others, 2004; Osborn and others, 2007; Thomas, 2000). The model advances at 3,450 cal yr. B.P. (ELA 1,800 m) are larger than the similarly dated Burroughs Mountain advance (Crandell and Miller, 1974) and is coeval with an advance in the southern Coast Range of British Columbia (Osborn and others, 2007).

Mount Rainier is the most glaciated peak in the contiguous 48 U.S. states, and future research should continue in efforts to better understand current climate-paleoclimate relationships, glacier and paleo-glacier relationships, and how such may have affected early users on the mountain. The paleoclimatic record in the U.S. Pacific northwest is relatively rich spatially and temporally but more could be done to understand the different influences of the two SST records especially as they diverged in the late Holocene. Radiocarbon dating other McNeeley II moraines around the large valley glaciers would further constrain its glacial extent and address spatial variability. Radiocarbon dating of Burroughs Mountain moraines would be beneficial because the spatial and temporal data is limited. More sophisticated climate models should account for non-linear accumulation and ablation data, the diminished snowfall elevation such as the accumulation peak at 2,200 m on the Nisqually Glacier, greater seasonality, and length of season. Modeling ELA and glacier extents would benefit from more years of

mass balance data, mass balance data from higher elevations, and a continuous model that can test high advance and retreat rates and can be stopped at various time periods. Energy balance modeling could also test high advance and retreat rates. More current (21st century) glacial retreat rates from the region would benefit comparisons with Mount Rainier. Analysis of resulting AARs and comparisons between the models and other glaciers in the region would make glacial extent models more robust.

6. REFERENCES

Ahlmann, H.W.:. 1924. Le niveau de glaciation comme fonction de l'accumulation d'humidité sous forme solide. Méthode Pour le Calcul de L'humidité Condensée Dans la Haute Montagne et Pour L'étude de la Fréquence des Glaciers. *Geografiska Annaler,* **6**, 223-272.

Alley, R.B. 2000. The Younger Dryas cold interval as viewed from central Greenland. *Quaternary Science Reviews,* **19**, 213-226.

Alley, R.B. and P.U. Clark. 1999. The Deglaciation of the Northern Hemisphere: A Global Perspective. *Annual Review of Earth and Planetary Science,* **29**, 149-182.

Alley, R.B., P.A. Mayewski, T. Sowers, M. Stuiver, K.C. Taylor and P.U. Clark. 1997. Holocene climatic instability: a prominent widespread event 8200 yr ago. *Geology,* **25**, 483-486.

Anderson, B. and A. Mackintosh. 2006. Temperature change is the major driver of late-glacial and Holocene glacier fluctuations in New Zealand. *Geology,* **34**(2), 121-124.

Anslow, F.S., S.W. Hostetler, W.R. Bidlake and P.U. Clark. 2007. Distributed energy balance modeling of South Cascade Glacier, Washington and assessment of model uncertainty. *Journal of Geophysical Research-Earth Surface,* **113**(F02019), 1-18.

Baker, B.B. and R.K. Moseley. 2007. Advancing Treeline and Retreating Glaciers: Implications for Conservation in Yunnan, P.R. China. *Arctic, Antarctic, and Alpine Research,* **39**(2), 200-209.

Balascio, N.L., D.S. Kaufman and W.F. Manley. 2005. Equilibrium-line altitudes during the Last Glacial Maximum across the Brooks Range, Alaska. *Journal of Quaternary Science,* **20**(7-8), 821-838.

Barnosky, C.W., Anderson, P.M. and Bartlein, P.J. 1987. The northwestern U.S. during deglaciation: vegetational history and paleoclimatic implications. In Ruddiman, W.F. and Wright, H.E.J. eds *North America and adjacent oceans during the last deglaciation.* Boulder, Geological Society of America, 289-321.

Barron, J.A., L. Heusser, T. Herbert and M. Lyle. 2003. High-resolution climatic evolution of coastal northern California during the past 16,000 years. *Paleoceanography,* **18**(1), 1-19.

Bartlein, P.J., K.H. Anderson, P.M. Anderson, M.E. Edwards and C.J. Mock. 1998. Paleoclimate simulations for North America over the past 21,000 years: features of

the simulated climate and comparisons with paleoenvironmental data. *Quaternary Science Reviews,* **17**, 549-585.

Benn, D.I. and A.M.D. Gemmell. 1997. Calculating equilibrium-line altitudes of former glaciers by the balance ratio method: a new computer spreadsheet. *Glacial Geology and Geomorphology,* (tn01), 1-7.

Berger, A. 1988. Milankovitch theory and climate. *Review of Geophysics,* **26**, 624-657.

Betts, A.K. and W. Ridgeway. 1992. Tropical boundary layer equilibrium in the Last Ice Age. *Journal of Geophysical Research-Earth Surface,* **97**, 2529-2534.

Bilderback, E. L. 2004. Timing and Paleoclimatic Significance of Latest Pleistocene and Holocene Cirque Glaciation in the Enchantment Lakes Basin, North Cascades, WA. (M.S. Thesis, Western Washington University.)

Bitz, C.M. and D.S. Battisti. 1999. Interannual to Decadal Variability in Climate and the Glacier Mass Balance in Washington, Western Canada, and Alaska. *Journal of Climate,* **12**(11), 3181-3196.

Briles, C.E., C. Whitlock and P.J. Bartlein. 2005. Postglacial vegetation, fire, and climate history of the Siskiyou Mountains, Oregon, USA. *Quatern.Res.,* **64**(1), 44-56.

Brown, K.J., R.J. Fitton, G. Schoups, G.B. Allen, K.A. Wahl and R.J. Hebda. 2006. Holocene precipitation in the coastal temperate rainforest complex of southern British Columbia, Canada. *Quaternary Science Reviews,* **25**(21-22), 2762-2779.

Brugger, K.A. and Goldstein, B.S. 1999. Paleoglacier reconstruction and late Pleistocene equilibrium-line altitudes, southern Sawatch Range, Colorado. In Mickelson, D.M. and Attig, J.W. eds *Geological Society of America Special Paper 337-Glacial Processes Past and Present.* Boulder, CO, Geological Society of America, 103-112.

Burbank, D.W. 1981. A chronology of late Holocene glacier fluctuations on Mount Rainier, Washington. *Arctic and Alpine Research,* **13**(4), 369-386.

Burbank, D.W. 1982. Correlations of climate, mass balances, and glacial fluctuations at Mount Rainier, Washington, U.S.A., since 1850. *Arctic and Alpine Research,* **14**(2), 137-148.

Burtchard, G.C. 1998. Environment, prehistory and archaeology of Mount Rainier National Park, Washington.

Butler, D.M. and L.M. DeChano. 2001. Environmental change in Glacier National Park, Montana: an assessment through repeat photography from fire lookouts. *Physical Geography,* **22**(4), 291-304.

Cane, M.A., A.C. Clement, A. Kaplan, and others. 1997. Twentieth-Century Sea Surface Temperature Trends. *Science,* **275**(5302), 957-960.

Clague, J.J. and R.W. Mathewes. 1989. Holocene thermal maximum in western North America: new evidence from Castle Peak, British Columbia. *Geology,* **17**, 277-280.

Coleman, C.G., S.J. Carr and A.G. Parker. 2009. Modelling topoclimatic controls on palaeoglaciers: implications for inferring palaeoclimate from geomorphic evidence. *Quaternary Science Reviews,* **28**, 249-259.

Corripio, 2007. *Javier Corripio Solar Insolation Calculator.* http://www.geo.ed.ac.uk/~jgc/sunshine.html. Last accessed 11/15/2007.

Crandell, D.R. 1969. Surficial geology of Mount Rainier National Park, Washington. *U.S. Geologcial Survey Bulletin* **1288.**

Crandell, D.R. and Miller, R.D. 1974. Quaternary stratigraphy and extent of glaciation in the Mount Rainier Region, Washington 847. Washington, D.C., United States Government Printing Office, 59.

Cuffey, K.M., G.D. Clow, R.B. Alley, M. Stuiver, E.D. Waddington and R.W. Saltus. 1995. Large Arctic Temperature Change at the Wisconsin-Holocene Glacial Transition. *Science,* **270**(5235), 455-458.

Daly, C., W.P. Gibson, G.H. Taylor, G.L. Johnson and P. Pasteris. 2002. A knowledge-based approach to the statistical mapping of climate. *Climate Research,* **22**, 99-113.

Daly, C., R.P. Neilson and D.L. Phillips. 1994. A Statistical-Topographic Model for Mapping Climatological Precipitation over Mountainous Terrain. *Journal of Applied Meteorology,* **33**, 140-158.

Davis, P.T., B. Menounos and G. Osborn. 2009. Holocene and latest Pleistocene alpine glacier fluctuations: a global perspective. *Quaternary Science Reviews,* **28**, 2021-2033.

Driedger, C.L. and P.M. Kennard. 1984. Ice volumes on Cascade Volcanoes : Mount Rainier, Mount Hood, Three Sisters, and Mount Shasta . *US Geological Survey Open-File Report* **84-581.**

Dunwiddie, P.W. 1986. A 6000-year record of forest history on Mount Rainier, Washington. *Ecology,* **67**(1), 58-68.

Friele, P.A. and J.J. Clague. 2002. Younger Dryas readvance in Squamish river valley, southern Coast mountains, British Columbia. *Quaternary Science Reviews,* **21**, 1925-1933.

Furnbish, D.J. and J.T. Andrews. 1984. The use of hypsometry to indicate long-term stability and response of valley glaciers to changes in mass transfer. *Journal of Glaciology,* **30**(105), 199-211.

Gavin, D.G., J.S. McLachlan, L.B. Brubaker and K.A. Young. 2001. Postglacial history of subalpine forests, Olympic Peninsula, Washington, USA. *Holocene,* **11**(2), 177-188.

Gesch, D.B. 2007. The National Elevation Dataset. In Maune, D. eds *Digital Elevation Model Technologies and Applications: The DEM Users Manual.* Bethesda, Maryland, American Society for Photogrammetry and Remote Sensing, 99-118.

Gesch, D.B., M. Oimoen, S. Greenlee, C. Nelson, M. Steuck and D. Tyler. 2002. The National Elevation Dataset. *Photogrammetric Engineering and Remote Sensing,* **68**(1), 5-11.

Green, D.G. and G.S. Dolman. 1988. Fine resolution pollen analysis. *Journal of Biogeography,* **15**, 685-701.

Greene, S.E. and M. Klopsch. 1985. Soil and Air Temperatures for Different Habitats in Mount Rainier National Park. **PNW-342.**

Guido, Z.S., D.J. Ward and R.S. Anderson. 2007. Pacing the post-Last Glacial Maximum demise of the Animas Valey glacier and the San Juan Mountain ice cap, Colorado. *Geology,* **35**, 739-742.

Hall, M.H.P. and D.B. Fagre. 2003. Modeled climate-induced glacier change in Glacier National Park, 1850-2100. *BioScience,* **53**(2), 131-140.

Hallett, D.J., D.S. Lepofsky, R.W. Mathewes and K.P. Lertzman. 2003. 11 000 years of fire history and climate in the mountain hemlock rain forests of southwestern British Columbia based on sedimentary charcoal. *Canadian Journal of Forest Research,* **33**(2), 292-312.

Harper, J.T. and N.F. Humphrey. 2003. High altitude Himalayan climate inferred from glacial ice flux. *Geophysical Research Letters,* **30**(14), 1764-1767.

Harrison, A.E. 1956. Fluctuations of the Nisqually Glacier, Mt. Rainier, Washington, since 1750. *Journal of Glaciology,* **2**(19), 675-683.

Hayes, P.S., L.A. Rasmussen and H. Conway. 2002. Estimating precipitation in the central Cascades of Washington. *Journal of Hydrometeorology,* **3**(3), 335-346.

Heine, J.T. 1996. New limiting ages for tephra layer R on Mount Rainier, Cascade Range. Geologic Society of America Cordilleran Section Meeting, *Abstracts with Programs,* **74**

Heine, J.T. 1998. Extent, timing, and climatic implications of glacier advances on Mount Rainier, Washington, USA, at the Pleistocene/Holocene transition. *Quaternary science reviews,* **17**(12), 1139-1148.

Heusser, C.J. 1977. Quaternary palynology of the Pacific slope of Washington. *Quaternary Research,* **8**, 282-306.

Huang, S. 2004. Merging information from different resources for new insights into climate change in the past and future. *Geophysical Research Letters,* **31**(L13205), 1-4.

Huybers, P. 2006. Early Pleistocene Glacial Cycles and the Integrated Summer Insolation Forcing. *Science,* **313**, 508-511.

ICOADS, 2008. *NOAA Earth System Research Laboratory, Physical Sciences Division, International Comprehensive Ocean-Atmosphere Dataset, 2-degree.* http://www.cdc.noaa.gov/cdc/data.coads.2deg.html. Last accessed 1/08/2008.

IPCC 2007. Climate Change 2007: The Physical Science Basis, Contribution of Working Group I to the Fourth Assessment Report of the Intergovernmental Panel on Climate Change.

Jackson, K.M. and A.G. Fountain. 2007. Spatial and morphological change on Eliot Glacier, Mount Hood, Oregon, USA. *Annals of Glaciology,* **46**, 222-226.

Jianping, Y., D. Yongjian, C. Rensheng, L. Shiyin and L. Anxin. 2003. Causes of glacier change in the source regions of the Yangtze andYellow rivers on theTibetan Plateau. *Journal of Glaciology,* **49**(167), 539-546.

Jouvet, G., M. Picasso, J. Rappaz and H. Blatter. 2008. A new algorithm to simulate the dynamics of a glacier: theory and applications. *Journal of Glaciology,* **54**(188), 801-811.

Kerschner, H.H. and S. Ivy-Ochs. 2008. Palaeoclimate from glaciers: Examples from the Eastern Alps during the Alpine Lateglacial and early Holocene. *Global Planet.Change,* **60**(1-2), 58-71.

Kienast, S.S. and J.L. McKay. 2001. Sea Surface Temperatures in the subarctic Northeast Pacific reflect millennial-scale Climate Oscillations during the last 16 kyrs. *Geophysical Research Letters,* **28**(8), 1563-1566.

Laabs, B.J.C., M.A. Plummer and D.M. Mickelson. 2006. Climate during the last glacial maximum in the Wasatch and southern Uinta Mountains inferred from glacier modeling. *Geomorphology (Amsterdam, Netherlands),* **75**(3-4), 300-317.

LaChapelle, E. 1960. The Blue Glacier. Final Report, Project 1959 and 1960.

Leonard, E.M. 1989. Climatic change in the Colorado Rocky Mountains: estimates based on modern climate at late Pleistocene equilibrium lines. *Arctic and Alpine Research,* **21**(3), 245-255.

Letreguilly, A. 1988. Relation between the mass balance of Western Canadian mountain glaciers and meteorological data. *Journal of Glaciology,* **34**, 11-18.

Licciardi, J.M., P.U. Clark, E.J. Brook, D. Elmore and P. Sharma. 2004. Variable responses of western U.S. glaciers during the last deglaciation. *Geology,* **32**(1), 81-84.

Lie, O.O. and O. Paasche. 2006. How extreme was northern hemisphere seasonality during the Younger Dryas? *Quaternary Science Reviews,* **25**(5-6), 404-407.

Mann, M.E., R.S. Bradley and M.K. Hughes. 1999. Northern Hemisphere Temperatures During the Past Millennium: Inferences, Uncertainties, and Limitations. *Geophysical Research Letters,* **26**(6), 759-762.

Mann, M.E. and C.D. Jones. 2003. Global surface temperatures over the past two millennia. *Geophysical Research Letters,* **30**(15), 1820.

Mann, M.E., S. Rutherford, R.S. Bradley and M.K. Hughes. 2003. Optimal surface temperature reconstructions using terrestrial borehole data. *Journal of Geophysical Research-Earth Surface,* **108**(D7), 4203-4213.

Marcott, S. A. 2005. A Tale of Three Sisters: Reconstructing the Holocene glacial history and paleoclimate record at Three Sisters Volcanoes, Oregon, United States. (M.S. Thesis, Portland State University.)

Marcott, S.A., A.G. Fountain, J.E. O'Connor, P.J. Sniffen and D.P.:. Dethier. 2009. A latest Pleistocene and Holocene glacial history and paleoclimate reconstruction at Three Sisters and Broken Top Volcanoes, Oregon, U.S.A. *Quatern.Res.,* **71**(2), 181-189.

McCabe, G.J. and A.G. Fountain. 1995. Relations between Atmospheric Circulation and Mass Balance of South Cascade Glacier, Washington, U.S.A. *Arctic and Alpine Research,* **27**(3), 226-233.

Meier, M.F. and A.S. Post. 1962. Recent variations in mass net budgets of glaciers in western North America. *Publication-De l'Association Internationale d'Obergurgl,* **58**, 63-77.

Menounos, B., J. Koch, G. Osborn, J.J. Clague and D. Mazzucchi. 2004. Early Holocene glacier advance, southern Coast Mountains, BritishColumbia, Canada. *Quaternary Science Reviews,* **23**, 1543-1550.

Menounos, B., G. Osborn, J.J. Clague and B.H. Luckman. 2009. Latest Pleistocene and Holocene glacier fluctuations in western Canada. *Quaternary Science Reviews,* **28**, 2049-2074.

Meyer, H.W. 1992. Lapse rates and other variables applied to estimating paleoaltitudes from fossil floras. *Palaeogeography, Palaeoclimatology, Palaeoecology,* **99**(1-2), 71-99.

Miller, G. 2002. Pacific Northwest Weather: But my barometer says fair! Portland, Frank Amato Publications, 174.

Moss, M.L., Peteet, D.M. and Whitlock, C. 2007. Mid-Holocene culture and climate on the Northwest Coast of North America. In Anderson, D.G., Maasch, K.A. and Sandweiss, D.H. eds *Climate Change and Cultural Dynamics: A Global Perspective on Mid-Holocene Transitions.* San Diego, Elsevier, Inc., 491-529.

Mote, P.W. 2003. Trends in temperature and precipitation in the Pacific Northwest during the twentieth century. *Northwest Science,* **77**(4), 271-282.

Mullineaux, D.R. 1974. Pumice and other pyroclastic deposits in Mount Rainier National Park, Washington. *U.S. Geologcial Survey Bulletin* **1326.**

NWCC, 2008. *National Water and Climate Center, Natural Resource Conservation Service, SNOTEL Site Information and Reports.* http://www.wcc.nrcs.usda.gov/snow/. Last accessed 1/15/2008.

Nylen, T. H. 2001. Spatial and temporal variations of glaciers (1913-1994) on Mt. Rainier and the relation with climate. (MSc thesis, Portland State University.)

Nylen, T.H., A.G. Fountain and C.L. Driedger. 2000. Temporal and spatial variation of glaciers on Mount Rainier. *Washington Geology,* **28**(1-2), 27-28.

Oerlemans, J. 2005. Extracting a Climate Signal from 169 Glacier Records. *Science,* **308**, 675-677.

Ohmura, A. 2001. Physical basis for the temperature-based melt-index method. *Journal of Applied Meteorology,* **40**, 753-761.

Ohmura, A., P. Kasser and M. Funk. 1992. Climate at the equilibrium line of glaciers. *Journal of Glaciology,* **38**, 397-411.

Osborn, G., B. Menounos, D. Koch, J.J. Clague and V. Vallis. 2007. Multi-proxy record of Holocene glacial history of the Spearhead and Fitzsimmons ranges, Southern Coast Mountains, British Columbia. *Quaternary Science Reviews,* **26**, 479-493.

Paterson, W.S.B. 1994. The Physics of Glaciers. Tarrytown, New York, Elsevier Science Inc., 480.

Pelto, M.S. 1989. Time-series analysis of mass balance and local climatic records from four northwestern North American glaciers. In Colbeck, S.C. eds *Snow Cover and Glacier Variations.* Great Yarmouth, UK, IAHS, 95-102.

Pelto, M.S. 2000. Mass balance of adjacent debris-covered and clean glacier ice in the North Cascades, Washington. In Nakawo, M., Raymond, C.F. and Fountain, A.G. eds *Debris-Covered Glaciers.* Seattle, WA, IAHS, 288.

Peteet, D.M. eds 1993. *Global Younger Dryas, a special issue of Quaternary Science Reviews.* 277-355-355.

PRISM, 2007. *PRISM Group, Oregon State University.* http://www.prismclimate.org. Last accessed 2/8/2008.

Rasmussen, L.A. and H. Conway. 2001. Estimating South Cascade Glacier (Washington, U.S.A.) mass balance from a distant radiosonde and comparison with Blue Glacier. *Journal of Glaciology,* **47**(159), 579-588.

Rasmussen, L.A., H. Conway and P.S. Hayes. 2000. The accumulation regime of Blue Glacier, U.S.A., 1914-96. *Journal of Glaciology,* **46**(153), 326-334.

Rasmussen, L.A. and J.M. Wenger. 2009. Upper-air model of summer balance on Mount Rainier, USA. *Journal of Glaciology,* **55**(192), 619-624.

Reasoner, M.A., G. Osborn and N.W. Rutter. 1994. Age of the Crowfoot advance in the Canadian Rocky Mountains: A glacial event coeval with Younger Dryas oscillation. *Geology,* **22**, 439-442.

Riedel, J.L. unpublished information. Glacier Monitoring Program. North Cascades National Park

Rupper, S.S. and G. Roe. 2008. Glacier Changes and Regional Climate: A Mass and Energy Balance Approach*. *J.Clim.,* **21**(20), 5384-5401.

Rutherford, S., M.E. Mann, T.J. Osborn, and others. 2005. Proxy-Based Northern Hemisphere Surface Temperature Reconstructions: Sensitivity to Method, Predictor Network, Target Season, and Target Domain. *Journal of Climate,* **18**, 2308-2329.

Scott, K.M. and J.W. Vallance. 1995. Debris Flow, Debris Avalanche, and Flood Hazards At and Downstream from Mount Rainier, Washington. **U.S. Geological Survey Hydrologic Investigations Atlas HA-729.**

Scott, K.M., J.W. Vallance and P.T. Pringle. 1995. Sedimentology, Behavior, and Hazards of Debris Flows at Mount Rainier, Washington. *U.S. Geologcial Survey Professional Paper* **1547.**

Sea, D.S. and C. Whitlock. 1995. Postglacial vegetation and climate of the Cascade Range, central Oregon. *Quaternary Research,* **43**, 370-381.

Stuiver, M. and P.J. Reimer. 1993. Extended 14 C data base and revised CALIB 3.0 14 C age calibration program. *Radiocarbon,* **35**, 215-230.

Tangborn, W.V. 1980. Two Models for Estimating Climate-Glacier Relationships in the North Cascades, Washington, U.S.A. *Journal of Glaciology,* **25**(91), 3-21.

Thomas, P.A. 2000. Early holocene glaciation on Mount Baker: Washington State, USA. *Quaternary Science Reviews,* **19**(11), 1043-1046.

Thompson, R.S., Whitlock, C., Bartlein, P.J., Harrison, S.P. and Spaulding, W.G. 1993. Climatic Changes in the Western United States since 18,000 yr B.P. In Wright, H.E.,Jr., Kutzbach, J.E., Webb, T.,III, Ruddiman, W.F., Street-Perrott, F.A. and Bartlein, P.J. eds *Global Climates Since The Last Glacial Maximum.* Minneapolis, University of Minnesota Press, 468-513.

Topinka, L. 1997. Location Map. Vancouver, Washington, USGS/CVO,

Tsukada, M., Sugita, S. and Hibbert, D.M. 1981. Paleoecology in the Pacific Northwest I. Late Quaternary vegetation and climate. International Association of Theoretical and Applied Limnology, **21**730-737.

Tweiten, M.A. 2007. The Interaction of Changing Patterns of Land Use, Sub-Alpine Forest Composition and Fire Regime at Buck Lake, Mount Rainier, National Park, USA. *International Archeological Research Institute, Inc.*

Vacco, D.A., P.U. Clark, A.C. Mix, H. Cheng and R.L. Edwards. 2005. A speleothem record of Younger Dryas cooling, Klamath Mountains, Oregon, USA. *Quaternary Research,* **64**, 249-256.

Viau, A.E., K. Gajewski, M. Sawada and P. Fines. 2006. Millennial-scale temperature variations in North America during the Holocene. *Journal of Geophysical Research-Earth Surface,* **111**(D09102), 1-12.

Walsh, M.K., C. Whitlock and P.J. Bartlein. 2008. A 14,300-year-long record of fire-vegetation-climate linkages at Battle Ground Lake, southwestern Washington. *Quaternary Research,* **70**(2), 251-264.

Whiteman, C.D. 2000. Mountain Meteorology Fundamentals and Applications. New York, Oxford University Press, 355.

Whitlock, C. 1992. Vegetational and climatic history of the Pacific Northwest during the last 20,000 years: implications for understanding present-day biodiversity. *The Northwest Environmental Journal,* **8**(1), 5-29.

Whitlock, C., A.M. Sarna-Wojcicki, P.J. Bartlein and R.J. Nickmann. 2000. Environmental history and tephrostratigraphy at Carp Lake, southwestern Columbia Basin, Washington, USA. *Palaeogeography Palaeoclimatology Palaeoecology,* **155**(1-2), 7-29.

Williams, M., Dunkerley, D., De Deckker, P., Kershaw, P. and Chappell, J. 1998. Quaternary Environments. London, Arnold, 329.

Wolfe, J.A. 1992. An Analysis of Present-Day Terrestrial Lapse Rates in the Western Coterminous United States and Their Significance to Paleoaltitudinal Estimates. *U.S. Geologcial Survey Bulletin* **1964.**

WRCC, 2008. *Western Regional Climate Center, Historical Climate Information.* http://www.wrcc.dri.edu/index.html. Last accessed 1/15/2008.

Zemp, M.M., M. Hoelzle and W. Haeberli. 2007. Distributed modelling of the regional climatic equilibrium line altitude of glaciers in the European Alps. *Global Planet.Change,* **56**(1-2), 83-100.